1969/12/30

EHD Research: Final report for the year 1968-69

Biblarz, Oscar

Monterey, California. Naval Postgraduate School

NPS-57ZI9121A

United States
Naval Postgraduate School

EHD RESEARCH

FINAL REPORT FOR THE YEAR

1968-69

by

Oscar Biblarz

30 December 1969

NAVAL POSTGRADUATE SCHOOL
Monterey, California

Rear Admiral R. W. McNitt, USN
Superintendent

R. F. Rinehart
Academic Dean

ABSTRACT:

Interest in electrohydrodynamics (EHD) stems mainly from its potential application in electrical power generation. The principle is that a stream of insulating fluid, which contains charged particles viscously coupled to it, moves charges against an electric field. In this fashion, the mechanical power of the flowing medium is converted directly into electrical power. EHD generators offer some promise of being simple, reliable, compact, and light.

The present research is concerned with how charged particles can be generated in the laboratory with a potentially useful range of sizes, of charge, and of number density. It is suggested that refined measurement techniques are needed to check on just what is being injected into the flow. The effects of turbulence on the EHD process and, particularly, on breakdown are being studied. The report discusses in some detail the possible role of turbulence on the mean effective mobility of charged particles.

On the experimental side, a laboratory facility has been built and then improved by the addition of a larger test section and other equipment. Work is proceeding to further develop and refine the instrumentation. Two types of injectors have been operated, namely, molecular and two-phase and the latter shows potential for efficient operation.

It has been concluded tentatively that turbulence in the carrier fluid increases its breakdown potential, and that turbulent air may be a suitable medium for the EHD energy conversion process.

Research plans for the coming year are outlined in the report.

This task was supported by: Navy Department, Naval Air Systems Command
AIRTASK No. A34340/551/69R01002010

Oscar Biblarz
Assistant Professor of Aeronautics

Approved by:

R. W. Bell
Chairman
Department of Aeronautics

Released by:

C. E. Menneken
Dean of Research Administration

NPS-57ZI9121A
30 December 1969

FOREWORD

The program on EHD Research was started on September of 1968 at the Naval Postgraduate School, Monterey, California. This work was sponsored by the Naval Air Systems Command under the technical cognizance of Mr. Milton A. Knight.

The following personnel contributed to the work during the reporting year: Assistant Professor Oscar Biblarz (Principal Investigator), Assistant Professor D. C. Wooten, and Professor T. H. Gawain. Professor Wooten left the program in June of 1969 and Professor Gawain joined in July of 1969. Two Master theses we generated during this year and they are included as Appendices C and D in this report.

The help of Mr. Patrick Hickey in the laboratory is gratefully acknowledged.

Since September of 1968, Associate Professor K. E. Woehler of the NPS Physics Department has joined the program.

TABLE OF CONTENTS

LIST OF FIGURES (MAIN TEXT)

LIST OF TABLES

LIST OF SYMBOLS

A = Area of duct

D = Diffusion coefficient, drag force

D_i = Diffusion coefficient for ions

D_p = Diffusion coefficient for particles

D_e = Diffusion coefficient for electrons

$\mathscr{D}_i$ = Space charge diffusion coefficient for ions

$\mathscr{D}_p$ = Space charge diffusion coefficient for electrons

d = Cylinder diameter

E = Electric field

E_x = Electric field in the axial direction

E_r = Electric field in the radial direction

E_b = Breakdown field

E_s = Space charge field

e = Charge on an electron

F_E = Electrical force

F_G = Pressure force

F_V = Viscous force

G = Pressure gradient ($-dp/dx$)

h = Height of test section

I_g = Collector current

I_T = Total current at corona needle

K = Proportionality constant for drag law

k = Boltzmann's constant

L = Distance between corona ring and EHD collector

ℓ = Typical apparatus dimension, length of duct

$\mathcal{L}_s$ = Dimensionless loss parameter

n = Specie density

n_p = Number of particles

P_e = Electrical power output

P_f = Fluid power input

P_e^* = Dimensionless power density parameter

P_f^* = Dimensionless fluid power

Q = Total charge of space charge cloud

Q_p = Volumetric flow rate for carrier gas

$\bar{q}$ = Total charge per particle

R = Particle radius

R_e = Reynolds number based on the diameter

r = Radius

r_o = Initial space charge radius

$r_o)_{max}$ = Maximum value of r_o

S_c = Schmidt number

$S_c)_\ell$ = Laminar flow Schmidt number

$S_c)_t$ = Turbulent flow Schmidt number

T = Absolute temperature

U_∞ = Free stream velocity

$\bar{u}_p$ = Particle velocity

V_c = Corona voltage

v_D = Drift velocity

W = Width of the test section

X = Flow direction

x^* = Distance for which $\bar{u}_p/U_\infty = 0.99$

Z = Number of electronic charges

Γ = Specie flux

$\delta\bar{m}_p$ = Mass of particles

$\delta\bar{u}_p$ = Volume of particles

ε_v = Eddy diffusivity (momentum)

ε_m = Eddy diffusivity (mass)

ε_o = Permitivity of free space

η_i = Efficiency of the idealized energy converter

μ = Mobility of particles

μ_o = Mobility of particles for $\delta\bar{m}_p\ \delta\bar{u}_p \to 0$

μ_∞ = Viscosity of carrier gas

ν = Molecular diffusivity (momentum)

ρ_{p_e} = Electrical power density

ρ_{p_f} = Fluid power density

ρ_p = Particle density

ρ_∞ = Carrier gas density

τ_v = e-folding time for particle velocity charges

I. Introduction

A. General

Electrohydrodynamics (EHD) is the study of the interaction of a non-neutral fluid with an electric field. The fluid contains charged particles which are viscously coupled to the surrounding fluid particles and, since one polarity prevails, there can be an exchange of energy between the fluid and the electric field. The unipolar charged particles must be introduced into a highly non-conducting fluid since it must support high voltages without any appreciable flow of current. The fluid can be either a liquid or a gas, and in the latter case the name electrogasdynamics (EGD) is commonly used. Since the injected particles must, in general, be quite different from the enveloping medium, we speak of EHD flows as two-phase flows (i.e., solid or liquid particles suspended in a gas).

Interest in EHD stems from its potential application as a mechanism for "direct" power generation. Here, the flow energy of an insulating fluid is transformed into electrical energy. The principle of operation is that of the Van de Graaff generator where the moving belt has been replaced by a moving fluid stream. There are three basic steps in the EHD generator which are charge injection, charge convection by the fluid against the resistance of the elctrical field, and charge collection. Power levels of the order of one kilowatt per generator unit are anticipated with a variety of energy sources. A substantial EHD interaction, if it can be achieved, can also be used for purposes other than power generation, such as for propulsion and for diagnostic schemes in fluid dynamics. A number of practical applications are thus envisioned, but these await a better understanding of the underlying phenomena.

A striking feature of the EHD process is that it permits the conversion of fluid kinetic energy into electrical power without the need to employ or interpose turbomachinery. This absence of moving mechanical parts is a strong practical advantage in some applications

and can be an important factor in enhancing reliability. EHD, moreover, offers advantages over sister schemes such as magnetohydrodynamics (MHD) since it generates higher voltages and operates at more moderate temperatures. The lower operating temperatures of the carrier fluid present significantly fewer material problems when compared to MHD, and the absence of a magnetic field in EHD makes for inherently simpler equipment and lighter weight.

During the past decade, there has been considerable interest in direct energy conversion devices. The use of EHD generators for this purpose has great appeal because of their simplicity of operation, i.e., they involve no bulky equipment and need only a very short start-up time. Also, they are inherently light weight and, therefore, portable. Moreover, EHD devices have potential use as smog control devices since many of the pollutants can be charged and then precipitated.

There are at present three major groups in this country who have interest in EHD generators, viz., the Marks Polarized Company[1,2], Gourdine Systems Inc[3,4], and the Air Force (WPAFB) under the direction of Dr. H. von Ohain.[5,6].

B. Background

It was first thought that EHD is innately an inefficient process. More detailed and sophisticated studies have shown, however, that theoretical possibilities exist for reaching good performance. Of course, the phenomena involved are complex and subtle, and the ultimate attainment of these possibilities will require scientific work of high order. Before any potential benefits of EHD can be practically attained, it is essential to improve our understanding of the basic phenomena. Consequently, the present research is aimed primarily at the study of such fundamentals.

There are several problems that research efforts in EHD must overcome before producing practical results. For example, because the medium has to be highly stressed electrically, one has to contend with the numerous ways that nature would like to relieve that stress.

These include surface leakage through impurities on insulators, corona discharges from sharp metallic surfaces, spark breakdown, etc.

A major problem in this connection is that of electrical breakdown of the carrier gas. Breakdown represents an upper limit of operation in the sense that once the fluid begins to generate charge carriers, it is no longer an insulator. Breakdown can be most likely attributed to the presence of free electrons which gain enough energy from the electric field to ionize a molecule upon collision with it. Obviously, the geometry of the flow field and the electron scavenging properties of the gas are going to affect breakdown. Such scavenging decreases the free electron concentration. Additives[8] such as SF_6 or CCl_2F_2 (Arctron -12) can also be introduced for just this purpose. The geometry can have the effect of creating an inhomogeneous field. Consequently ionization may take place at lower overall voltage than would otherwise be the case, such as in the corona discharge.

Free electrons always exist in a medium due to a variety of natural sources. These electrons need minimum energy for ionization. Also there must be a cumulative series of ionizing collisions so that there is an avalanche effect and the ionization build-up can overcome the losses between the electrodes. The gas density also comes into play since there must be enough molecules to ionize (here we get the familiar Paschen law[9] for spark breakdown). In gases with additives, or in gas mixtures[10], complex interactions can take place which may aid or hinder the cumulative processes needed for breakdown. It has been found[8] that, at pressures above atmospheric, the electrode material also becomes a significant item in breakdown. There is yet another factor which affects breakdown and that is the motion of the gas. Because of the strong frictional coupling the charged particles follow the gas motion and because of the strong electrical coupling the electrons must follow the particles closely (otherwise space charge fields could develop which might easily become larger than the external field). Hence, the movement of the gas and, in particular, the degree of turbulence

of the flow[11] has an effect on the breakdown. This last item will be of particular concern to us.

Another fundamental problem in EHD energy conversion pertains to the mobility of the charged particles. Mobility is defined as the average drift velocity per unit electric field. It describes how well a charged particle couples the long range electric forces to the short range forces effective during collisions with surrounding molecules. The mobility parameter arises from the observation that in a collision-dominated system, particles achieve a terminal drift velocity relative to surrounding medium which is proportional to the strength of the electric field. This, in essence, is a simplified solution of the momentum equation for the charged species. The lower the mobility the more highly coupled the particles (and hence the electric field) to the fluid. Analyses have shown conclusively that low molecular weight ions are too mobile for most cases of interest; larger particles that range up to micron dimensions and which carry one or a few charges per particle are needed to maintain the mobility at the requisite low values. A drift velocity which is smaller than the gas velocity by a factor of at least ten is necessary. Low mobility particles not only couple the flow field to the electric field but reduce particle diffusion to the insulator walls.

Fig. 1 shows the mobility of water droplets in air as calculated by Barreto.[14] Such theoretical predictions of mobility take into account particle size and charge. Other effects should be included, such as the role of the free electrons which might possibly exist, the effects of charge exchange collisions, etc. Moreover, experimental measurements of mobility are also difficult to perform. Because of these complexities, the most comprehensive calculations to date have not been fully borne out by experimental observations.

Even though we can presumably manufacture particles which follow the gas because of their low mobility (i.e., no slip), we must somehow also arrange that the relative density of the flow of charged particles

be sufficiently high. Obviously, if there are only a few charged particles, this will translate into a small amount of electrical energy.

The theoretical relations governing power generation for an idealized case are given in Appendix A. These show the basic importance of mobility and relative density as mentioned above.

Other fundamental problems pertain to particle losses and frictional losses. A judicious choice of velocities and channel geometries will be necessary in order to minimize these losses. It is interesting to note here the "slender" versus "broad" channel controversy.[4] If we consider the flow in a generator channel to be axisymmetric, then we have to contend with a radial as well as an axial component of the electric field as obtained from Poisson's equation. In a "broad" channel the axial spacing is small so that one may neglect the radial motion of the ions. But this configuration has a pressure drop limited by the breakdown field to an unattractively small value. The "slender" channel attempts to increase the pressure drop by lengthening the channel and accounting for radial ion movement to the walls. Neither configuration has proven ideal but the problems here have received more attention than those mentioned in earlier paragraphs.

C. Method of Approach

Our approach has been to focus on the fluid dynamics of an EHD generator utilizing a gas for the carrier medium. The need to build an experimental facility, however, has prompted us to consider all of the relevant EHD effects. A review of the work of other investigators was initiated (see Chapter II) and a facility which operates with air at subsonic speeds has been constructed (see Chapter III).

An important objective of our program is to study the influence of turbulence on the EHD process. Present evidence suggests that this factor has a very significant effect on the operation of EHD generators. A highly turbulent flow can be shown to yield favorable results in increasing the breakdown potential of the carrier gas. It also has the collateral effect of strongly affecting the mean effective mobility of

the charged particles. The main disadvantage associated with turbulence is the larger fluid dynamic losses involved. Figure 2 illustrates schematically the application of this principle. The role of turbulence is discussed further in Chapter IV.

Since the manner by which charges are introduced into the carrier gas is the most critical in the EHD process and the most complicated in practice, the injector is another main concern in this program. Analysis based strictly on mobility arguments can be used[2] to show a certain optimum range of charged particle sizes. The mobility relations in terms of frictional forces, as given in Appendix B, are relevant in this regard. Also, on the experimental side we have operated two types of injectors, namely, molecular and two-phase, and conclude that the two-phase injector has a good potential for efficient operation. Appendices C and D are two Master Theses done at the Naval Postgraduate School in this connection.

Chapter VI presents some tentative conclusions from this work. Our proposed endeavors for the year 1969-70 are mentioned in Chapter VII.

II Survey of Work in the Field

The principles of EHD generation are based on phenomena which have been studied for over a century. Armstrong (1843) found that a steam jet which contained minute water drops would charge up an insulated body. He found no such effect with dry steam. Babat (1936) operated a generator using a supersaturated mercury jet which picked up charged particles as it passed through a discharge. Babat actually generated about 5 watts but since the particles moved in a collisionless regime, his was actually a "ballistic" generator. M. Mureau-Hanot[23] charged coal and glass dusts in order to obtain more massive charge carriers. Recently, W. E. Bennett[24] (1959) revived the idea of the gaseous Van de Graaff with some experimental results and with a discussion of the advantages of such generators.

O. Stuetzer[25] has been active in the field of EHD for many years. His early concerns have been the pumping of liquids (Ion Drag Pumps) and he has made contributions to the ion injector problems and to the understanding of space charge flow. More recently, he has done work on EHD flow control which consists of an electrically induced transition from turbulent to laminar flow and some control on boundary layer separation. All his work has been with insulating liquids. H. R. Velkoff[26] of Ohio State University has done wome work on EHD effects on gas flows.

The survey that follows is intended to be neither comprehensive nor exhaustive since the work has been summarized elsewhere.[1,5,15,26] We intend to present here a partial account of generator work which is largely derived from impressions during visits to the various companies and laboratories presently doing EHD research.

Pioneering efforts in EHD power generation were made by Alvin Marks who proposed the use of a charged aerosol.[12] He recognized the importance that ion mobility plays in the performance of EHD devices. Marks has worked on generators and smog control units and holds many patents. He has proposed a "mixture-condensation" process[1] for the formation of the charged aerosol which attempts to overcome some of the difficulties

inherent in the generator. Marks forsees the EHD generator breaking the monopoly of large utility companies by making possible the generation of smaller amounts of electrical power economically. He has also proposed that a fluid with low mobility, unipolar ions be studied as a new thermodynamic working medium.

The Air Force has sponsored several programs[5] in this field with a strong in-house capability (WPAFB) headed by Dr. H. von Ohain. Contributions of his group include an electrostatic analysis of generator configuations which singles out regions of undesirably high electric fields and predicts the performance of a given configuration, the use of guard electrodes to improve injector operation, and the design and operation of high pressure hardware. The scaling laws for EFD (electrofluiddynamic) generators based on a simplified version of the physics have been formulated. A two-fluid system (ejector cycle) has been proposed to overcome the low pressure ratios of the generators.

Dr. M. C. Gourdine in the late 1950's carried out a one dimensional gas dynamic analysis of EHD flows.[3] He concluded that the energy extraction was so minimal that the gas dynamic equations could be uncoupled from the electrodynamics. His analysis shows that the electric field can have its highest value at the injector and, thus, breakdown there may be a problem. Later he became a proponent of the "slender channel" generator configuration.[4,13] Briefly, in an axially symmetric flow, the axial electric field (x-direction) is assumed relatively constant so that Poisson's equation can be simplified by an order of magnitude argument, i.e.,

$$\frac{\partial E_x}{\partial X} << \frac{1}{r}\frac{\partial}{\partial r}(rE_r) \qquad (2\text{-}1)$$

Theoretical predictions made on this basis show an advantage over "broad" channels, but these predictions have not been borne out by experiments. A large scale generator system has been attempted using

coal dust charged in a corona discharge. Louvers are used to "contain" several parallel slender generator channels in a common vessel. Selected charge-bleeds to ground from these louvers are used in an attempt to minimize the effects of charge build up. Gourdine has marketed an electrostatic paint spray-gun which has a built-in EHD generator which provides all the high voltage electricity needed for the operation of the gun.

An allied but separate effort has been carried out at the Curtiss-Wright Corporation under several investigators.[7,13,14,15] They have worked with the slender channel with a charged air-water aerosol at both subsonic and supersonic speeds. Charged particle mobility measurements have been studied. Since the one-dimensional analysis of the generator has met with little success, a two-dimensional one has been carried out which accounts for the radial space charge field. Two-dimensional effects are shown to affect the generator load characteristics, although the theory agrees only qualitatively with experiements.

None of the above efforts, however, have convincingly shown that a substantial amount of flow energy has been transformed into electricity. Many ingenious schemes have evolved from these efforts, but progress in solving basic problems has been sporadic.

III Hardware

We have chosen to use air as the carrier medium because of its accessibility in the laboratory. A Carrier three-stage centrifugal compressor has been used which has a maximum flow rate of 4,000 CFM (inlet air). Its maximum pressure ratio is two and the exit air temperature can be varied from 80° to 240°F with an after cooler. While free from pump oil, the air contains moisture and whatever impurities it has at the inlet which do not precipitate at the pump. Before entering the test apparatus, the air is metered with a sharp-edged orifice built to ASME standards, and its temperature is also measured.

The test region is preceded by a plenum which serves to reduce the level of free stream turbulence to an intensity of 0.14% RMS in the test section. The flow straighteners in the plenum consist of a series of honeycomb and screen sections. In this plenum, additives to the flow may be introduced. The plenum is followed by a nozzle and then the test section. The test section is a rectangular channel 6" long of cross section 1" by 2". Typical runs are made at a Mach number of 0.3 and atmospheric conditions. The building material for the plenum and test section is Plexiglass, chosen for its excellent insulating properties, its ease of fabrication, and its transparency. This facility is described by Wallace (Appendix D). A new plenum-test section has been constructed which has increased the test section dimensions to 2" by 4". In addition, it permits the removal to the test section from the nozzle. This is shown in Figure 3.

The turbulent region of interest is the wake of a cylinder. The injector unit is incorporated into the trailing edge of the cylinder. Of the two types of injector tried the one that supplies air ions, of course, is the simpler to manufacture. It consists of a needle imbedded in the cylinder and recessed from the ring so that the electric field produces a velocity which is partially in the flow direction. As would be expected, these ions are too mobile in spite of the turbulent field.

This type of injector is discussed in Appendix C. The two-phase injector consists of a corona discharge within a metallic nozzle where supersaturated steam is accelerated to sonic-velocities. The initial unit is also reported in Appendix C. The results obtained are a considerable improvement over the air ions, but they are not as good as we had hoped. Hence, a new nozzle was built of teflon with a metallic insert at the throat which acts as the corona ring. This causes a more stringent condition for the corona operation since the spacing between the ring and needle is quite influential as to whether or not breakdown occurs before the onset of the corona current. However, better success has been achieved with this unit and it is the subject of Chapter V. The generator mode investigated so far has been the "short-circuit" case because we are interested primarily in injector performance at this time. We may note here that the internal impedance of the generator is so high that a usual type of application will not noticeably load it (except for the condition of load matching for maximum power). The diode bank used in conjunction with the collector has a resistance of about 3 megohms (see Figure 8, Chapter V) which is low compared to the generator internal impedance. The diode bank calibration curve is shown in Figure 4.

The injector does not fill all of the channel cross section and leaves ample space between the conversion region and the channel walls, as depicted in Figure 5. The flowing air is an excellent insulator and no problems have been encountered with shorting. The collector is a traversable needle mounted through the back of the channel. This needle collector offers less resistance to the flow than a screen. It was found that the sharp needle would back-corona and hence overshadow the EHD process. Subsequently, a guard ring was unsuccessfully installed. This ring can presumably shield the corona high voltage (at the nozzle exit ring) from the collector which, like the corona needle, is grounded. It is conceivable that the geometry of the injector-collector-guard ring system could be improved, but since we wanted to traverse the

collector this seemed like a rather involved operation. Instead, the series of diodes (or electronic valves) were installed which force the needle to operate in the generator mode. More recently we have blunted the collector tip somewhat.

Mappings of the collector current vs. space are not complete to date but we have observed small changes of planes cross wise to the flow and an expected decay in the axial direction. The collector area, in any event, is very difficult to define because of the back-corona effect, and because water condenses everywhere and particularly at the collector probe.

The high voltage is supplied by a Sorensen High Voltage DC power supply, with a range of 0 - 30 KV and 0 - 20 ma and with adjustable scales on its meters. It has a relay that disconnects the supply when a current surge exceeds 2 ma. All high voltage leads are properly labelled and provisions for high voltage safety are incorporated in the room. The high voltage connections are terminated in spherical brass balls so as to minimize corona discharges.[13] All cable used is good in excess of 40,000 volts.

Two high voltage voltmeters are available, a Singer (Sensitive Research) electrostatic voltmeter which measures 0 - 40 KV in four scales and is calibrated to 1% of full scale, and a High Voltage Engineering generating voltmeter which has essentially infinite DC impedance. This generating voltmeter has been mounted in a set of Rogowski electrodes to insure a homogenous capacitance.

Currents have been measured by a Calico digital multimeter, a Keithley Picoammeter, and an assortment of Simpson microammeters. These current measurements have always been made to ground.

Additional measurements of pressure, temperature, and humidity are made with conventional metering equipment.

For the study of turbulence some additional special instrumentation has been obtained. A voltage divider and current probe, which measures DC to 50 MHZ, have been obtained for Tektronix oscilloscopes.

In addition a Hewlett-Packard X-Y display scope and a General Radio real time analyzer have been purchased.

High pressure Heise manometers for future expansion into above atmospheric operation are available and metallic and nonmetallic submicron powders have also been purchased for future use.

IV Effects of Turbulence

The definition of the effects of fluid dynamic turbulence is a significant portion of this program. Bela Karlowitz[11], in his work on enhancing the enthalpy of flames by the addition of electrical energy, has found that strong, free stream turbulence acts to suppress filamentary discharges in plasmas and hence to increase the breakdown potential. We propose to study how turbulence affects breakdown and in particular, how it affects the behavior of free electrons, ions, and charged particles in the flow. There are always some free electrons present in a space charge flow, and because of their lower mass they can be accelerated to ionization energies much more readily than ions. An appropriate cumulative effect would cause enough volume ionization to short-out the high voltages necessary for EHD operation. Breakdown of the carrier gas is a severe practical limitation and an increase of the breakdown potential of air by a factor of ten would expand the applications of EHD to areas such as boundary layer control.

The analysis presented here is somewhat heuristic. Because of the high electric fields and the large disparity of mass of the charged species (electrons, ions, and particles) the definition of mean effective transport coefficients is somewhat difficult. Moreover, a rigorous statement of the problem would involve a coupling of the equations of turbulent flow with the electrodynamic equations. Needless to say, this is a complicated task, and we shall not undertake it here.

Let us first look at the case for a plasma, where the diffusion of charges is ambipolar.[17] The ratio of the diffusivity of momentum to that of mas is given by the Schmidt number (Sc) defined as

$$S_c)_\ell = \nu/D \qquad \text{(laminar)} \qquad (4\text{-}1)$$

$$S_c)_t = (\varepsilon_v + \nu)/(\varepsilon_m + D) \qquad \text{(turbulent)} \qquad (4\text{-}2)$$

where ν = molecular diffusivity (momentum)

ε_v = eddy diffusivity (momentum)

D = mass or charge diffusivity

ε_m = eddy mass or charge diffusivity

Now, according to the Reynolds analogy[27],

$$\varepsilon_v \approx \varepsilon_m \tag{4-3}$$

and

$$\varepsilon_v >> \nu \tag{4-4}$$

$$\varepsilon_m >> D \tag{4-5}$$

so that

$$S_c)_t \approx 1.0 \tag{4-6}$$

That is, the turbulent diffusivities for mass and momentum are said to be the same at any point in the flow and much larger than their corresponding laminar values. The turbulent coefficients, unlike their laminar counterparts, depend strongly on the flow field. The laminar flow coefficients are functions of molecular phenomena and, thus, are true coefficients. Note that simple kinetic theory predicts the Schmidt number to be unity. This suggests that the simplified mechanisms for momentum and mass transfer are the same for laminar and turbulent flows. We expect the Reynolds analogy to be a useful tool even though it may not be entirely accurate in the present case.

Let us consider air at standard temperature and pressure flowing around a cylinder. (We acknowledge the fact that this is a "poor" plasma)

$\nu = 1.5 \times 10^{-5}$ m^2/sec

$\varepsilon_v = 0.016\ U_\infty\ d$ (wake of the cylinder)[16] (4-7)

and take $U_\infty = 100$ m/sec (free stream velocity)

$d = 10^{-2}$m (cylinder diameter)

so that $\varepsilon_v = 0.016$ m^2/sec $\approx \varepsilon_m$

Note that the turbulent diffusivity is larger by a factor of about 10^3 than the molecular value. Under our present treatment, this fact is not expected to affect greatly the Schmidt number of the ions. However, the electrons because of their low mass do not exchange momentum by collision with neutrals very efficiently and hence are somewhat uncoupled from the flow pattern (this is the same argument used in the two-temperature plasma). In the other hand, particles are more highly coupled than ions because of their large size and we might expect a change of the Schmidt number.

We will assume that the Einstein relation[17] between the diffusion and the mobility applies to the charged species.

$$D = \frac{kT}{e}\,\mu = \frac{T}{11{,}606}\,\mu \qquad (4\text{-}8)$$

T = temperature (°K)

μ = mobility

The above relation expresses diffusion as motion due to thermal energies. More accurately, we can state that the ration D/μ represents the average energy of the species. For the ions and particles it is given by the gas temperature. For the electrons, however, it is considerably above the gas temperature because of the presence of the electric field.

For molecular air ions at 300°K, the ion mobility is[9]

$$\mu_i \simeq 2\times10^{-4}\ m^2/\text{volt-sec}$$

whereupon the Einstein relation gives

$$D_i \simeq 5.2 \times 10^{-6}\ m^2/\text{sec}$$

whereas for a 0.1 μm diameter particle we have (see Fig. 1)

$$\mu_p \simeq 1\times10^{-7}\ m^2/\text{volt-sec}$$

and $D_p \cong 2.6 \times 10^{-9}$ m^2/sec

We are picking this size particle merely because it is a representative one, somewhat independent of the method of charging, rather than because it is an optimum.

For electrons, the situation is somewhat more complicated since the mobility is a function of the electric field. However, for an electric field of the order of the breakdown potential in air (3×10^6 v/m) we can estimate the mobility to be[9,10]

$$\mu_e \cong 0.1 \text{ m}^2/\text{volt-sec}$$

and

$$D_e \cong 2.6 \times 10^{-3} \text{ m}^2/\text{sec}$$

(This is perhaps not fair in the sense that the breakdown potential of a plasma is actually lower than that for un-ionized air, but it will suffice for now.) The electron mobility at lower fields is higher than the value quoted. There is also some question as to whether or not the electron temperature should be higher than the gas temperature because of the electric field but, again, we will not dwell upon that here.

The resulting Schmidt numbers are shown in Table I.

TABLE I Schmidt Numbers for Ambipolar Diffusion

Mobility (m^2/v-sec)	$(S_c)_\ell$	$(S_c)_t$
A. IONS		
2×10^{-4}	3	$\sim$1
B. PARTICLES		
1×10^{-7}	5,800	$\sim$1(?)
C. ELECTRONS		
1.0×10^{-1}	5.8×10^{-3}	5.8

For the ions, Table I shows that there is no substantial difference between the laminar and the turbulent case. The apparent undesirable increase of diffusion in the turbulent case is not large enough to be meaningful under our stated approximations. Experience shows, moreover, that the drift velocity of ions in both laminar and turbulent fields is too high so that the ambipolar conditions must not fully prevail in our case, i.e., we would anticipate that the Schmidt number of ions would be less than one.

The charged particles, as expected, appear quite strongly coupled to the laminar flow field ($S_c >> 1$) but seem somewhat uncoupled in the turbulent case. This, of course, is a direct result of Reynold's analogy. Experimentally, particles perform rather well in both laminar and turbulent flows which casts some doubts on the validity of the result shown in Table I. One may argue, for example, that ambipolar conditions do not prevail. There is also another point to be considered, namely, the equilibration time for the particles. As shown in Appendix B, the e-folding time[20] for a micron-size water droplet can be calculated to be 10^{-5} sec; turbulent fluctuations of frequency higher than 100 kHz could thus not be followed by the particles and it is doubtful that the diffusion coefficient could rise to the full value of the momentum coefficient. Certainly, particles bigger than a micron have much larger equilibration times.

For electrons, the Schmidt number appears to be quite revealing. The laminar case shows that the diffusion rates dominate the momentum transfer rates ($S_c << 1$). These electrons, hence, are not influenced by the flow field. The turbulent case shows that the opposite begins to be true and we see that the flow field can carry the diffusing electrons. In particular the flow field can alter the electron diffusion pattern in space and thus break up filamentary discharges. We have to note here that we have assumed no enhanced electron diffusion by the turbulent field because of the weak collisional coupling.

Let's look now at the case of space charge flow. The charged species equation (electrons, ions, particles) is[17]

$$\Gamma = -D\nabla n + n\mu E_S \tag{4-9}$$

where Γ = specie flux

n = specie density

E_S = space charge field

Using the Einstein relation

$$\Gamma = Dn\left(-\frac{\nabla n}{n} + \frac{e}{kT} E_S\right) \tag{4-10}$$

In the case of ions and particles, we can argue that the flux will be predominantly due to the space charge field, except for a small region in the neighborhood of the injector where the density gradient may approximate a step function (i.e., $\nabla n \cong \infty$). This space charge predominance can be shown to exist for a Gaussian distribution of particles at the densities of interest.

Now, for the electrons the electric field is the same; however, the number density is considerably smaller and the temperature (energy) considerably larger than that for the others. This can be argued to mean that, for electrons, diffusion can be important over a considerably greater region of space than for the ions or particles. Even if this region does not cover the entire typical dimension of the EHD channel, it will suffice to assume that this region is finite in extent and, hence, we may say that there is some region where our results for ambipolar diffusion apply. Electron densities can be quite low in a space charge flow because of the absence of sources at the surfaces and because of high recombination rates in the gas.

Since we assume that the space charge diffusion is dominant for ions and particles, let's estimate the Schmidt number on the basis.

We can say,

$$n\mu E_S = \mu E_S \ell \ (n/\ell) \tag{4-11}$$

and

$$\mathscr{D} = \mu E_S \ell \ \text{("diffusion" coefficient)} \tag{4-12}$$

ℓ = characteristic length

If we pick ℓ to be the apparatus length (1 cm) and E_S to be $0.1E_b$ ($3\text{x}10^5$ v/m) or pick ℓ as 1 mm and E_S as $3\text{x}10^6$ v/m, then

$$\mathscr{D} \simeq 3\text{x}10^{+3}\mu$$

which for ions becomes

$$\mathscr{D}_i \simeq 0.6 \ m^2/\text{sec}$$

and particles

$$\mathscr{D}_p \simeq 3\text{x}10^{-4} \ m^2/\text{sec}$$

The results are shown in Table II. Note that we are somewhat arbitrarily carrying over the previous results for the electrons.

TABLE II Schmidt Numbers for Space Charge Flow

Mobility (m^2/v-sec)	$S_c)_\ell$	$S_c)_t$
A. IONS		
2×10^{-4}	$2.5\text{x}10^{-5}$	$2.6\text{x}10^{-2}$
B. PARTICLES		
$1\text{x}10^{-7}$	$5\text{x}10^{-2}$	0.98
C. ELECTRONS (Ambipolar)		
0.1	$5.8\text{x}10^{-3}$	5.8

In the case of ions in turbulent flow, the Reynolds analogy seems to break down since the value of ε_m is not much greater than $\mathscr{D}$.

We could, however, not argue further because of the arbitrariness of δ at the present stage.

The picture presented by Table II is quite different from Table I. Both ions and particles see an improvement with the turbulent field and the particles are always more closely coupled to the flow than the ions. This should satisfy our intuition but, obviously, the ideas presented above are not complete and we must await the results of better calculations before feeling satisfied we understand the role of turbulence.

We have consistently observed an effect of the flow with our air corona discharges. As mentioned earlier, the molecular ion injector was mounted on the wake of the cylinder, and a typical improvement of 200 to 400 volts in the breakdown potential was recorded. Breakdown, moreover, was arrested so that it generally never surged to the 2 ma needed to operate the trip-mechanism in the power supply. In the case of the steam injector, to be discussed in Chapter V, no corona operation could be obtained without the flow of steam in the nozzle, so that here turbulence (of a level not defined here) also plays a desirable role. Table III shows some of the increases in breakdown potential that we have measured as a result of the turbulence at the wake of a cylinder 1 cm diameter (see Appendix D). There is some uncertainty in the role that impurities might have played in data reproducibility and, hence, we are refraining from making a more quantitative estimate of the role of turbulence here. The data are shown for various corona units.

TABLE III

Effect of Turbulent Flow on Breakdown of Air Corona

Type of ion	No Flow Breakdown Potential - Kilovolts -	Breakdown Potential (Free stream velocity) - Kilovolts (m/sec) -
Negative	5.05	> 5.5 (100)
Positive	6.60	6.8 (104)
"	"	7.2 (72)
"	"	7.0 (100)
Negative	5.6	> 6.0 (100)

V Injector Work

As was mentioned earlier, the injector is the most critical component of the EHD system. This is because the size, charge, and density of ions must lie within a narrow spread of the optimum values. Moreover, corona type injectors utilize electrical energy which must not be wasted in creating an assortment of ion sizes (even though we could provide a scheme to select out the correct ion to be injected into the flow). We are pursuing the injector problem both analytically and experimentally. In our analysis, the definition of injector parameters parallels that of other investigators.[7,14]

The experimental challenge is perhaps the more crucial here. Some work (but not enough) has been done elsewhere[1,14] in growing aerosols by condensation and in developing techniques for measuring ion size. We have so far concerned ourselves with the air corona in the turbulent wake and with the supersaturated steam injector. Both of these are described in some detail in Appendix C. In this chapter, we will be only concerned with the work on the steam injector. This injector is an improvement over the one reported by Ober. Supersaturated steam passes through a corona discharge which is made up of a needle inserted through the front of a Teflon cylinder and a ring imbeded at the exit of the nozzle. The spacing between the needle and ring can be adjusted. The nozzle is at the wake of the cylinder facing downstream and the cylinder provides a reservoir of steam for the expansion. In this new design the cylinder is made also of Teflon. The design is shown in Figure 6. Steam is fed from a boiler, through a heated line, to this cylindrical reservoir which at the same time is used to generate the strong turbulence region.

This nozzle has been run with some success and Figure 7 shows data obtained by traversing the collector needle back and forth along the centerline of the nozzle. Here we plot the ratio of the current at the collector to the current issuing from the corona needle versus the corona voltage.[18] Below about 1.4 KV the system gets into a very

unstable mode and above about 2.5 KV the field is so strong that only a few percent of the total current is convected by the flow. This flow, incidentally, is about 1.5×10^{-3} lbm/sec of steam and the conditions at the throat are sonic. The electrical circuit used to obtain the data of Figure 7 is shown in Figure 8. As mentioned previously, we had to use a diode bank to prevent the back-corona. If this unstable mode were not present the efficiency of the injector could be improved by lowering the corona voltage. This is certainly obvious from Figure 7 for the smallest spacing (L = 0.075 cm). The higher spacings along the centerline show a maximum which is to be expected in such cases. In fact, Figure 9, shows a plot of these maxima versus distance and we may attribute the shape of the curve to the ion depletion in the free jet.[18] All of these data were obtained with the main flow off.

We have recently improved the injector performance by running it just above the condition where droplets form at the throat and short the corona. This condition might be referred to as maximum wetness inside the nozzle. We have also recently purchased a steam generator which permits continuous running, in contrast to the one hour limit of the previous unit.

More work needs to be done regarding the condensation (see Hill[19] and the Curtiss-Wright report[14]) of steam around the ionic nuclei created in the corona discharge, specifically towards a uniform formation of charged particles.

VI Summary, Conclusions, and Recommendations

A. Summary

Electrohydrodynamics embraces a series of specialized fields of endeavor. A partial list of these is given below:

1) High voltage technology -- the large voltages involved require the best insulation available. But, beyond that, surface impurities such as moisture and corona discharges from sharp points can leak enough current to mask those currents being measured. High voltage, low current metering equipment is rather specialized and safety procedures are more involved than with usual electrical equipment.

2) Two phase flow -- the gas dynamics of two phase flow, including condensing vapors (see Marble[20]), is a relatively sophisticated field. The extension is needed to a charged aerosol flow.

3) Injector -- the injector has to meet some fairly exacting requirements as to ion size and charge. To do this job efficiently may be too demanding of some of the present schemes.

4) Breakdown -- air is the most convenient carrier medium for open EHD systems but its characteristics are marginal because of the low breakdown field. The presence of free electrons in the flow affect the breakdown. Electron sources such as sharp corners also affect breakdown.

B. Conclusions and Recommendations

Based on our work to date, the following conclusions can be put forth:

1) Strong, free stream turbulence appears to increase the breakdown potential of the carrier medium, mainly through its effect on the free electrons. Our present estimates are somewhat intuitive and point out the need for (further) study of the fundamental relations involved.

2) Air with electronegative additives and high turbulence may be an acceptable medium for EHD schemes.

3) The definition of optima for particle sizes awaits experimental confirmation. It is not necessary to begin with an efficient injector, but rather with one that manufactures the desired size and charge. This could be done by "filtering out" the undesirable ions and only injecting the proper ones.

4) A confirmation is needed of the assumptions used to carry out EHD generator analyses. This will require some rather sophisticated diagnostics.

VII New Research

The project is continuing through Fiscal Year 69-70 in basically the same form it was initiated. The injector work has continued and a study of turbulent spectrum both with an EHD probe and a hot wire anemometer has been initiated. The use of a Langmuir probe is presently under study in conjunction with Professor Woehler of our Physics Department. An investigation of the possible use of EHD for boundary layer control is being conducted. In addition, a theoretical study of the effects of the turbulence is being undertaken by Professor Gawain of our Aeronautics Department.

Our aim is to better define some of the work that, by necessity, has been sketchily presented here. In particular, it is desirable to develop appropriate mathematical models to describe at least the major phenomena encountered in our system.

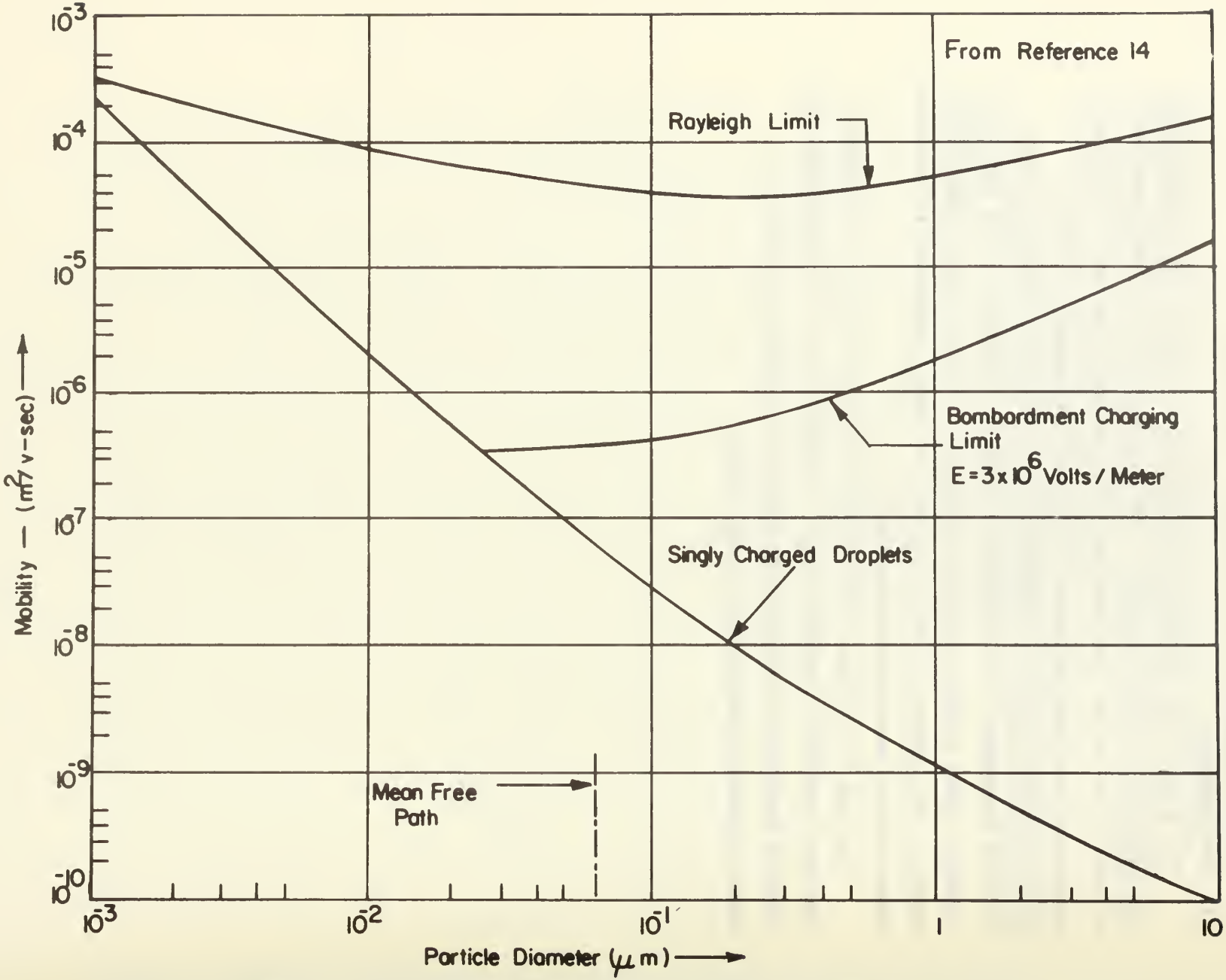

FIGURE I MOBILITY OF WATER DROPLETS IN AIR AT I-ATM. AND 20°C

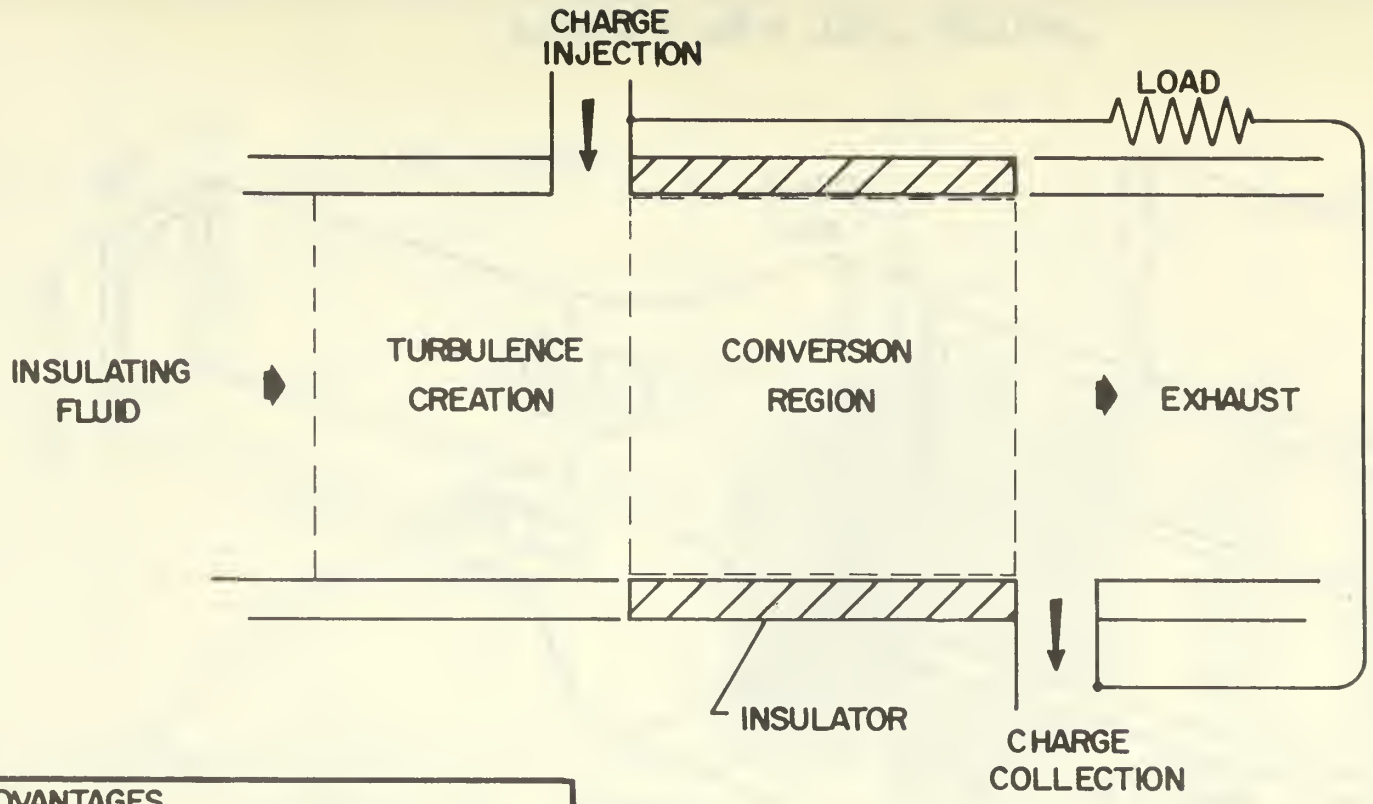

ADVANTAGES

1. INCREASED BREAKDOWN POTENTIAL OF CARRIER GAS.
2. MORE HOMOGENEOUS CHARGED PARTICLE MIXING.

DISADVANTAGES

ADDED FRICTIONAL LOSSES

FIGURE 2 HIGH FREE STREAM TURBULENCE EHD GENERATOR

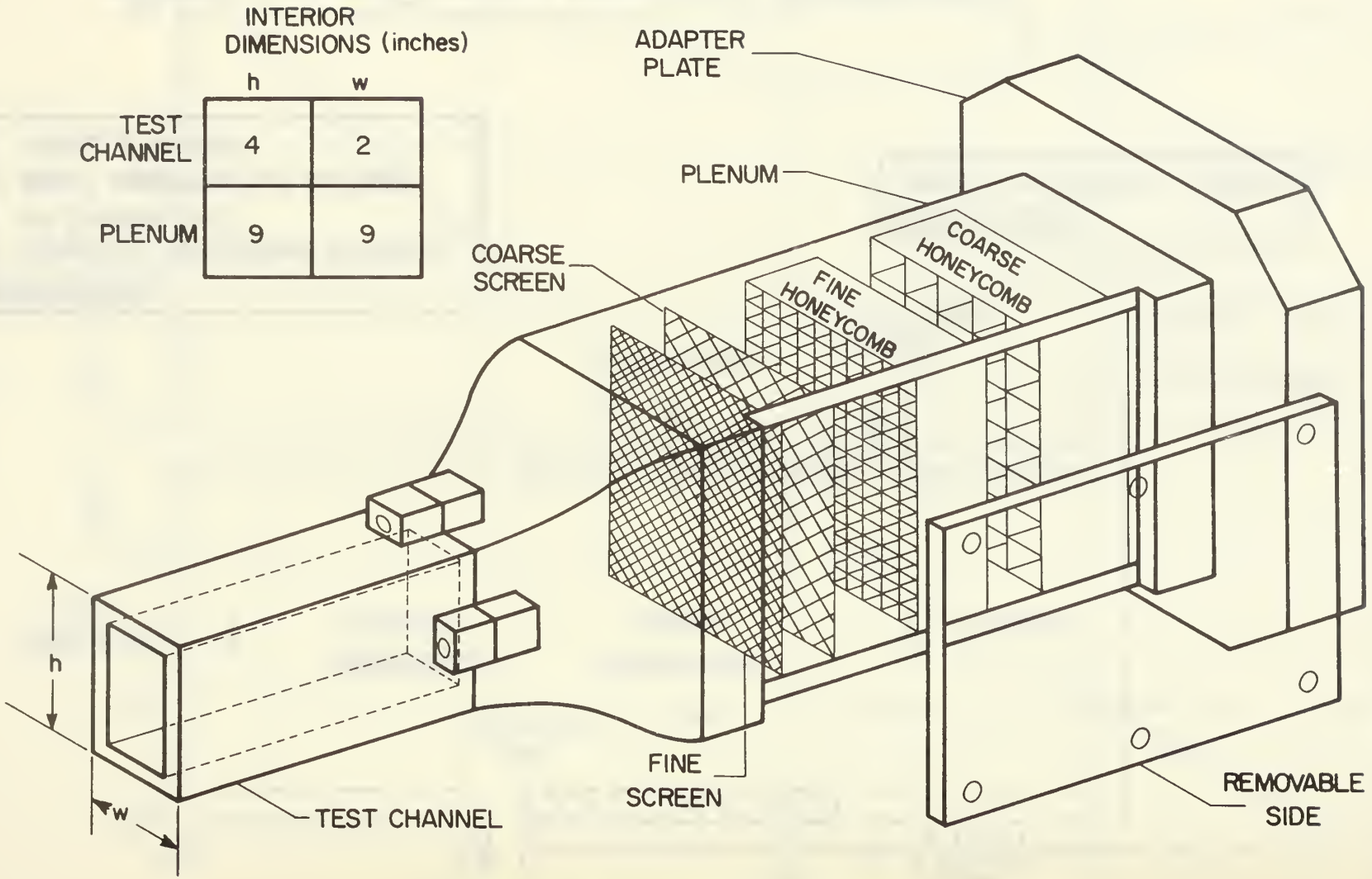

FIGURE 3 "NEW TEST SECTION"

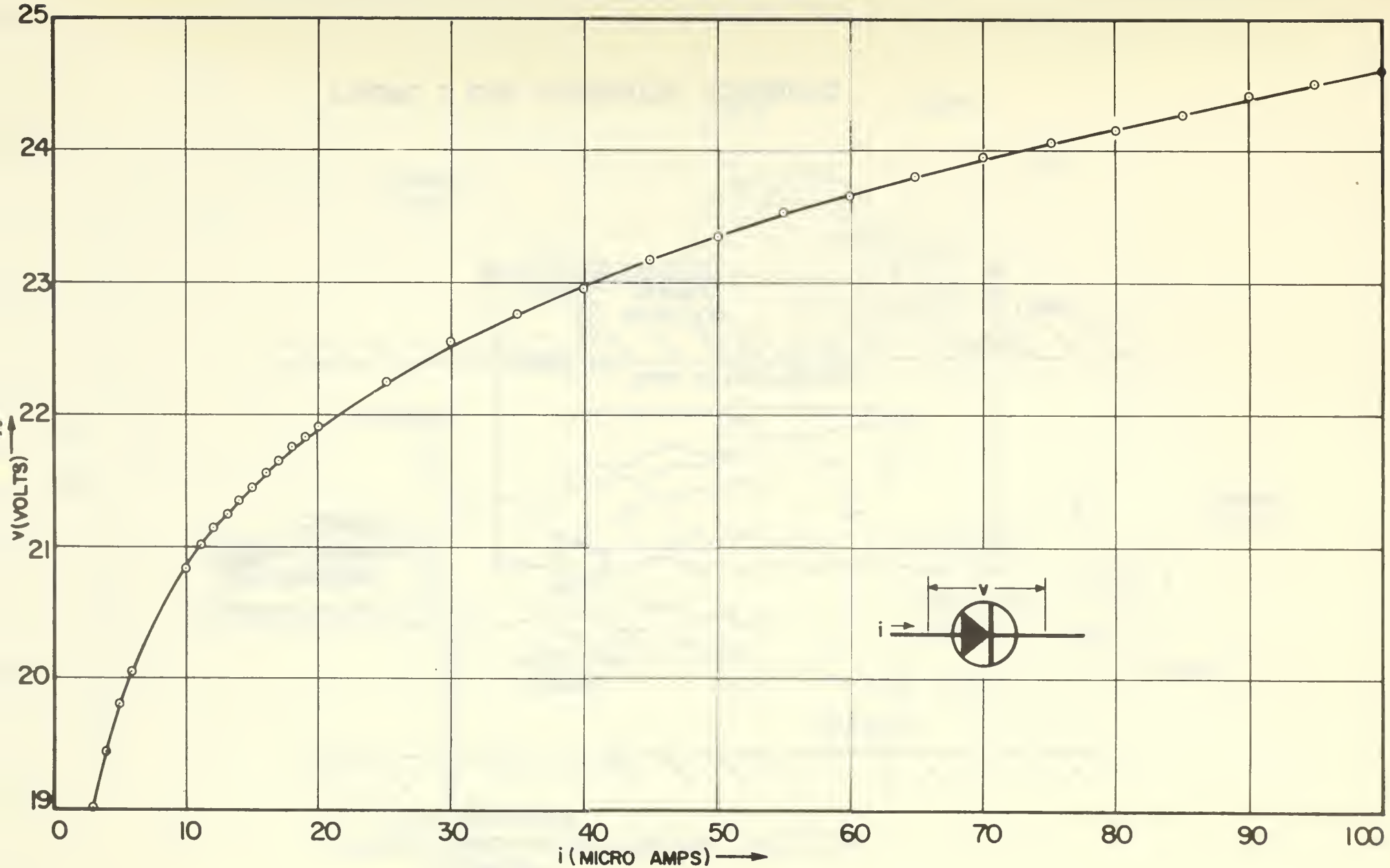

FIGURE 4 DIODE CALIBRATION CURVE

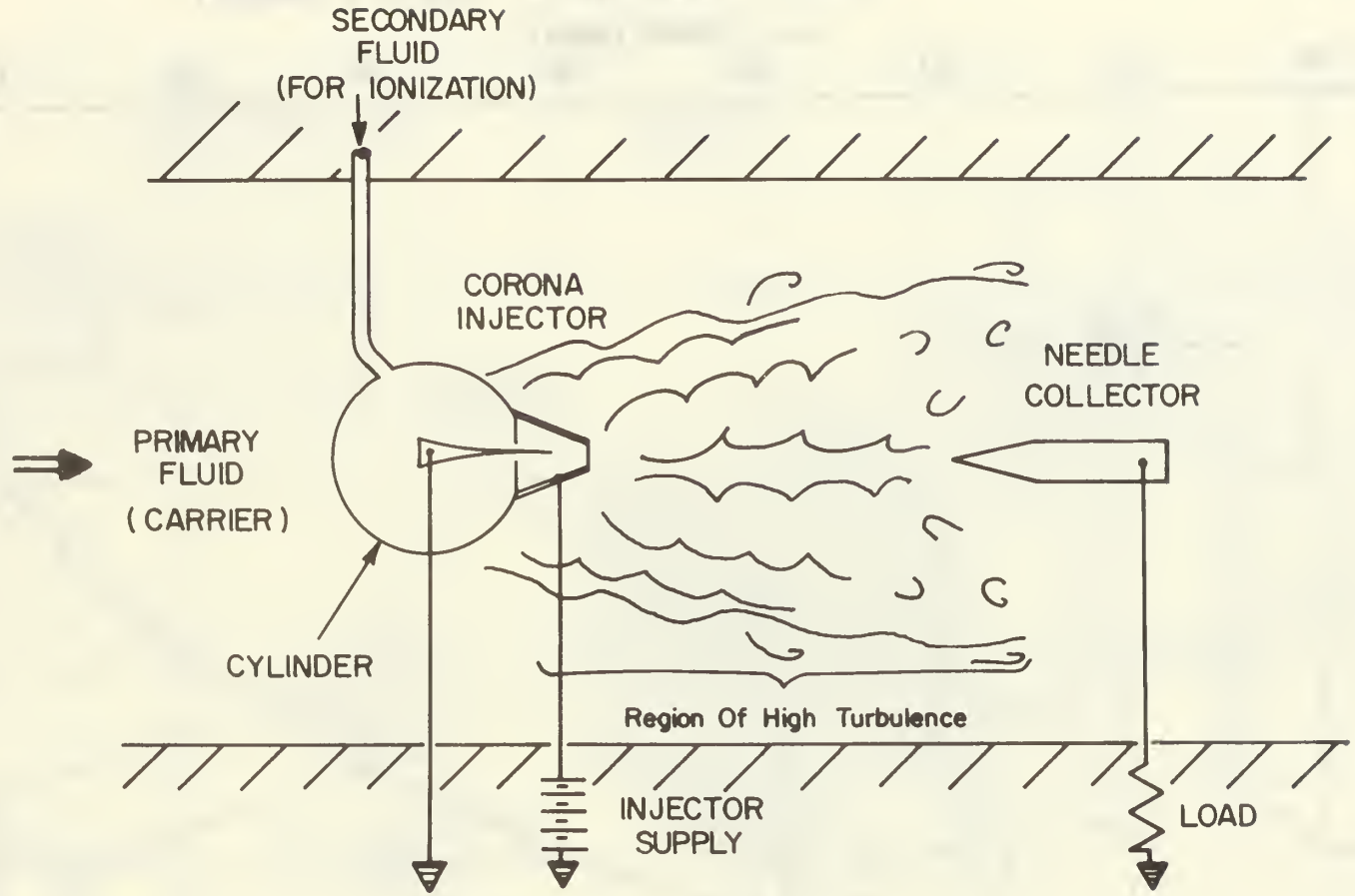

FIGURE 5 EHD GENERATOR SCHEMATIC

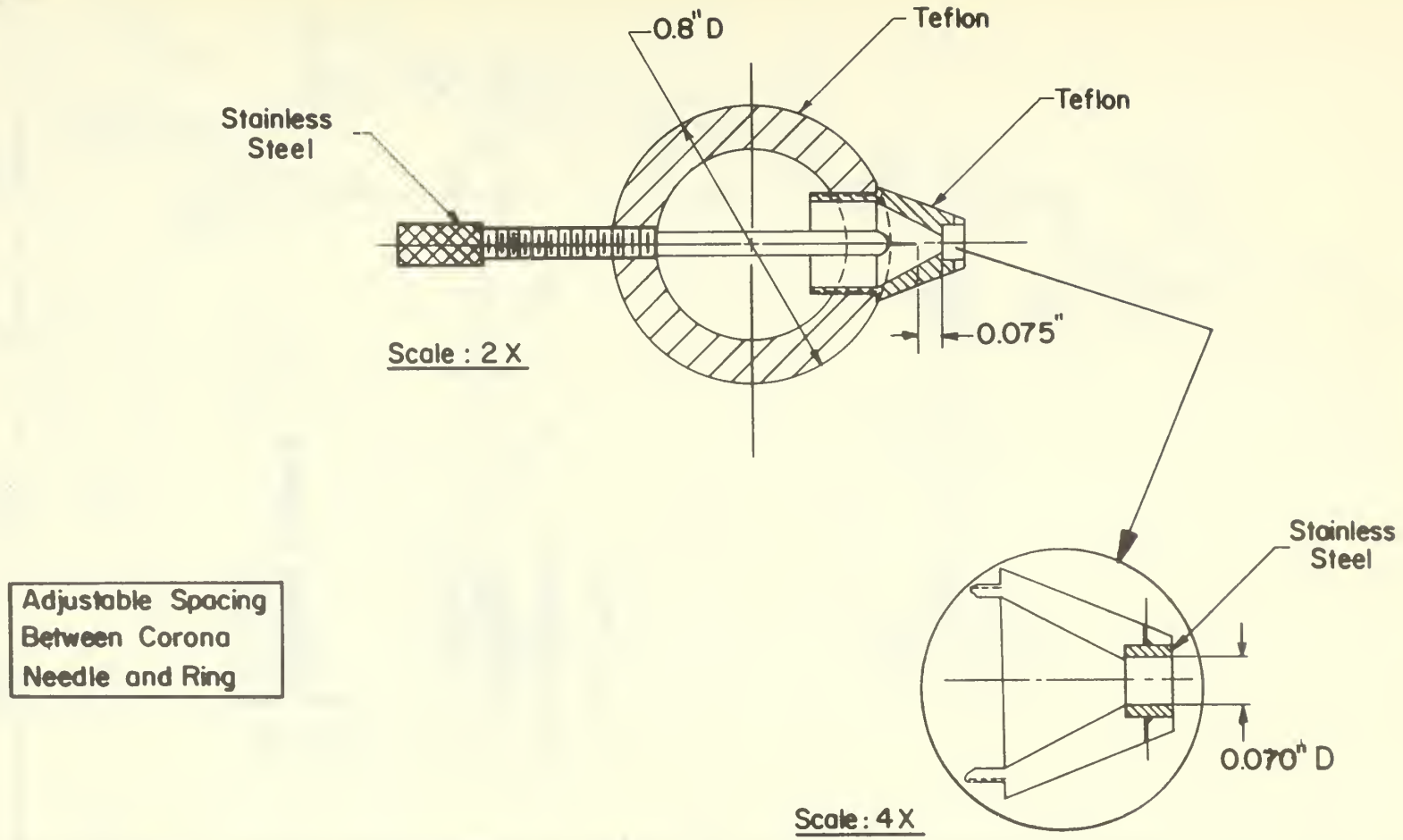

FIGURE 6 AIR–WATER AEROSOL INJECTOR

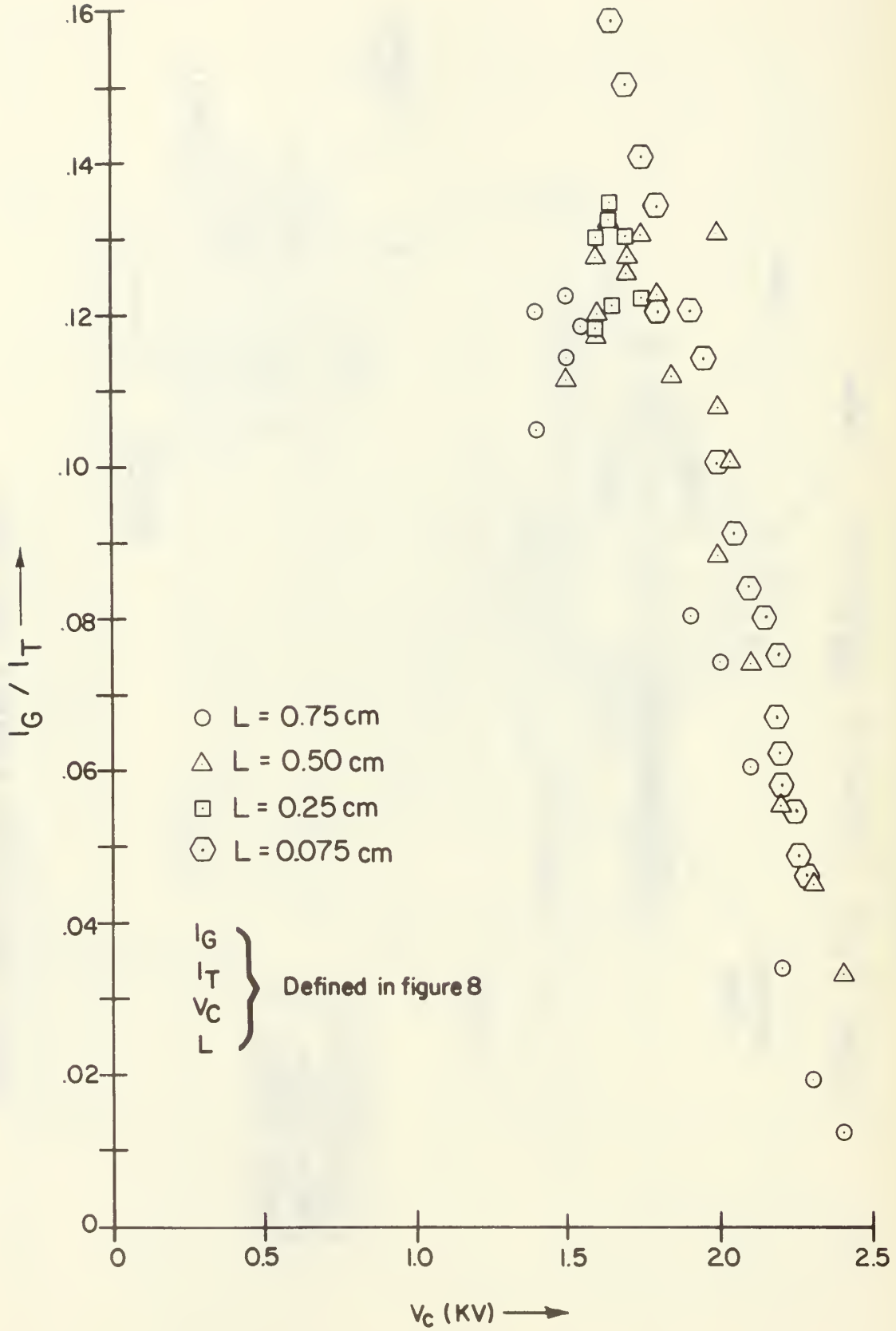

FIGURE 7 TEFLON NOZZLE STEAM INJECTOR

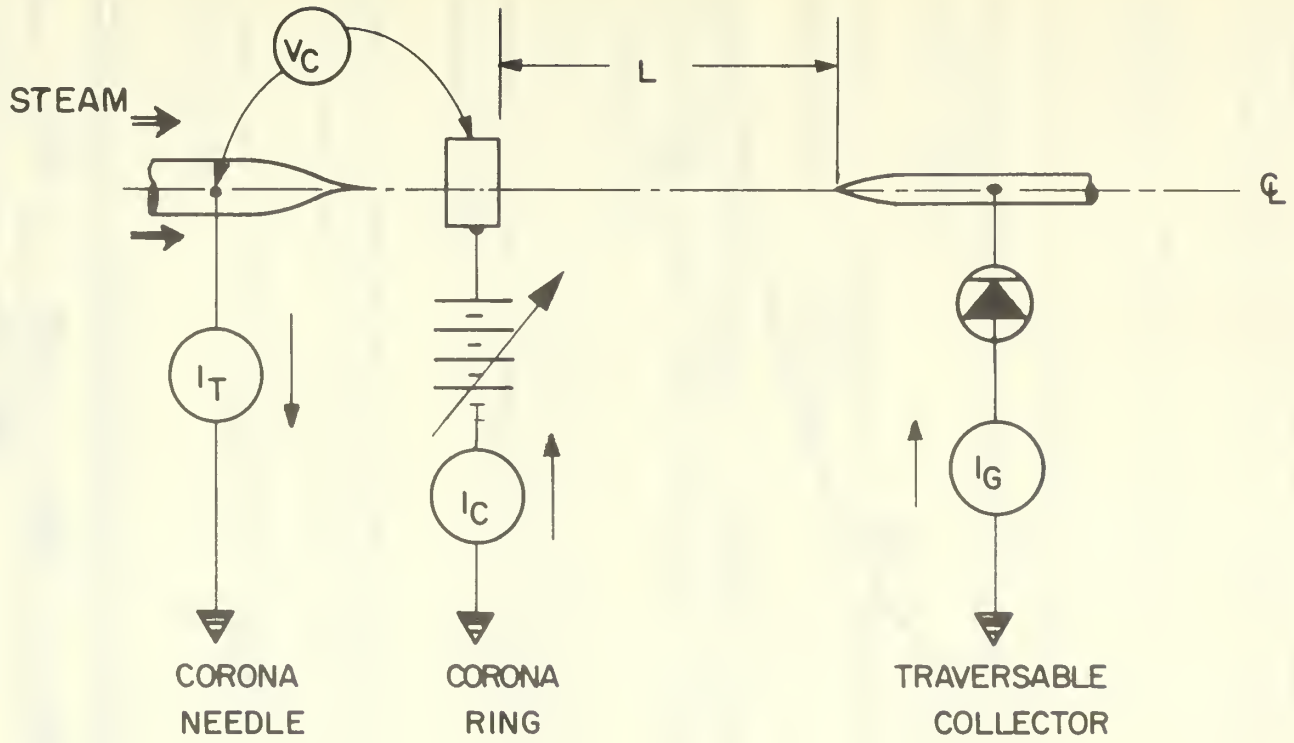

FIGURE 8 ELECTRICAL CIRCUIT FOR INJECTOR STUDY

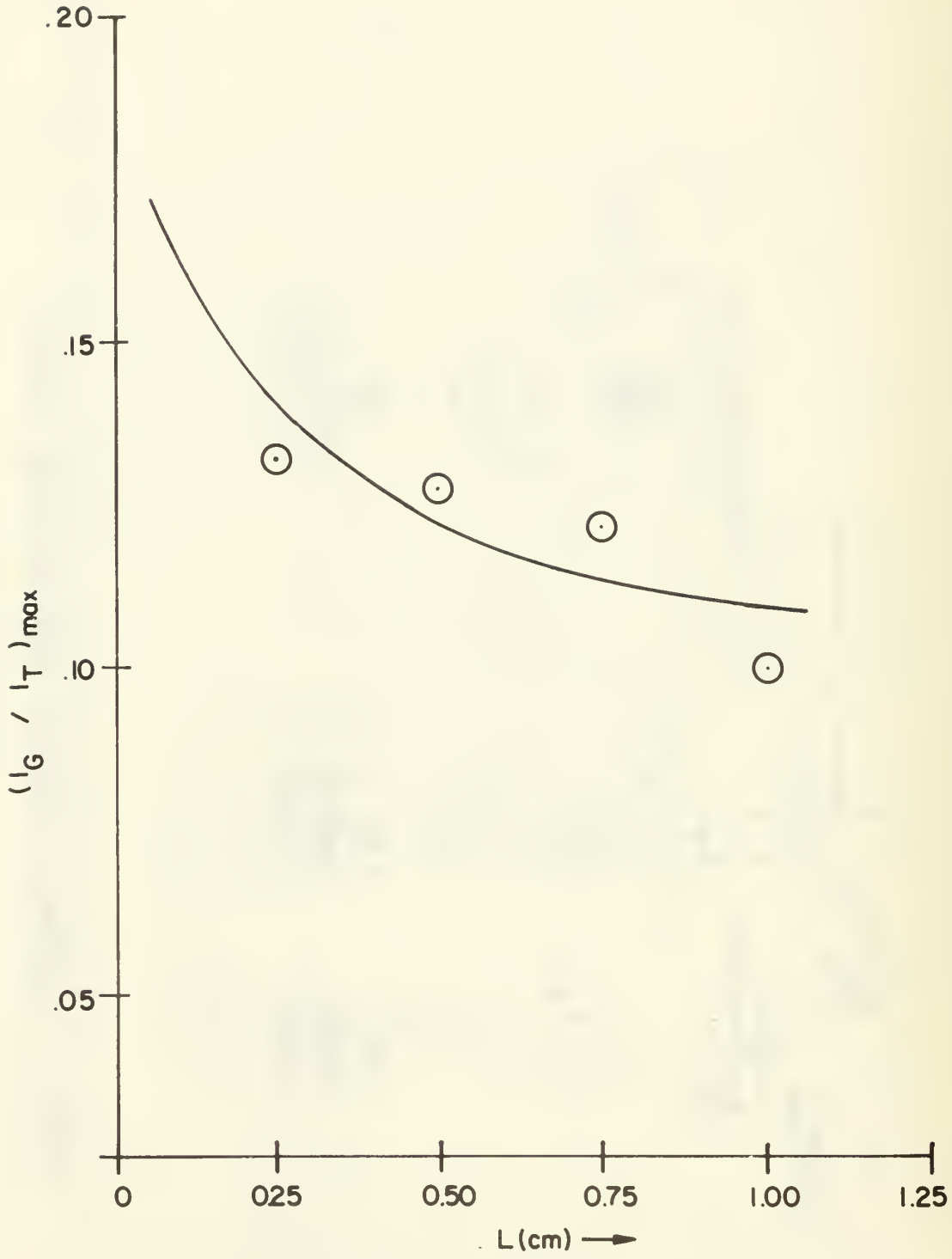

FIGURE 9 MAXIMUM RATIO VERSUS SPACING

REFERENCES

1) Marks, A. M., "Economic Implications of Charged Aerosol and Dipole Technology," paper presented before the Senate Subcommittee on Antitrust and Monopoly, Sen. P. A. Hart, chairman (October 1967).

2) Marks, A. M., Barreto, E., and Chu, C. K., AIAA Journal, 2, 45 (1964).

3) Gourdine, M. C., "Power Generation by Means of the Electric Wind," JPL TN 32-6 (1960); "Electrogasdynamic Channel Flow," JPL TN 34-5 (1960).

4) Collier, E. L., and Gourdine, M. C., "Resistive EGD Channel," AIAA Journal, 6, 2278 (1968).

5) Lawson, M., and Wattendorf, F. (Editors) "Selected Topics in Electrofluid Dynamic Energy Conversion," AGARDograph 122 (December 1968).

6) Decaire, J. A., and Lawson, M. O., "Electrofluiddynamic Power Generation Trends and Expectations," Eight Symp. on MHD, Stanford, (1967).

7) Kahn, B. "A Continuation of the Basic Study of Slender Channel Electrogasdynamics," (Curtiss-Wright Corp.) ARL 65-4 (January 1965).

8) Alston, L. L. (Editor), High Voltage Technology, Oxford University Press (1968).

9) Cobine, J. D., Gaseous Conductors, Dover (1958).

10) Loeb, L. B., Basic Processes of Gaseous Electronics, University of California Press, (1960).

11) Karlowitz, B., "Flames Augmented by Electrical Power," Pure and Applied Chemistry 5, 557 (1962).

12) Marks, A. M., Patent No 2,638,555 (May 1953).

13) Kahn, B., and Gourdine, M. C., "A Basic Study of Slender Channel Electrogasdynamics," (Curtiss-Wright Corp), ARL 63-205 (Nov. 1963).

14) Brandmaier, H. E., Dimmock, T. H., and Kahn, B., "Research on Power Generation Electrogasdynamic Energy Conversion," (Curtiss-Wright Corp), ARL 67-0008 (January 1967).

15) Brandmaier, H. E., and Dimmock, T. H., "Factors Influencing Electro-Fluid Dynamic Power Generation," Journ. Spacecraft and Rockets, 4, 961 (1967).

16) Hinze, J. O. Turbulence, McGraw-Hill (1959).

17) Brown, S. C., Introduction to Gas Discharges, John-Wiley (1966).

18) Witby, K. T., "Generator for Producing High Concentrations of Small Ions," Review of Scientific Instruments, 32, 1351 (1961).

19) Hill, P. G. "Condensation of Water Droplets During Supersonic Expansion Nozzles," Journ. of Fluid Mechanics, 25-3, 593 (1966).

20) Marble, F. E., "Gasdynamics of Condensing Vapors," (Calif. Inst. of Tech), ARL 69-0040 (March 1969).

21) Megaw, W. J., and Wells, A. C., Nature, 219, 259 (July 20, 1968).

22) Fuchs, N. A. and Stechkina, M. Trans. Faraday Sc. 58, 1949 (1962).

23) Mureau-Hanot, M., "Transport of Ions by a Gaseous Current," C. R. Academic Sciences, Paris (1939).

24) Bennet, N. E., "The Generation of Direct Current at High Potential," Research. App. in Industry, 12, 455 (1959).

25) Stuetzer, O. M., Journ. App. Phys., 984 (July 1959); Journ. App. Phys., 136 (Jan 1960); Rev. Sci. Instr. 16 (Jan 1961).

26) Velkoff, H. R., "Electrostatically - Induced Secondary Flows in a Channel," Int. Symp. on EHD, MIT (1969).

27) Kays, W. M., Convective Heat and Mass Transfer, McGraw-Hill (1966).

28) Schlichting, H., Boundary Layer Theory, McGraw-Hill, Sixth Ed., (1968).

APPENDIX A

Idealized Analysis of Basic Energy Conversion Process in EHD Flows

In this appendix we will discuss some of the relations pertinent to power and efficiency of an EHD generator. Here, we will also focus on the power loss due to ion slip.

1) Assumptions

The carrier fluid moving at velocity U_∞ entrains charged particles and moves them at velocity $\overline{u}_p$ against the resistance E of the electrical field. Velocities are maintained constant by a driving pressure gradient G in the direction of flow. We consider particle sizes to be much larger than the mean free paths of the molecules in the carrier gas so that we can speak of a pressure force on the particle.

The particles are treated as being all of identical volume $\delta\overline{v}_p$, identical charge $\overline{q}$ and moving with identical velocity $\overline{u_p}$.

Quantities E, G, U_∞, $\overline{u_p}$, A, --- are constants.

The only loss considered in this analysis is that associated with the mobility or slip of the charged particles relative to the carrier fluid. Figure A1 depicts the system under study.

Steady, incompressible flow is assumed. Friction and viscosity are neglected except for the viscous drag of the charged particles moving in the carrier fluid. It is assumed that Stokes' drag law for a sphere applies. In the range of particle size considered, the spherical shape turns out to be a good approximation.

2) Forces on a Particle

$$\overline{F}_E = E\overline{q} = \text{Electrical Force} \qquad \text{(A-1)}$$

$$\overline{F}_G = G\delta\overline{v}_p = \text{Pressure Force} \qquad \text{(A-2)}$$

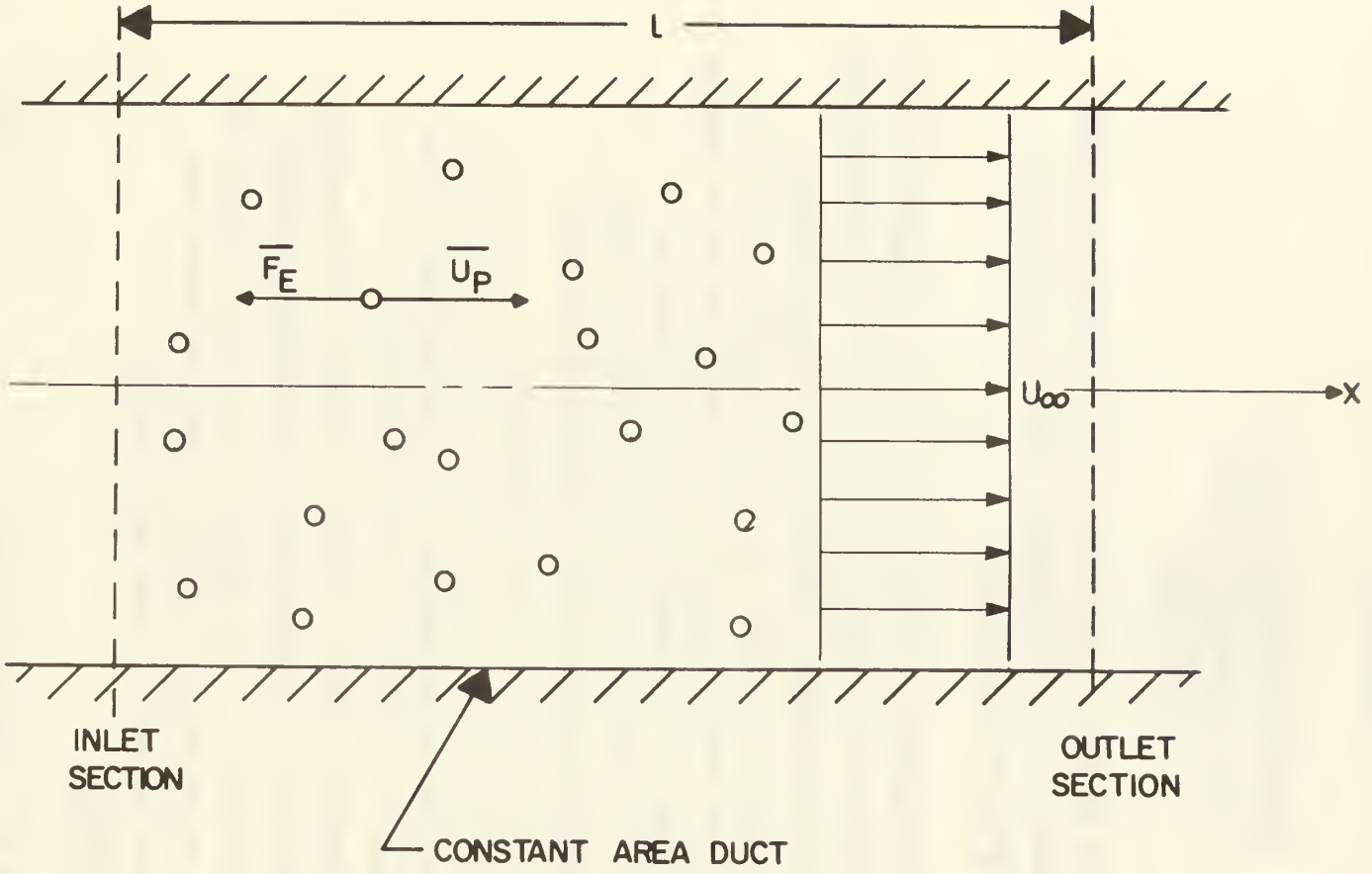

FIGURE A1. SYSTEM FOR ANALYSIS

$$\bar{F}_V = K\,(U_\infty - \bar{u}_p) = \text{Viscous Force} \qquad \text{(A-3)}$$

where $K = 6\pi R\mu_\infty$ according to Stokes' drag law.

Hence the equation of motion becomes -

$$-E\bar{q} + G\delta\bar{v}_p + K\,(U_\infty - \bar{u}_p) = \delta\bar{m}_p\left(\frac{d\bar{u}_p}{dt}\right) \qquad \text{(A-4)}$$

3) Momentum Equation for Two Phase Flow

We apply the momentum theorem to the working section of the duct, which lies between inlet and outlet cross-sections. Fluid and particle velocities both remain constant, hence there is no change in momentum. Viscous interaction forces between carrier fluid and particles are equal and opposite on fluid and particles and vanish in the summation over both phases. Therefore

$$\underbrace{+ G\ell\, A}_{\text{Pressure Force}} \underbrace{- n_p\, A\, \ell\, E\, \bar{q}}_{\text{Electrical Force}} = 0 \qquad \text{(A-5)}$$

Hence

$$G = n_p \bar{q}\, E \qquad \text{(A-6)}$$

Balance of pressure and electrical forces

4) Mobility vs Viscous Drag Factor

Mobility μ is defined by the expression,

$$(U_\infty - \bar{u}_p) \equiv \mu E \qquad \text{(A-7)}$$

subject to the restriction that U_∞ and $\bar{u}_p$ have reached constant limiting values. Under these conditions (A-4) becomes

$$-E\bar{q} + G\delta\bar{v}_p + K\,(U_\infty - \bar{u}_p) = 0 \qquad \text{(A-8)}$$

Now substituting (A-6) and (A-7) into (A-8) gives

$$- E\overline{q} + n_p \overline{q}\, E\, \delta\overline{v}_p + K \mu E = 0 \qquad \text{(A-9)}$$

therefore

$$\mu = \frac{\overline{q}}{K} (1 - n_p \delta\overline{v}_p) \qquad \text{(A-10)}$$

which defines the relation between μ and K.

Consider the limiting case where $\delta m_p \delta\overline{v}_p \to 0$ then

$$\mu \to \mu_o = \frac{\overline{q}}{K} \qquad \text{(A-11)}$$

substituting this back into (A-10) gives

$$\mu = \mu_o (1 - n_p \delta\overline{v}_p) \qquad \text{(A-12)}$$

where μ_o is a constant. This shows that apparent mobility μ is a function of the volume ratio $n_p \delta\overline{v}_p$!

5) Power Relations

The ideal useful electrical power delivered by the charged particles moving against the resistance of the electrical field is

$$P_e = n_p A \ell\, \overline{q}\, E\, \overline{u}_p \qquad \text{(A-13)}$$

The ideal fluid power expended in pumping both the carrier fluid and the particles is

$$P_f = G \ell\, [Q_p + Q_f] \qquad \text{(A-14)}$$

where $Q_p = n_p \delta \bar{v}_p \, A \, \bar{u}_p$ Volumetric flow rate of particles (A-15)

$Q_f = (1 - n_p \delta \bar{v}_p) \, A \, U_\infty$ Volumetric flow rate of carrier fluid (A-16)

Substituting (A-6), (A-15) and (A-16) into (A-14) and rearranging gives

$$P_f = n_p \, A \, \ell \, \bar{q}_p E \left\{ U_\infty - n_p \delta \bar{v}_p \, (U_\infty - \bar{u}_p) \right\} \tag{A-17}$$

Now substituting (A-7) into (A-13) and (A-17) gives the two expressions --

$$\frac{P_e}{A\ell} = \rho_{p_e} = n_p \bar{q} \, e \, U_\infty \left(1 - \frac{\mu E}{U_\infty} \right)$$ Electrical power density (A-18)

$$\frac{P_f}{A\ell} = \rho_{p_f} = n_p q E \, U_\infty \left\{ 1 - n_p \delta \bar{v}_p \left(\frac{\mu E}{U_\infty} \right) \right\}$$ (A-19)

Fluid power density

The ratio of these two quantities fixes the efficiency of this idealized energy conversion process, that is

$$\frac{P_e}{P_f} = \eta_i = \frac{1 - \left(\frac{\mu E}{U_\infty} \right)}{1 - (n_p \delta \bar{v}_p) \left(\frac{\mu E}{U_\infty} \right)} \tag{A-20}$$

Moreover, we may substitute (A-12) into (A-18) and (A-20). The results are --

$$\left(\frac{P_e}{A\ell n_p q E U_\infty} \right) = P_e^* = 1 - (1 - n_p \delta \bar{v}_p) \left(\frac{\mu_o E}{U_\infty} \right) \tag{A-21}$$

and

$$\frac{P_e}{P_f} = \eta_i = \left\{ \frac{1 - (1 - n_p \delta \overline{v}_p) \left(\frac{\mu_o E}{U} \right)}{1 - n_p \delta \overline{v}_p \, (1 - n_p \delta \overline{v}_p) \left(\frac{\mu_o E}{U_\infty} \right)} \right\} \tag{A-22}$$

For the ideal case of zero mobility, $\frac{\mu_o E}{U_\infty} \to o$ and

$$\left. \begin{aligned} P_e^* &\to 1 \\ \eta_i &\to 1 \end{aligned} \right\} \tag{A-23}$$

6) Relative Power Loss Due to Slip

Let

$$P_e^* = \frac{P_e}{A \ell n_p \overline{q} \, E U_\infty} \tag{A-24}$$

$$P_f^* = \frac{P_f}{A \ell n_p \overline{q} \, E U_\infty} \tag{A-25}$$

$$\frac{P_e^*}{P_f^*} = \eta_i$$

The relative slip loss may be defined as

$$\mathcal{L}_s = \frac{P_f^* - P_e^*}{P_e^*} = \frac{1}{\eta_i} - 1 \tag{A-27}$$

Substituting from (6-10), we obtain --

$$\mathcal{L}_s = \frac{(1 - n_p \delta \overline{v}_p)^2 \left(\frac{\mu_o E}{U_\infty} \right)}{1 - (1 - n_p \delta \overline{v}_p) \left(\frac{\mu_o E}{U_\infty} \right)} \tag{A-28}$$

Eqs (A-21) and (A-28) show the importance of minimizing $\mu_o E/U_\infty$ and maximizing $n_p \delta\bar{v}_p$. It can be shown that for the range of micron size particles with between 1 and 100 charges the ratio $\mu_o E/U_\infty$ is acceptably small. Moreover, for n_p of the order of 10^{16} m^{-3}, the product $n_p \delta\bar{v}_p$ is negligible so that micron size particles meet the desirable criteria defined above. A realistic estimate of n_p can be made in terms of limitations at the injector (see Appendix B).

APPENDIX B

Charged Particle Mobility and Diffusion

I. We will concern ourselves with particles in the micron and submicron diameter range for which the flow is in the low Reynolds number regime (creeping flows). Classical calculations (such as the Stokes drag law[28] for a sphere), based upon the assumption of a continuum fluid with no fluid slip at the particle surface, are not valid as the particle radius approaches the order to magnitude of the mean free path of the gas in which it is moving. Megaw and Wells[21] have carried out mobility measurements with singly charged spherical polystyrene particles, which they compared to a theory due to Fuchs and Stechkina[22], as shown in the Figure B1. The theoretical line lies slightly above most of the experimental points.

As a comparison, the prediction based upon Stokes' drag law for a sphere is also shown on the figure. The data are seen to lie generally between the two theoretical curves. A possible explanation is that the Fuchs and Stechkina theory allows for too much slip at the particle surface, giving a high value of mobility; whereas the Stokes theory, which assumes no slip, gives a low value for the mobility. Note that the difference between the two theories for a 0.1-micron particle is a factor of two.

The calculation of the mobility of a charged sphere in air based upon Stokes' drag law is as follows: The force acting upon a particle carrying $\overline{q}$ charge in an electric field E is

$$\overline{F}_E = \overline{q}\, E \qquad \text{(newtons)} \tag{B-1}$$

$$\overline{q} = Z\, e \qquad \text{(coulombs)}$$

Z = number of electronic charges

e = charge of an electron

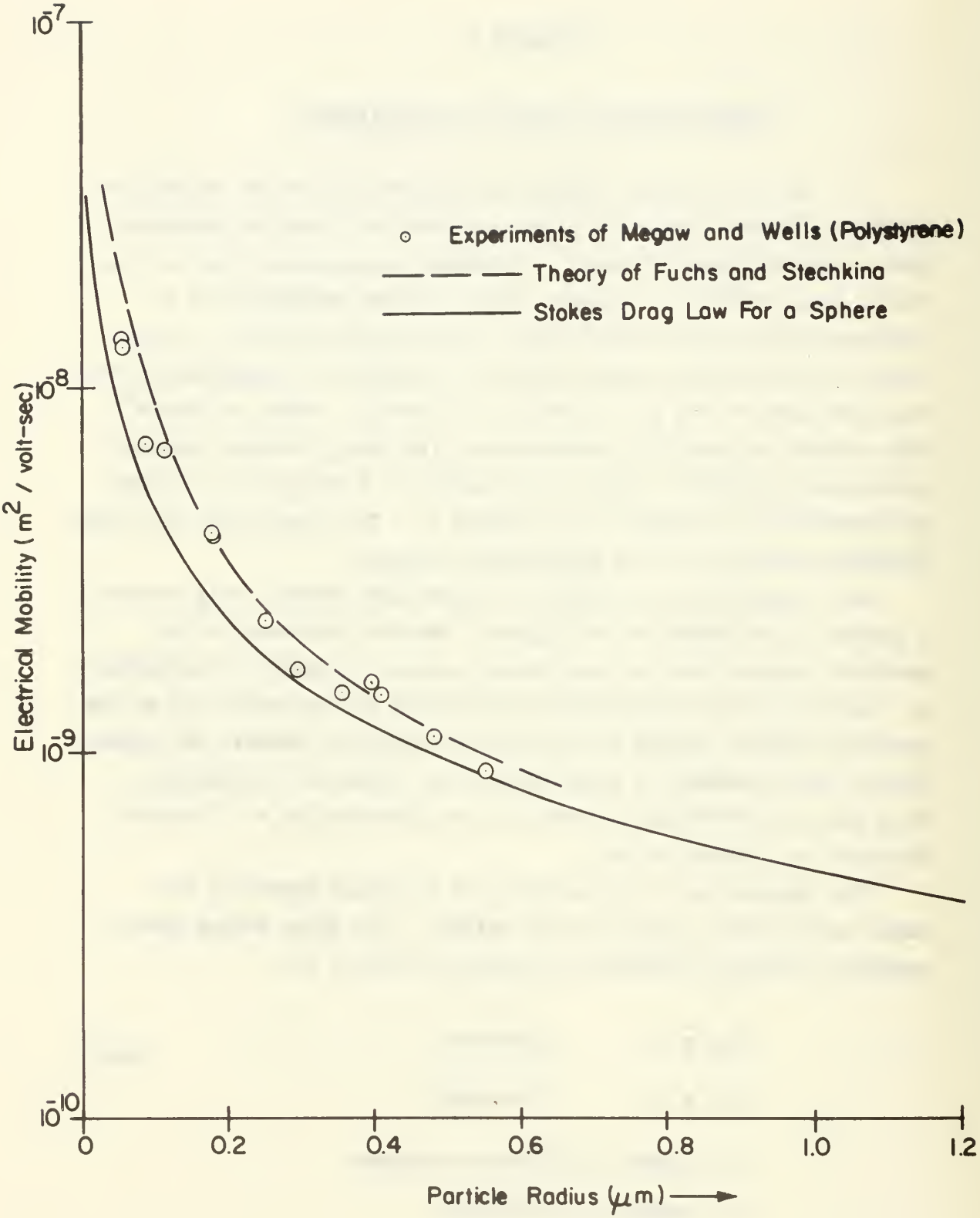

FIGURE B1. ELECTRICAL MOBILITY OF SINGLY CHARGED PARTICLES IN AIR AT STANDARD CONDITIONS

The Stokes' drag is

$$D = 6\pi R\mu_\infty (U_\infty - \bar{u}_p) \qquad \text{(newtons)} \qquad \text{(B-2)}$$

where $\bar{u}_p$ = particle velocity

U_∞ = gas velocity

R = particle radius

and

μ_∞ = gas viscosity

Mobility μ is defined as

$$\mu \equiv \frac{v_\infty - u_p}{E} \qquad \text{(B-3)}$$

In steady motion, which is assumed in the definition of mobility

$$\bar{F}_E = D$$

so

$$\mu = \frac{\bar{q}}{6\pi R\mu_\infty} \qquad \text{(B-4)}$$

For air at 20°C and 760mm Hg

$$\mu_\infty = 1.83 \times 10^{-5} \text{ Kg/m sec}$$

then

$$\mu = 2.94 \times 10^{3} \bar{q}/R \quad \text{m}^2/\text{volt sec}$$

where $\bar{q}$ is in coulombs and R is in m.

For a particle charged with one electronic charge

$$\mu = \frac{4.7 \times 10^{-10}}{R} \quad \frac{\text{m}^2}{\text{volt-sec}} \qquad \text{(B-5)}$$

where R is in microns. Equation 5 is the basis of the theoretical solid curve shown on the graph. This curve compares favorably with Figure 1 of the text.

For design purposes, either the simple Stokes' theory or the theory of Fuchs and Stechkina may be used. The actual mobility can reasonably be expected to fall between these two values. A more accurate evaluation of mobility, expecially for particles whose radius is less than about 0.1 microns, must await additional experimental data.

II. The distance that a particle must travel after being injected into the flow can be calculated with the aid of a few assumptions. Let us say that the ions are injected with no velocity component in the flow direction and that the Stokes drag law applies to this particle (since, whether or not the main flow is turbulent, the Reynolds number based on particle diameter is low). Then, equating forces,

$$6 \pi \mu_\infty R (U_\infty - \bar{u}_p) = \delta \bar{m}_p \bar{u}_p \frac{d\bar{u}_p}{dx} \qquad \text{(B-6)}$$

x = flow direction

$\delta \bar{m}_p$ = mass of particle

The characteristic time scale for which the droplet reaches the gas velocity or e-folding time[20] is

$$\tau_v = \frac{\delta \bar{m}_p}{6\pi R \mu_\infty}$$

So that for $x = 0$, $u = 0$ we have

$$\ell n \frac{1}{1 - \bar{u}_p/U_\infty} - \bar{u}_p/U_\infty = \frac{6\pi\mu_\infty R}{U_\infty \delta \bar{m}_p} \qquad \text{(B-7)}$$

but

$$\mu_\infty = \rho_\infty \nu \qquad \text{(B-8)}$$

$$\delta \bar{m}_p = \rho_p \left(\frac{4}{3} \pi R^3\right) \qquad \text{(B-9)}$$

ρ_p = particle density

Hence

$$\frac{6\pi\mu_\infty R}{U_\infty \delta m_p} x = \frac{9}{R_e} \frac{\rho_o}{\rho_p} \frac{x}{R} \tag{B-10}$$

where $R_e \equiv \frac{U_\infty (2R)}{\nu}$ (based on the diameter) (B-11)

Then, we can solve for x/R as

$$\frac{x}{R} = \frac{\rho_p}{\rho_\infty} \frac{R_e}{9} \left\{ \ell n \left(\frac{1}{1 - \bar{u}_p/U_\infty} \right) - \bar{u}_p/U_\infty \right\} \tag{B-12}$$

Taking $\bar{u}_p/U_\infty = 0.99$ since the free stream velocity is approached asymptotically, we have

$$\frac{x^*}{R} = 0.402 \frac{\rho_p}{\rho_\infty} R_e \qquad \text{for } \frac{\bar{u}_p}{U_\infty} = 0.99 \tag{B-13}$$

For water droplets in air and a Reynolds number of 1.0 we get

$$\frac{x^*}{R} = 328 \tag{B-14}$$

So that for a micron particle, x* will be 0.16 mm which is a relatively small distance. For higher Reynolds numbers (higher velocities for the same particle size), the distance x* will be proportionately higher but the Stokes law will begin to break down. Still, it is noteworthy that for channels of the size of a few millimeters, the distance over which micron size particles reach the gas velocity may not be negligible.

III. Let us treat briefly the space charge expansion due to its own electric field as treated in Chapter IV. We assume that

$$v_D = - \frac{D\nabla n}{n} + \mu E_S \approx \mu E_S \tag{B-15}$$

where v_D = drift velocity (ions or particles)

Now let's look at a spherical cloud of space charge. If the total charge is Q (in coulombs) and there are many ions or particles, then a surface ion can be taken as a test charge and the electrical force on it will be

$$F = \frac{\bar{q}\,(Q - \bar{q})}{4\pi\varepsilon_o r^2} \approx \frac{\bar{q}\,Q}{4\pi\varepsilon_o r^2} \qquad \text{(B-16)}$$

r = distance to the center of charge (radius of sphere), hence

$$E_r = \frac{Q}{4\pi\varepsilon_o r^2} \qquad \text{(B-17)}$$

where E_r is the radial field on the surface ion due to the space charge.

The expansion of the charged cloud will be radial, so that

$$v_D = \frac{dr}{dt} = \mu\left(\frac{Q}{4\pi\varepsilon_o r^2}\right) \qquad \text{(B-18)}$$

Integrating we get

$$\frac{r^3 - r_o^3}{3} = \frac{\mu Q}{4\pi\varepsilon_o}\,t \qquad \text{(B-19)}$$

where r_o is the radius at t = 0. Rearranging,

$$(r/r_o)^3 = 1 + \frac{3}{4}\left(\frac{\mu}{\pi\varepsilon_o}\right)\left(\frac{Q}{r_o^3}\right)\,t \qquad \text{(B-20)}$$

$$= 1 + \frac{\mu}{\varepsilon_o}(\bar{q}n_p)_0\,t \qquad \text{(B-21)}$$

$(\bar{q}n_p)_0$ = initial space charge density (corresponding to r_o)

Now for a constant velocity (U_∞) of the space charge cloud in the axial direction

$$U_\infty = \frac{dx}{dt} \qquad x = 0 \text{ at } t = 0 \qquad \text{(B-22)}$$

$$(r/r_o)^3 = 1 + \frac{\mu}{\varepsilon_o}(\bar{q}n_p)_0\frac{x}{U_\infty} \qquad \text{(B-23)}$$

Introducing the gas density

$$\delta_\infty = m_\infty n_\infty \tag{B-24}$$

we get

$$(r/r_o)^3 = 1 + \frac{\mu\delta_\infty}{\epsilon_o} \frac{\overline{q}}{m_\infty} \left(\frac{n_p}{n_\infty}\right)_o \frac{x}{U_\infty} \tag{B-25}$$

We can find by the equation above the spread of the space charge cloud as a function of x given μ, n_p/n_∞, and U_∞. Note that the product $\mu\delta_\infty$ is pressure independent. The expansion, then, will be as the ratio of radii cubed.

In order to prevent breakdown of the carrier gas, we must demand that

$$\frac{(\overline{q}n_p)_0 \quad (\frac{4}{3}\pi r_o^3)}{4\pi\epsilon_o r_o^2} < E_b \tag{B-26}$$

where E_b is the breakdown field of the carrier gas

or

$$r_o < \frac{E_b/n_\infty}{(\overline{q}n_p)_0/n_\infty\epsilon_o} \tag{B-27}$$

Using $\overline{q} = Ze$ we can evaluate the expression above for air.

$$r_{o)_{max}} \approx \frac{5.5\times10^{-12}}{z\ (n_p/n_\infty)} \quad \text{(meters)} \tag{B-28}$$

E_b/n_∞ is relatively constant between one and 100 atmospheres. The relationship for $r_{o)_{max}}$ is representative of a typical injector size and says that any initial radius of the space charge cloud greater than $r_{o)_{max}}$ will cause a breakdown.

United States
Naval Postgraduate School

THESIS

ION INJECTORS FOR SINGLE- AND TWO-

PHASE ELECTROGASDYNAMIC GENERATORS

by

William Taylor Ober II

June 1969

Ion Injectors for Single- and Two-Phase Electrogasdynamic Generators

by

William Taylor Ober II
Lieutenant (junior grade), United States Navy
B. S., United States Naval Academy, 1968

Submitted in partial fulfillment of the
requirements for the degree of

MASTER OF SCIENCE IN AERONAUTICAL ENGINEERING

from the

NAVAL POSTGRADUATE SCHOOL
June 1969

ABSTRACT

Systems suitable for the injection of ions into electrogasdynamic (EGD) generator devices were built and tested. The mechanism of injection was based on a corona discharge, whereby ions moving through an electric field can be intercepted by a gaseous flow. The intercepted ions are of one polarity, insuring selective ion injection. Two types of injector units were investigated. One was a molecular ion device which produced ions directly from the carrier gas, and the other created larger sized ions, resulting in an aerosol flow. The latter consisted of passing saturated steam through a corona discharge and injecting it into an air stream. In order to aid the injection process, the wake of a cylinder in the air stream was utilized in both cases. Most of the work done here was devoted to the design and testing of the aerosol flow device. The degree of success was moderate.

TABLE OF CONTENTS

LIST OF ILLUSTRATIONS

LIST OF SYMBOLS AND ABBREVIATIONS

E_b	electric field strength
EGD	electrogasdynamic
I_C	corona current
I_G	generator current
I-V	current-voltage
L	length
V_C	corona voltage
ν_D	charged particle drift velocity
μ	charged particle mobility
W	mass flow rate
A*	nozzle exit area for choked flow
k	C_p/C_v
R	steam gas constant
P_o	pressure
T_o	temperature

ACKNOWLEDGEMENT

The author wishes to express his deepest gratitude to Professor Oscar Biblarz for his invaluable guidance, to Pat Hickey for all the time and effort he devoted to this project and to Lieutenant (junior grade) Dave Wallace for his aid in co-ordinating this effort with his own.

I. INTRODUCTION

The principle of operation of an electrogasdynamic (EGD) generator is based on the fact that if a moving gas can displace ions away from their point of creation it can perform electrical work. The generator, therefore, consists of an ion injector, a conversion region (where the ion migration path is influenced by the direction of the gas flow), and a collector device to pick up the ions which have been carried downstream. Of these three basic components, the ion injector is the most complex and critical to the proper operation of the generator. The purpose of this work was to design and test two means of ion injection, classified by the nature of the ions desired in each case. The first injects molecular air ions into an air stream. The second one injects ionized water droplets into the air stream; this injection method will be alternately referred to as either a colloidal ion suspension or an aerosol flow.

The problem of creating an efficient EGD generator has been studied with considerable interest over the past seven years [1-5]. It was decided at the start of this project to employ a cylinder mounted spanwise in a subsonic test section to generate a two dimensional turbulent wake. It was thought that this wake would facilitate the removal of charged particles from their generation point and thus aid the process by which the air flow forces them downstream to a collector device. With this goal in mind all designs for the generation and injection of charged particles were incorporated with the cylinder. It was also felt that the turbulent wake would be instrumental in delaying electrical breakdown of the carrier gas.

Preliminary studies revealed that a corona discharge device would provide the most suitable means of ion injection because of the relatively high (atmospheric) pressures involved in the air flow in the cylinder wake[6,7]. The characteristics of a corona discharge which make it a favorable injector are given below.

One type of corona can be created when a sufficient voltage is placed across the gap between a circular ring and a centrally mounted needle tip. At voltages below that required to cause an arc discharge across the gap there exists a field of sufficient strength to ionize the gas in this region. The charges of polarity opposite to that of the tip are then trapped in a charge sheath about the needle tip. The effect of this sheath is to reduce the outer electric field strength. This fact when simply stated means that although a current still exists due to the migration of charges of the same polarity as the needle toward the ring, the migration occurs in a field of weakened strength and these ions can be more easily removed from the influence of this field. Thus, particles of a desired polarity can be forced away from the electric field of the corona unit (See Figure I).

II. MOLECULAR ION EXPERIMENTS

Preliminary work with molecular ions involved a study of the current voltage characteristics of a corona discharge unit which consisted of an aluminum ring mounted in a teflon block and a needle tip shaped from an iron nail (see Figure II). Current-voltage (I-V) curves from this setup are shown in Figure II. It was learned from this test that any sharp edges in the ring will act as discharge points, and therefore would cause the unit to deviate from its desired operational characteristics. It was also found that the position of the needle tip within the ring has a noticeable effect on the I-V characteristics. The test was also employed as a familiarization period on the safety requirements of high voltage work.

From this point the study was divided into two phases. Phase one involved the design and study of a small corona unit to be incorporated with the aforementioned cylinder. The cylinder was mounted in a test section through which air flowed at velocities in the vicinity of three hundred feet per second. In this phase then, the corona unit was employed to ionize air and the air flow would provide a carrier which would force some of the ions out from the inside of the ring and downstream to a collector.

For a drawing of the model chosen for this phase refer to Figure III. The ring was designed to be of a size which would insure that the whole unit would be within the wake of a one centimeter diameter cylinder. Braces on the ring attached it to the downstream side of the cylinder and the needle tip wire was placed through a hole drilled streamwise through the cylinder. Electrical leads were brought in through the test section

walls in such a manner as to provide contact with ring and needle at the ends of the cylinder.

If the needle were positively charged, positive air ions would migrate toward the ring, which would be at ground potential. As stated earlier, the migration would occur in a region of weak field strength due to a sheath of negative ions held in the vicinity of the needle tip. Thus for this polarity it should be possible in theory to remove some of these positive ions from this field by means of the air flow before they reach the ring. Similarly, electrons could be generated and removed by simply reversing the polarity of the device.

Initial tests were then made to determine I-V characteristics of the unit in stagnant air. These are shown for either polarity in Figure IV. The next series of tests involved taking I-V data with the cylinder and corona unit mounted in the test section with various air flow rates. The electrical and metering setup is shown in Figure V. At this point it was determined that our I-V data was not a true indication of what was happening within the corona unit. The wiring was crude at best and at higher voltages numerous corona discharges were occurring at several spots where sharp edges were exposed, providing parallel current paths and thus giving misleading data. In an attempt to remedy this situation, all leads were brought into two spherical brass junctions. Wherever any sharp edges were present an attempt was made to round them off. The I-V data then taken are shown in Figure VI. For a detailed report on the operation of the unit as a generator (with collector current data) and effectiveness of design innovations refer to reference 6.

III. COLLOIDAL ION SOURCE

A INTRODUCTION

The second phase of this study entails the major part of the research carried out in the preparation of this thesis. This phase is concerned with devising a means of injection of ions of a much greater size than ionized air into the air flow downstream from the cylinder.

An important consideration in the design of an effective EGD generator is the mobility of the charged particles which are to be forced out to the collector. Mobility is a measure of the velocity of a charged particle under the influence of an electric field. A high mobility indicates that it would be difficult to force the ions away from their migration path from the needle tip to the ring and therefore a low mobility is desirable. In a study[4] carried out for the Aerospace Research Laboratories published in 1964, it was reported that particle size is an important factor governing the mobility of the ions. As shown below, particles on the order of 10^{-7} meters to 10^{-6} meters (one micron) in diameter provide a somewhat optimal mobility for EGD considerations.

A comparison between the usefulness of molecular ions and larger sized ions can be made using the mobility calculations of reference 4. Consider the drift velocity of an ion charged in a corona device under an electric field of 3.0×10^{6} volts/m (breakdown potential (E_b) of air at STP). The respective drift velocities (v_D) are given below.

molecular ion: mobility (μ) $\cong 10^{-4}$ m^2/volt-sec

$$v_D = \mu E_b \cong 3.0 \times 10^{2} \text{ m/sec} \cong 9.84 \times 10^{2} \text{ ft/sec}$$

micron sized ion: $\mu \cong 10^{-6}$ m^2/volt-sec

$$v_D = \mu E_b \cong 3.0 \text{ m/sec} \cong 9.84 \text{ ft/sec}$$

As can be seen, the molecular ions can easily attain drift speeds greater than that of the main flow and little interception can be expected; whereas the micron sized ions drift relatively slowly and can be intercepted more readily by the flow. The situation improves further with particle sizes between 10^{-8} and 10^{-7} meters.

Having determined the desired size for the charged particles, and acting on the decision to retain the corona as a source of ion generation, it was then necessary to choose a means of producing charged particles which would be of the order of one micron in diameter. Three methods of producing micron-size particles were considered and are described below. The method employing saturated steam was chosen.

Method one involved the use of powder which is manufactured to have an average particle size of one micron. The powder could then be introduced to the air flow upstream of the cylinder and channeled through the corona unit. This is perhaps the simplest method and guarantees the proper particle size, but it does have the disadvantages of both the necessity of a large supply of powder and the discomfort of exhaust powder from the open system, which could provide a hazard to metering operation as well. Furthermore, it is difficult to produce homogeneous charged particle distributions.

The second method considered was to replace the needle tip of the corona with a hypodermic needle.[5] In this way a dielectric fluid could be forced out through the needle at a controlled rate. As droplets of dielectric form at the needle tip, the high electric field strength charges them and subsequently causes them to break up. Unfortunately, there is no good way with this method to insure proper particle size.[9]

Finally, a method has been studied whereby saturated steam is condensed by means of expansion through a nozzle.[2] The dry steam would

initially be forced through a corona unit as close as possible to the point of condensation. Then, in theory, the steam would saturate and condense about the ions, forming a colloidal suspension of charged water droplets in air. The steam is employed both as the dielectric and as the carrier gas to force the ions out of the nozzle. This method was chosen as the best suited for the work which has been done here although, admittedly, it also presents the problem of how to grow the proper ion size during condensation.

B. DESIGN OF COLLOIDAL ION GENERATOR

A design was sought which would incorporate the cylinder with a steam supply, a nozzle and a corona device. The design chosen involved a hollow teflon cylinder fitted with a stainless steel nozzle which would face the downstream direction of the flow. In this configuration the nozzle could serve a three fold purpose. It would act as a flow metering device, yielding any desired flow rate based on a supply of saturated steam (i.e., 250°F. and 15 psig). Additionally, it would serve as the ring of the corona unit and finally serve to condense the steam about the charged ions through expansion at the nozzle exit plane. A diagram of the nozzle and cylinder is shown in Figure VII. Sample calculations and principles for nozzle design are shown in the Appendixes. Three nozzles were constructed to have steam flow rates of .01 lbm/sec, .005 lbm/sec and .001 lbm/sec,all with a choked steam flow at the exit plane.

In order to have a generator capable of producing a constant supply of steam at the desired temperature and pressure it was decided that a sealed and reinforced aluminum container would be the most desirable. A pressure cooker served nicely for this purpose. The generated steam

would then be transported to the cylinder and nozzle by means of ¼-inch O.D. stainless tubing. A ball valve was placed into this line to serve as an on-off valve. Any excess pressure would be bled off by means of a needle valve installed on a length of tubing which led away from the main line. The total length of tubing from the pressure cooker to the cylinder was wrapped in heating tape to prevent condensation of the steam while it was in the line (see Figures VIII-IX). A pressure gauge was installed in the top of the cooker in order to provide a guide for pressure regulation.

Initial testing of this new unit was solely concerned with perfecting as much as possible the steam generation aspect of the system. A 4000 watt hot plate was found, which easily maintained a 15 psig pressure head. After completely insulating the top and sides of the pressure cooker with a layer of Sauereisen number 31 cement of approximately ½-inch in thickness and then another ½-inch thick layer of asbestos tape, condensation problems were solved well enough to maintain a steady flow of dry steam through the nozzle and thereby prevent any arcing of the corona due to spurts of condensed water. A length of twenty-thousandths-inch platinum wire was brought in from the upstream side of the cylinder and centered within the nozzle to serve as the needle tip of the corona unit (see Figure VII).

C. EXPERIMENTAL PROCEDURE

As previously mentioned, before any reliable electric data could be obtained, it was necessary to insure that a steady and dry steam flow would be emitted from the nozzle. To achieve this end the steam line was purged with a jet of high pressure air prior to each test. When this was accomplished the ball valve which separated the nozzle from the

pressure cooker was closed to seal off any steam flow in that direction. The four-quart pressure cooker was then filled to approximately three quarters of its capacity with distilled water and the hot plate was turned on to the maximum heating position.

It took about twenty minutes for the water to begin to boil. During this interim the heating tape, which was connected on line with a rheostat, was maintained at 400°F. to ensure that the inner tubing temperature would be greater than the temperature of the steam and thus aid in preventing any condensation in the line.

Initial data taking involved a set of I-V curves on the nozzle and needle as a corona unit. During these tests there was no steam flow through the nozzle. A set of these data is shown in Figure X. These tests were usually carried out during the period when the distilled water in the pressure cooker was being raised to the boiling point.

As soon as the water began to boil at a substantial rate all valves were closed until the internal pressure in the pressure cooker reached 15 psig. When this point was reached the bleed off needle valve was opened just enough to maintain this pressure. This action was continued for several minutes in order to insure that the water had reached its boiling point at the higher pressure. The ball valve was then opened to allow the steam flow to go up the line and through the nozzle as the needle valve was readjusted in order to steady the internal pressure at a constant 15 psig. It was also necessary to increase the rheostat setting, since the steam flow had a considerable cooling effect on the tubing. A heating tape temperature of about 350°F. (measured by a thermocouple mounted between the tape and the tubing) was found to be sufficient to avoid condensation.

When a steady steam flow was obtained I-V data were again taken on the corona within the nozzle. These data are shown in Figure XI. Electrical connections and metering setups are shown in Figure XII. At this point all systems were ready for a test of the unit as a generator (see Figures XIII, XIV and XV).

An iron nail, polished and sharpened, was insulated by plexiglass and mounted on a traversal mechanism. The tip of the nail served as the collector unit. It was wired to a microammeter and then to ground. Tests were then run measuring the corona voltage, corona current and collector current for both polarities on the corona. The collector position downstream of the nozzle was a variable as was the corona voltage. These tests were run at first using only the steam flow to force the charged particles out to the collector. A later test was made to determine the effect of the air flow in conjunction with the colloidal ion injection. Data are presented on Figures XVI, XVII and XVIII. Results and the effectiveness of system modifications are discussed in the Analysis of Results section of this paper.

IV. ANALYSIS OF RESULTS

The first test of the complete system proved rather discouraging as there was no measurable current flow from the collector. Two modifications in the system were simultaneously devised. A digital multimeter, capable of measuring down to one hundredth of a microampere, replaced the Simpson microammeter (see Figure XV). Secondly, it was deemed that with the configuration of the ion generator it would be advantageous to devise a means of aiding the process of getting the colloidal ions out into the region of the collector. As a solution of this problem the interior of the nozzle was coated with a thin layer of dielectric epoxy, with only a narrow band of steel at the throat of the nozzle left exposed, (see (Figure XIX). With the tip of the center needle recessed back into the nozzle, this would then align the direction of the electric force field toward the nozzle throat. Finally, to prevent the collector from acting as a discharge point when placed too near to the nozzle, a set of diodes was connected in series between the collector and the multimeter. With these improvements a measurable, though admittedly small, collector current was drawn, (see Figures XVI, XVII, and XVIII).

Three primary observations were made from the data thus obtained. First of these is that the ion density was primarily a function of streamwise distance from the nozzle exit plane. Positioning of the collector in various points off center of this axis had little effect on the current reading. Secondly, the collector current reading for the negative ion case was about double that for the positive ion case. Though consistent with the results of other researchers,[2] the reason

for this phenomenon remains to be uncovered. Thirdly, colloidal ion suspensions were shown to be considerably more effective in the generator operation than higher mobility air ions.[6]

The epoxy coating on the inside of the nozzle was helpful, but it was a crude solution at best. The ineffect of corona voltage increase on collector current may indicate a breakdown of the dielectric epoxy in this region. This hypothesis is based on the observation that at lower voltages on one test a significant self induced oscillation of corona current produced a proportional oscillation of collector current, (see Figure XVII). While on the same run at higher corona voltages and therefore increased corona current, the collector current was essentially constant, (see Figure XVIII). These higher voltage currents were far more stable than lower readings, but the point to be observed here is that the increased current did not proportionally increase the collector current as it had at lower voltage values.

Results given on this study are all for the nozzle designed to yield a flow rate of 0.001 lbm/sec. Use of the larger nozzles was attempted, but the present steam generator was not capable of maintaining a pressure head at these nozzles. A heating method with a greater BTU capacity and improved insulation would be required to overcome this hurdle.

The addition of air flow through the test section detracted from rather than aided the performance of the system. Admittedly little work was done with this configuration in air flow due to the time spent in perfecting the steam generator and achieving a non-air flow collector current. It is very possible that the injector design simply works better by relying only on steam for a carrier gas and expansion for condensation. It may also be that there is an air flow rate which would be favorable to the process. This study has yet to be carried out.

The data presented here must be interpereted taking into account the fact that the existence of micron sized particles was not proven by this study. Further, if they did exist, no attempt has been made to determine at what point in the flow they were condensed.

Finally, no leakage of current between the injector and the collector was anticipated. Therefore, no test of the generator unit was made without steam or air flow. The possibility of this leakage should, however, be considered in an analysis of this data.

V. CONCLUSIONS

The injector designs which were sought at the start of this project were built and successfully operated. A discussion of efficiency by usual standards at this point would be rather premature due to the somewhat limited state of development of the hardware. Positive, though not conclusive, results were obtained. It is hoped that these results prove helpful to future studies.

VI. RECOMMENDATIONS

The design of the colloidal ion generator should be reviewed. It would seem advisable to design a system which would employ the air flow to carry the colloidal ions out of the corona region, rather than rely so heavily on the steam flow. The use of the nozzle should be maintained, but an improved system should include a way to feed flowing air into the nozzle entrance plane without prematurely condensing the steam.

The system which has been used in this research could also be improved upon enough to bring about a marked increase in collector current. The first improvement needed here is to get a smooth dielectric coating on the inside of the nozzle, such as a thin teflon cone. This will lessen the doubts raised concerning the breakdown of the rough epoxy coating used in this work. Secondly, an increased steam flow rate would be greatly helpful in getting the colloidal ions out to where they can be gathered by the collector. The nozzles for this purpose have already been built. All that remains to be done is to generate steam fast enough to maintain the desired pressure head. Finally, a study with air flow should be made to determine the compatibility of this present system with original design criterion.

It is also noted here that there has been no attempt made as yet to determine at what distance from the nozzle exit plane the micron sized ions are condensed, if they existed at all. Several studies have been made of the rates of condensation which may prove useful to an investigation of this aspect of the EGD generator. Two of these are listed in the bibliography for future reference[10,11].

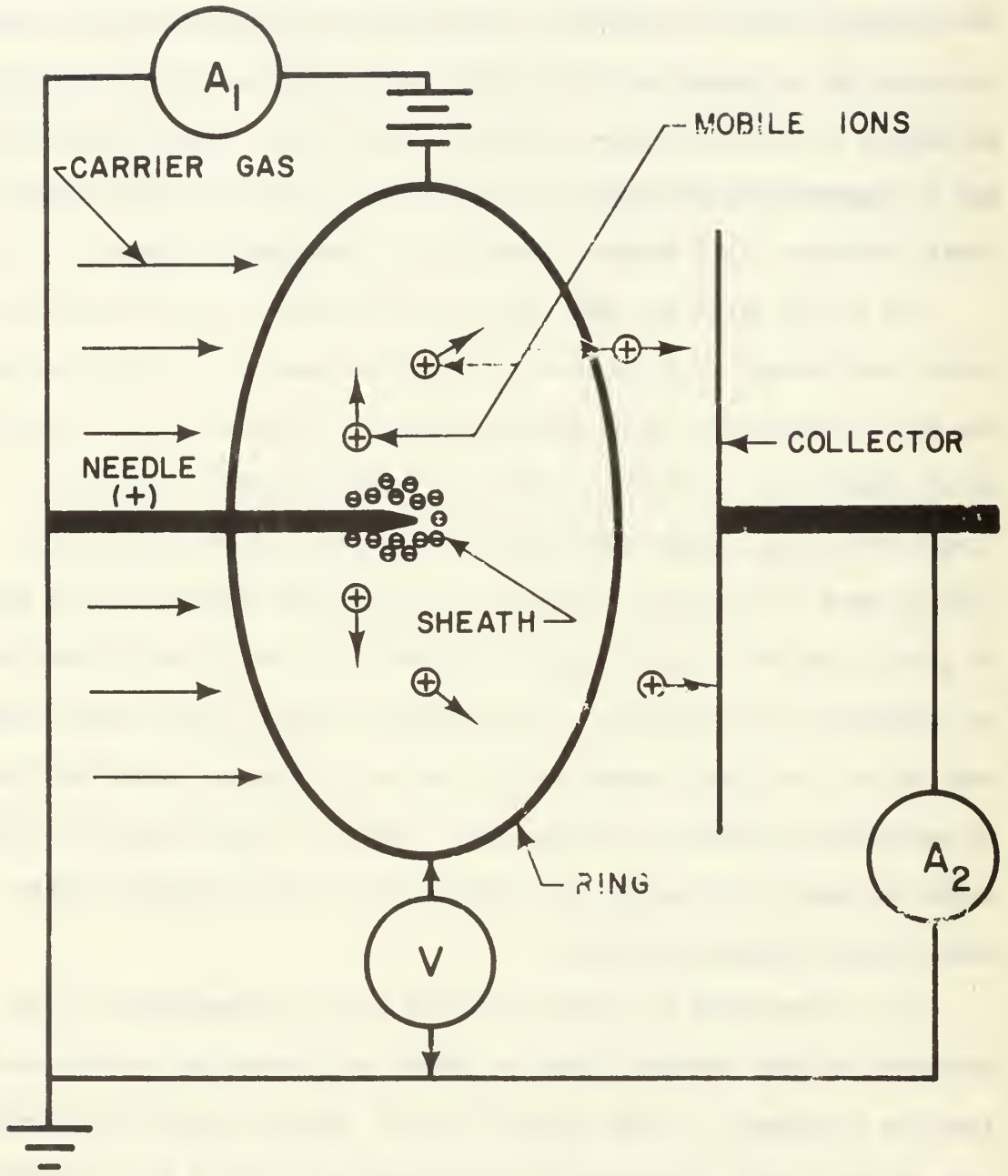

FIGURE I GENERATOR SCHEMATIC

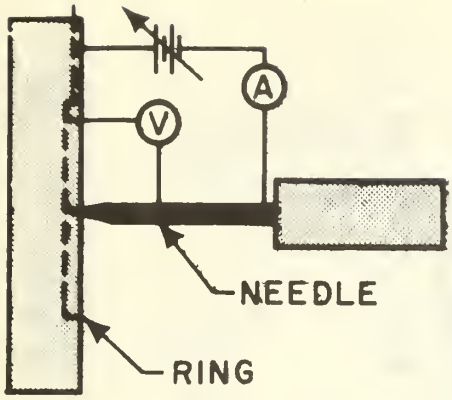

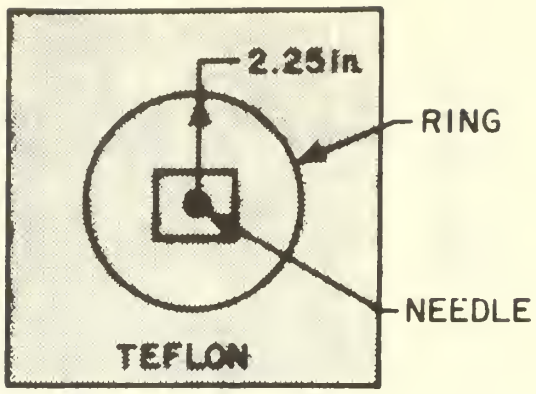

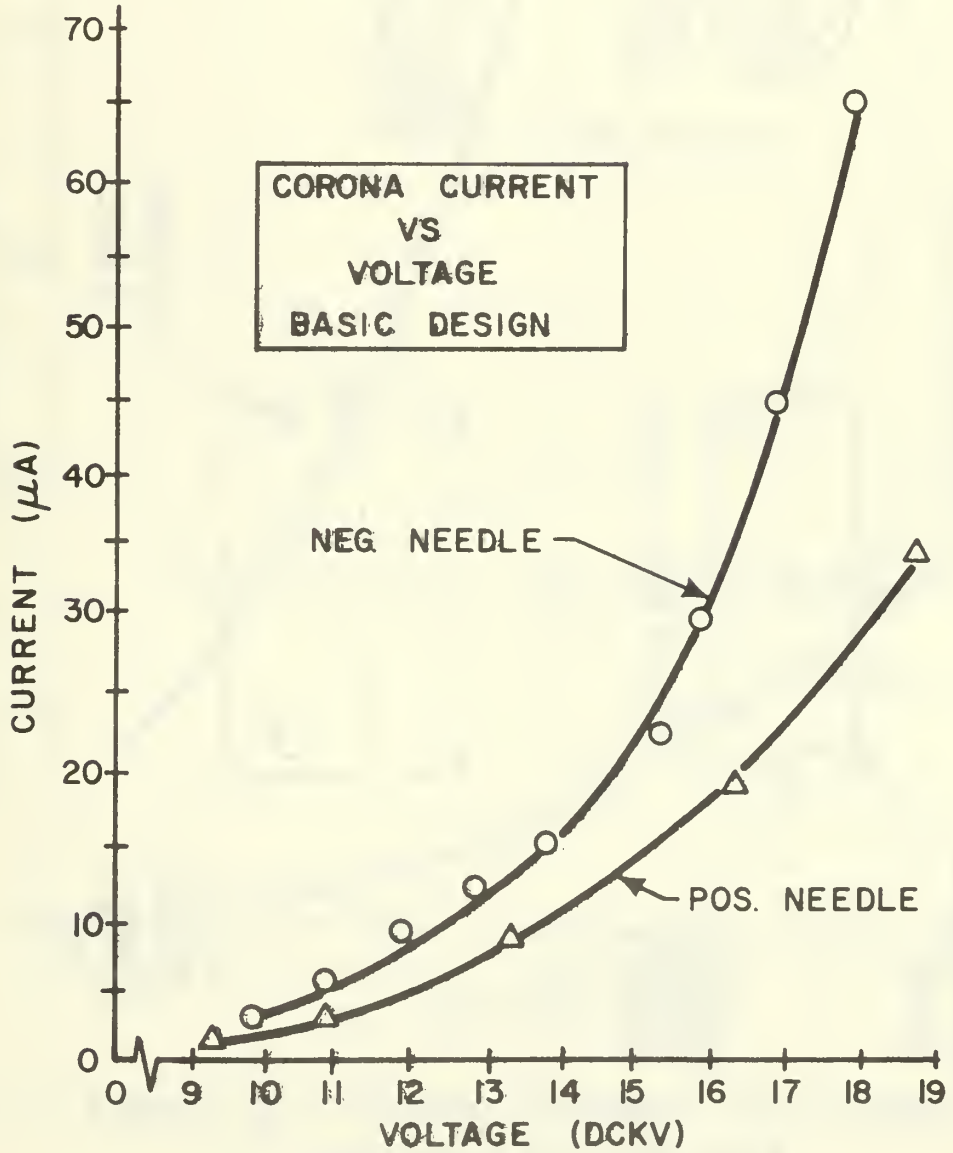

FIGURE II PRELIMINARY CORONA DEVICE

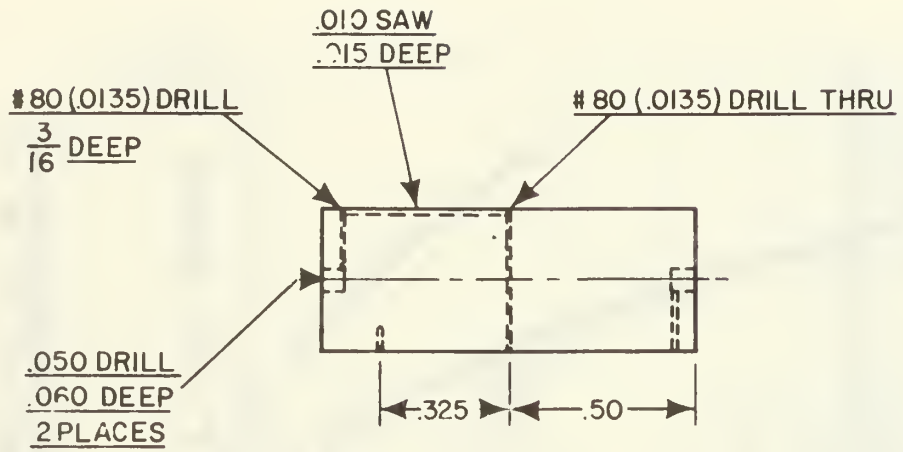

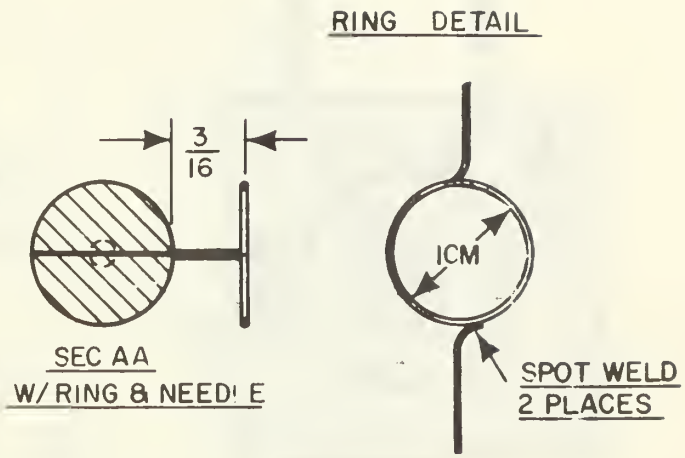

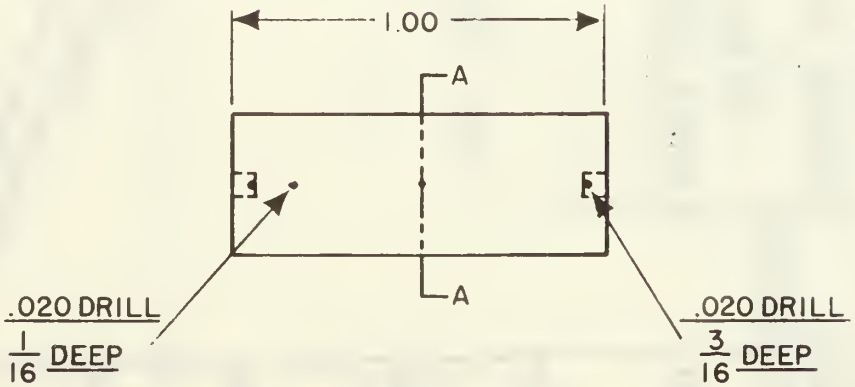

RING : .020 PLATINUM WIRE
NEEDLE: .010 PLATINUM WIRE
BODY MATERIAL: 3/8 DIA. PLEXIGLAS ROD

SCALE: 2X

FIGURE III MOLECULAR ION DEVICE

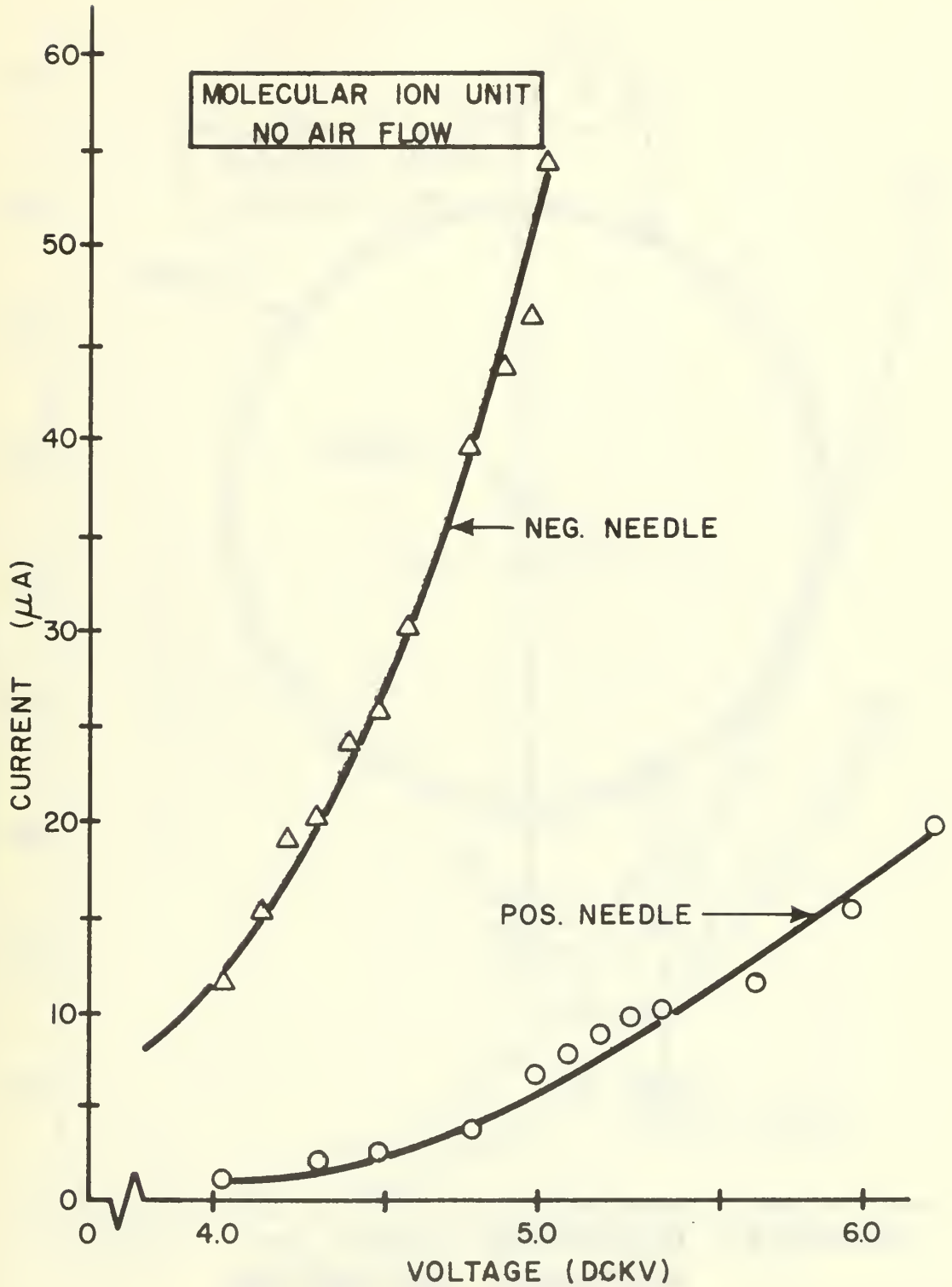

FIGURE IV CORONA CURRENT VS VOLTAGE
MOLECULAR ION UNIT

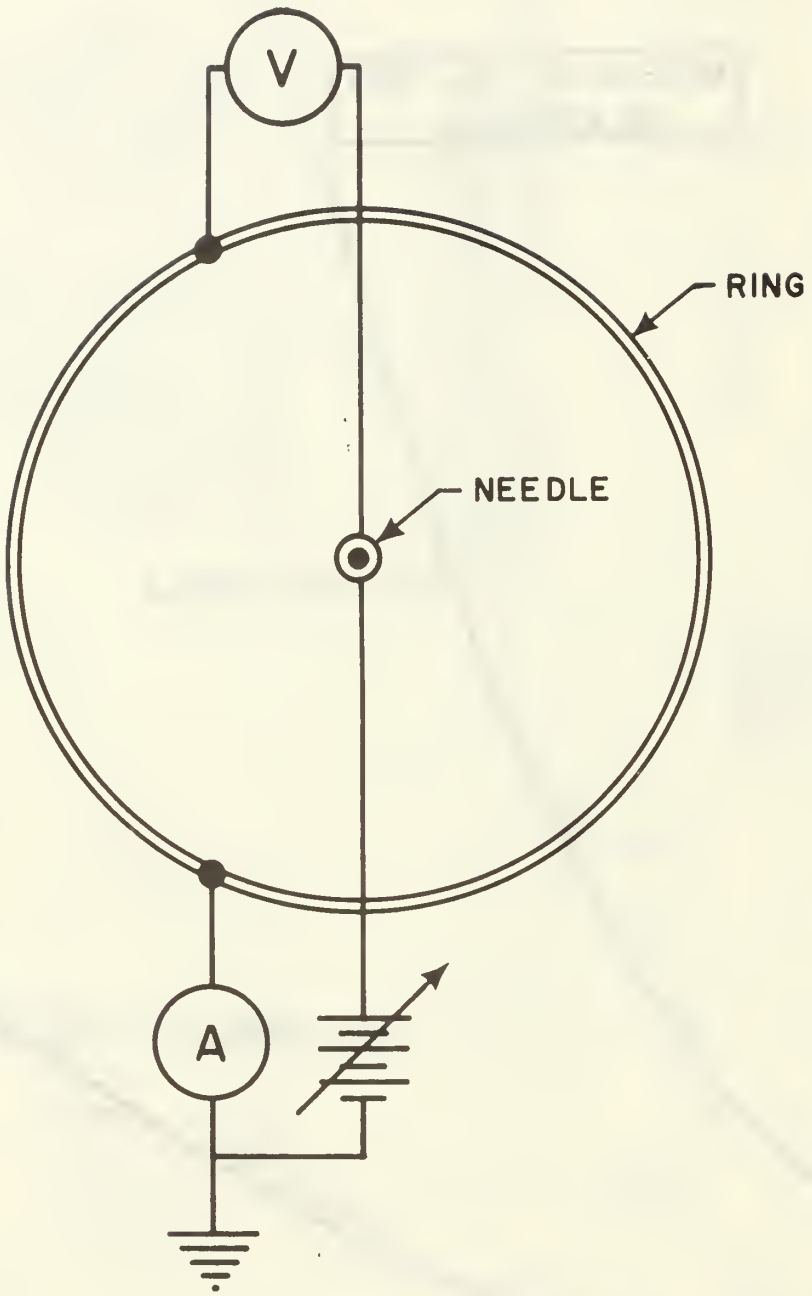

FIGURE V ELECTRICAL SETUP OF MOLECULAR ION INJECTOR

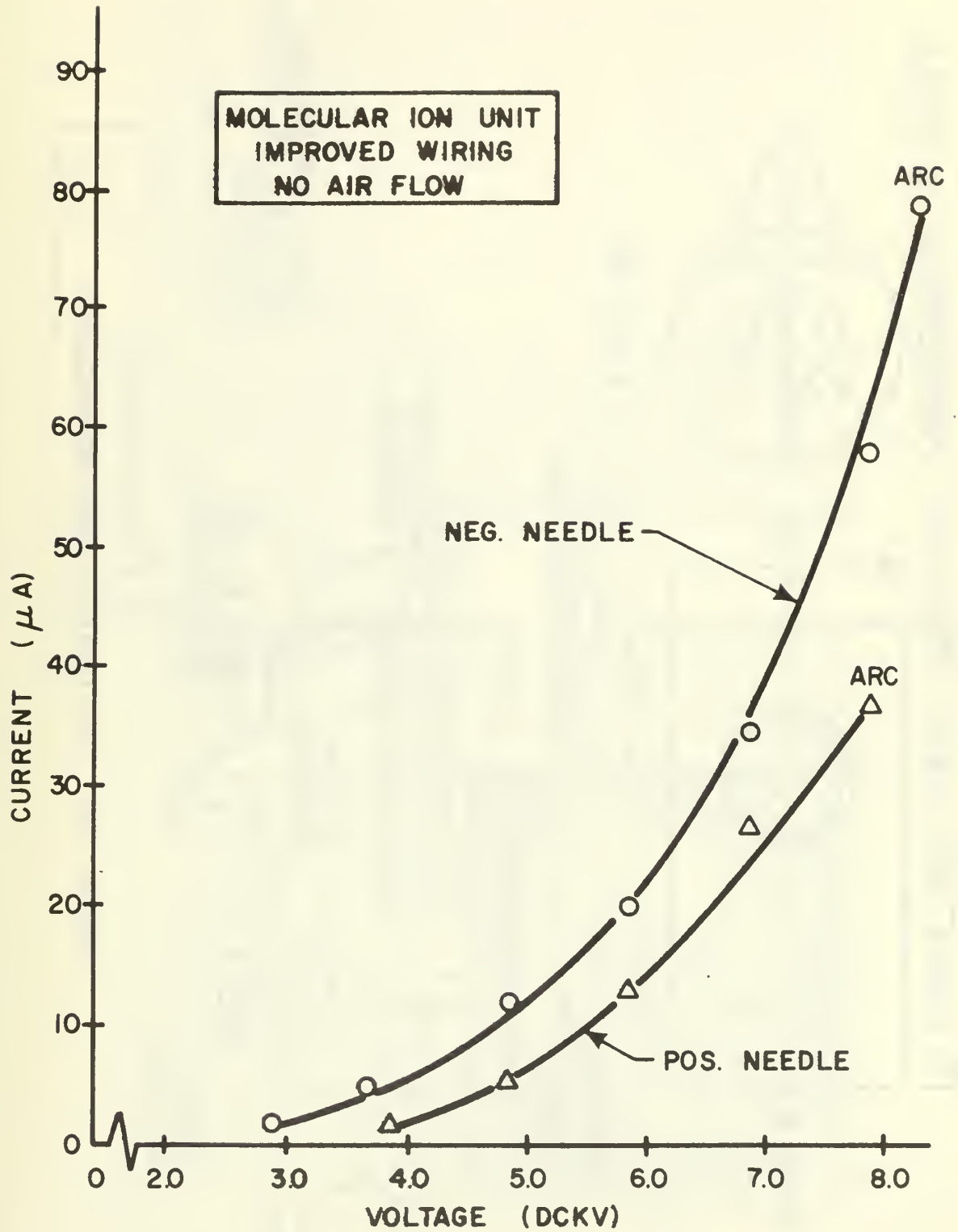

FIGURE VI CORONA CURRENT VS VOLTAGE
MOLECULAR ION UNIT

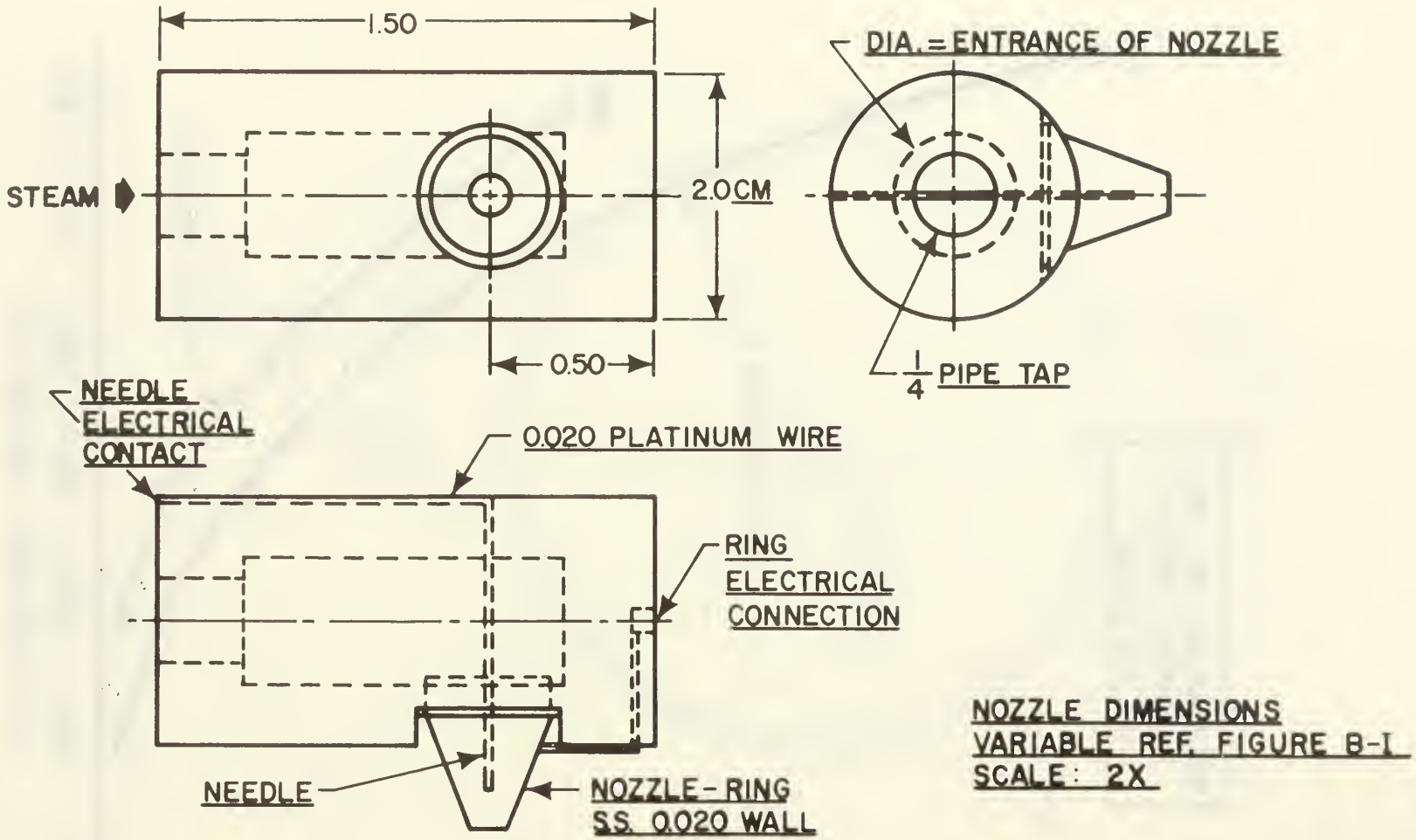

FIGURE VII COLLOIDAL ION GENERATOR

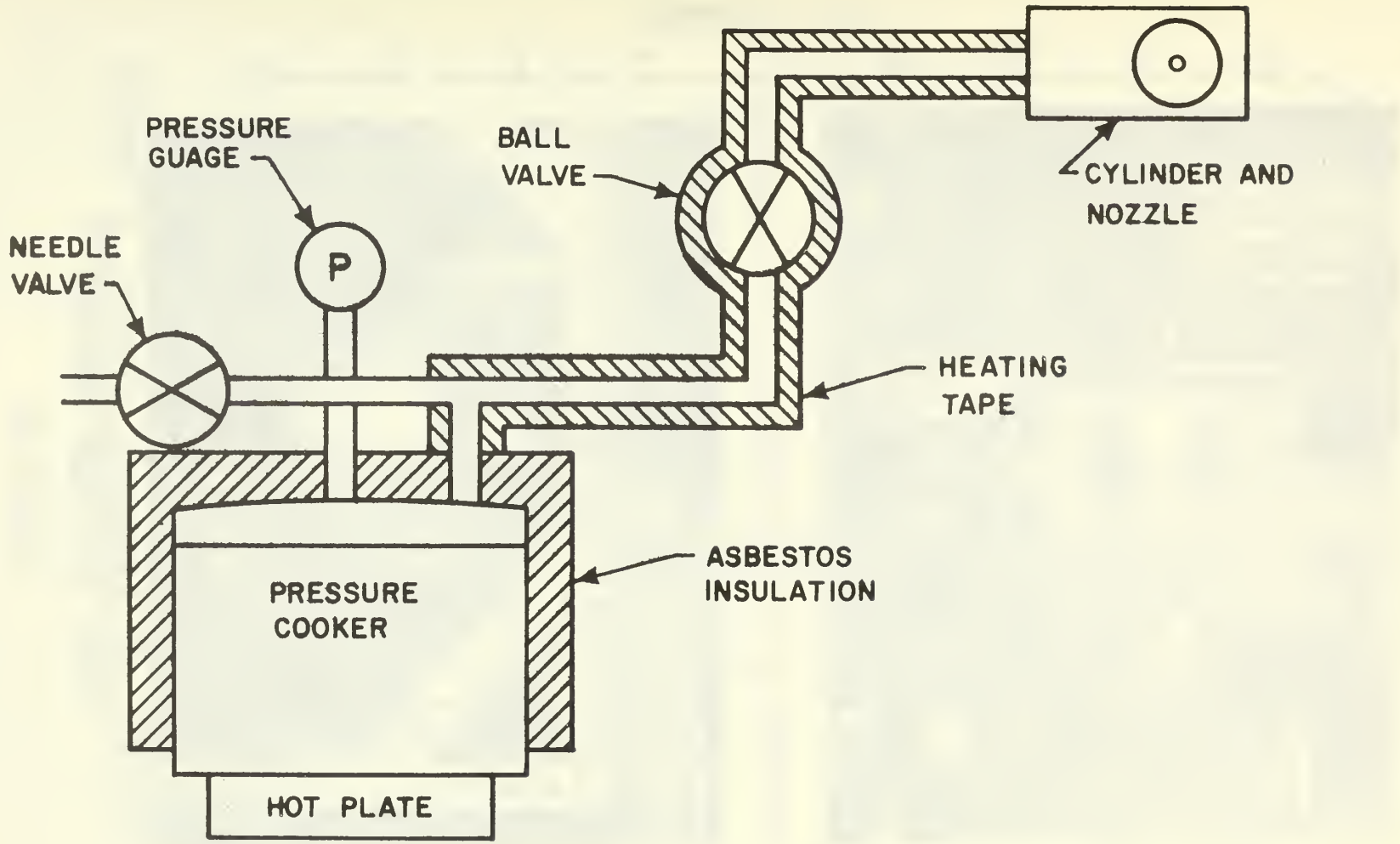

FIGURE VIII STEAM GENERATOR SCHEMATIC

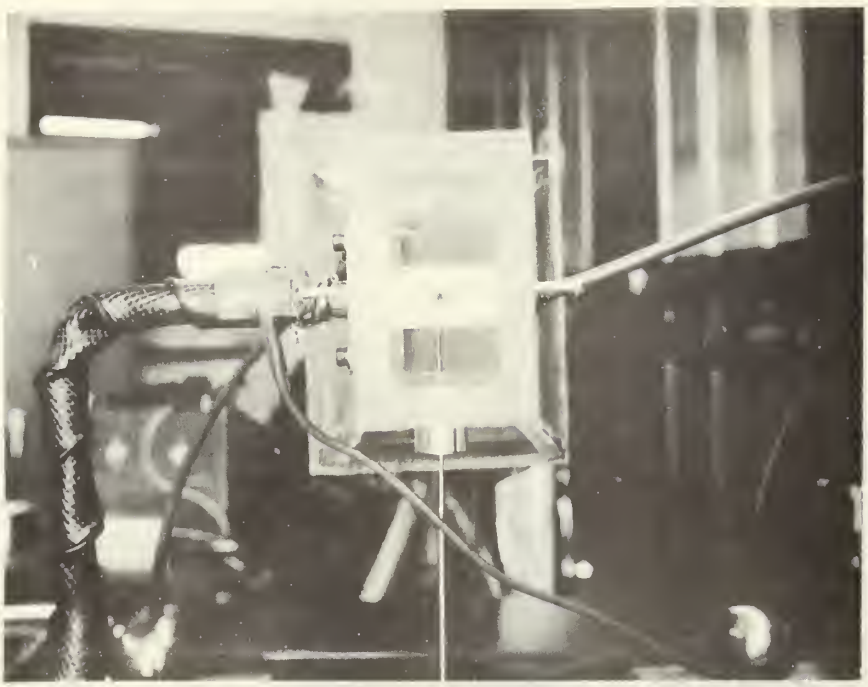

(i) VIEW OF STEAM UNIT IN TEST CHANNEL

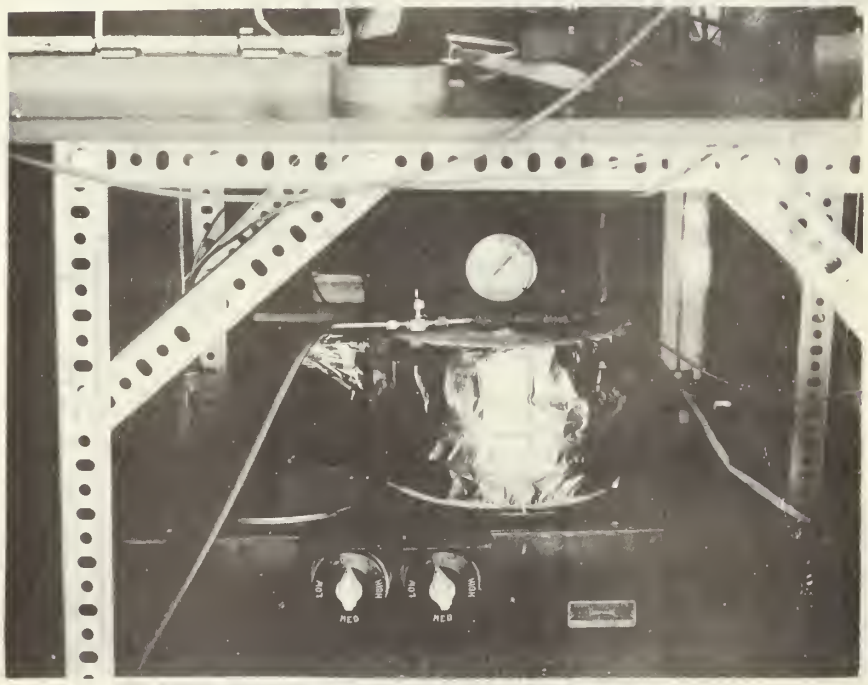

(ii) VIEW OF PRESSURE COOKER

FIGURE IX

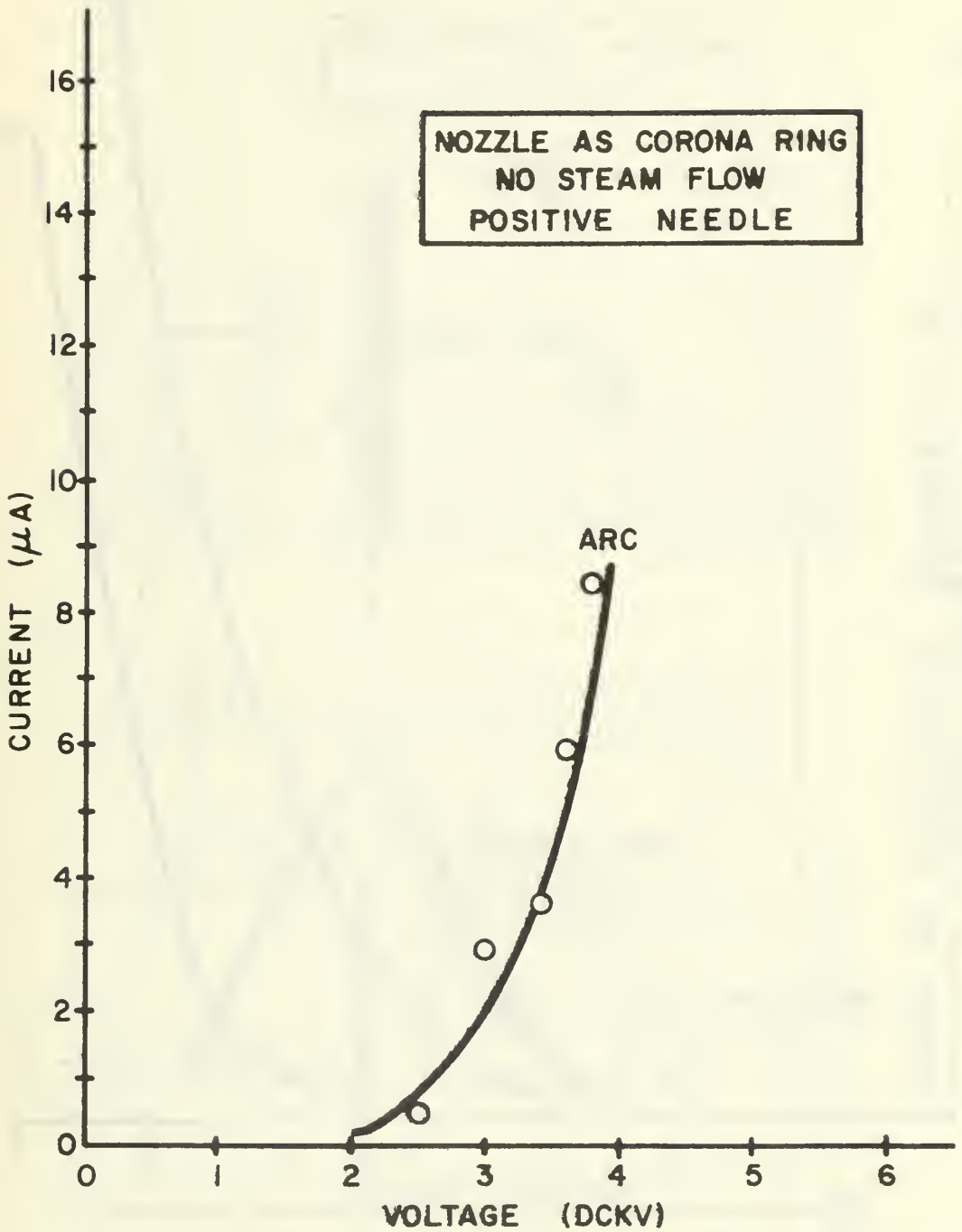

FIGURE X CORONA CURRENT VS VOLTAGE
MICRON INJECTOR UNIT

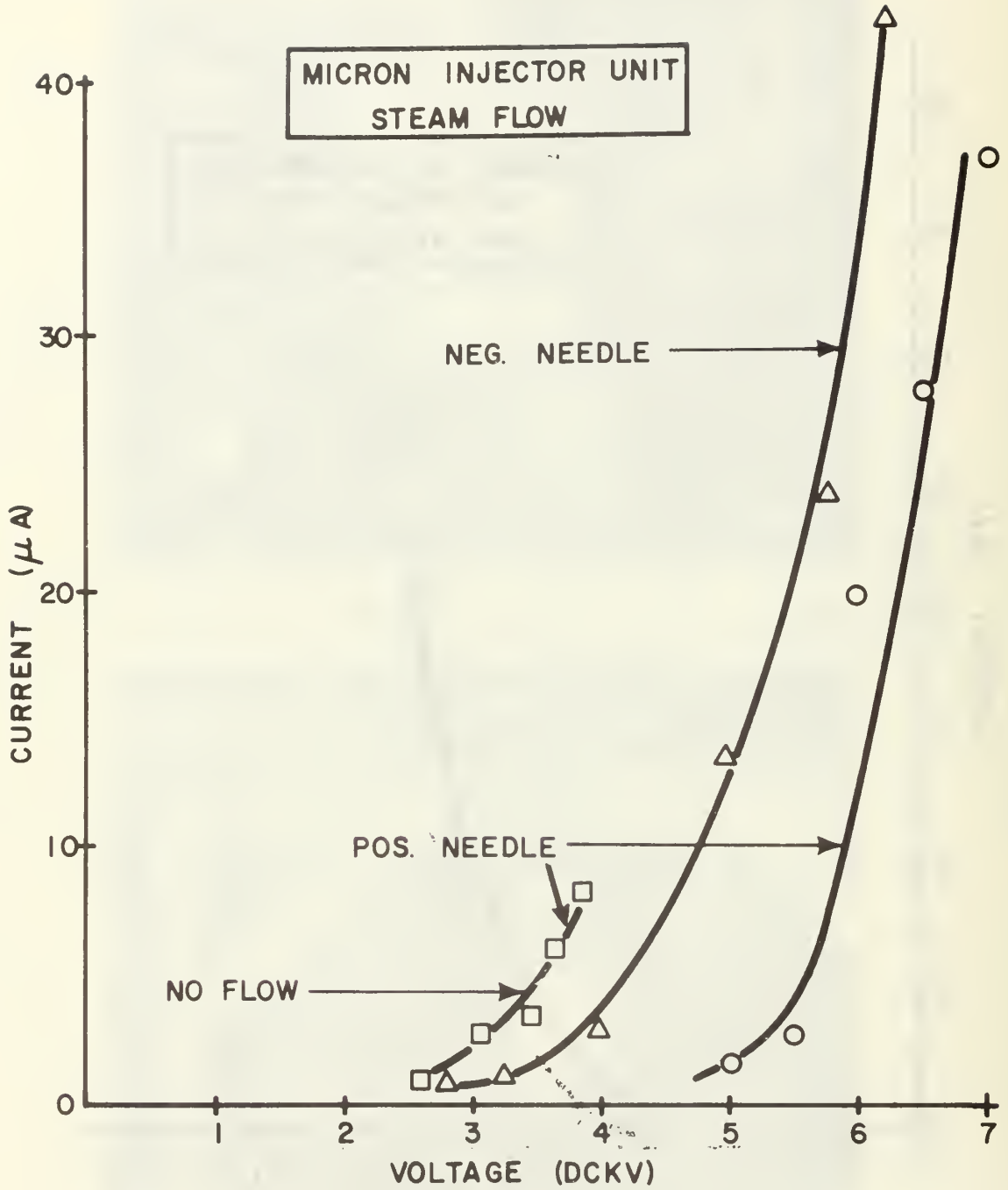

FIGURE XI CORONA CURRENT VS VOLTAGE
MICRON INJECTOR UNIT

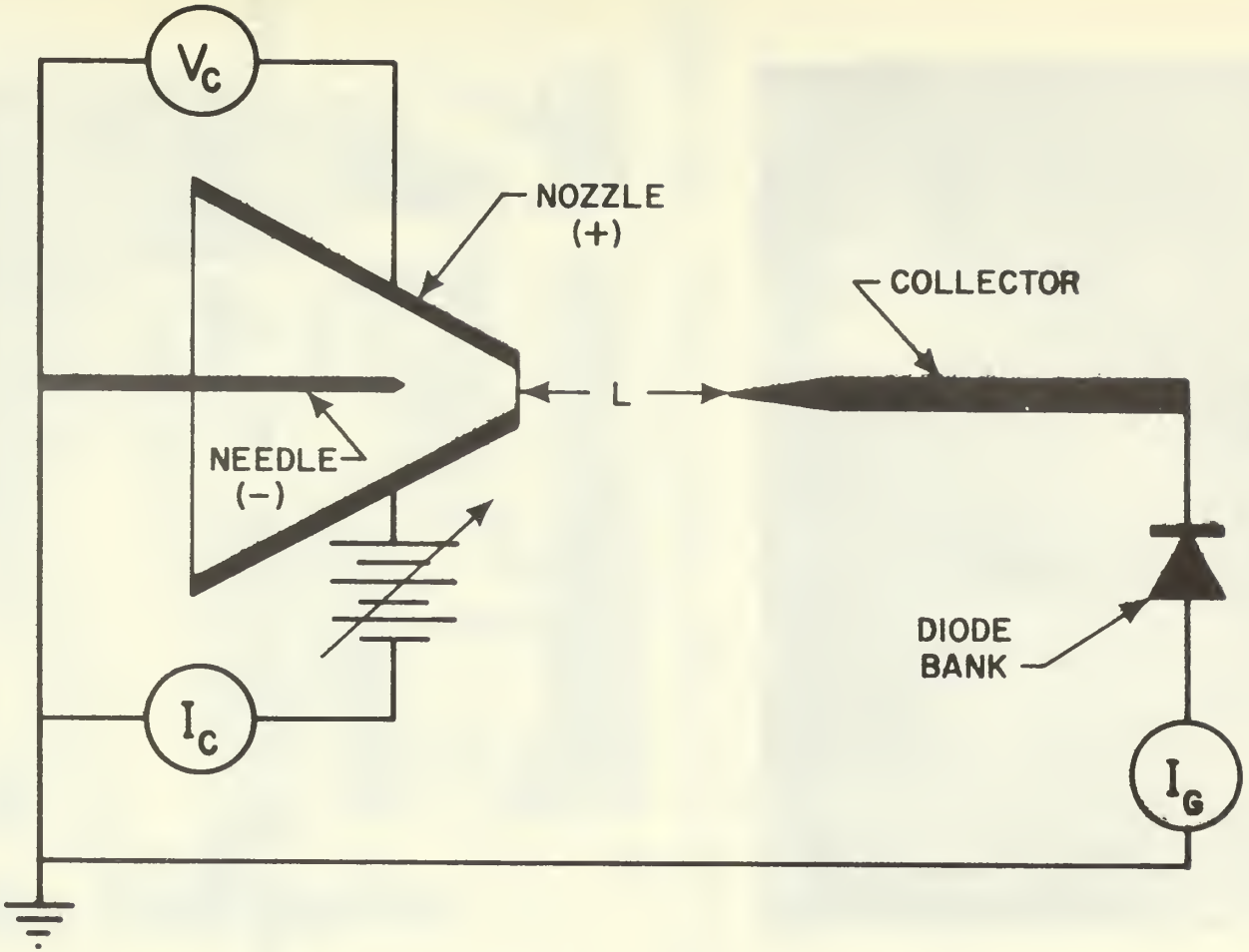

FIGURE XII ELECTRICAL SCHEMATIC OF MICRON INJECTOR UNIT

FIGURE XIII GENERATOR UNIT IN TEST SECTION

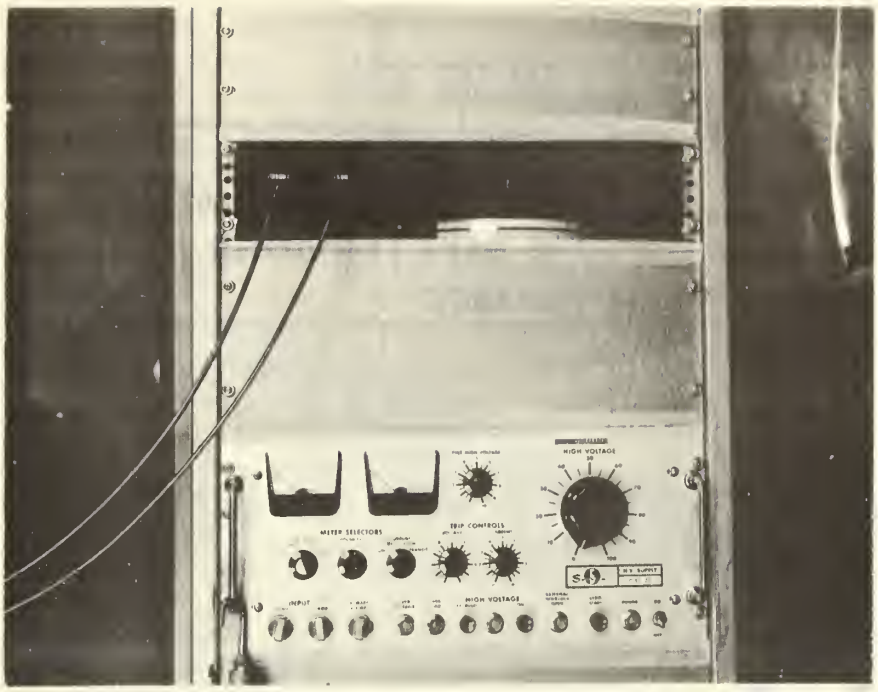

FIGURE XIV POWER SOURCE AND VOLTMETER

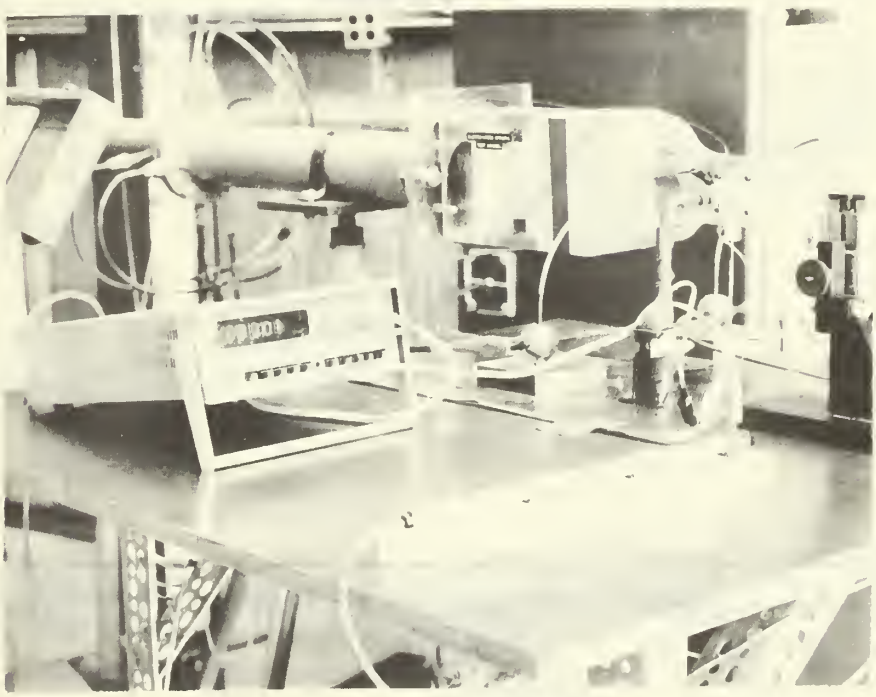

FIGURE XV MULTIMETER AND DIODE BANK

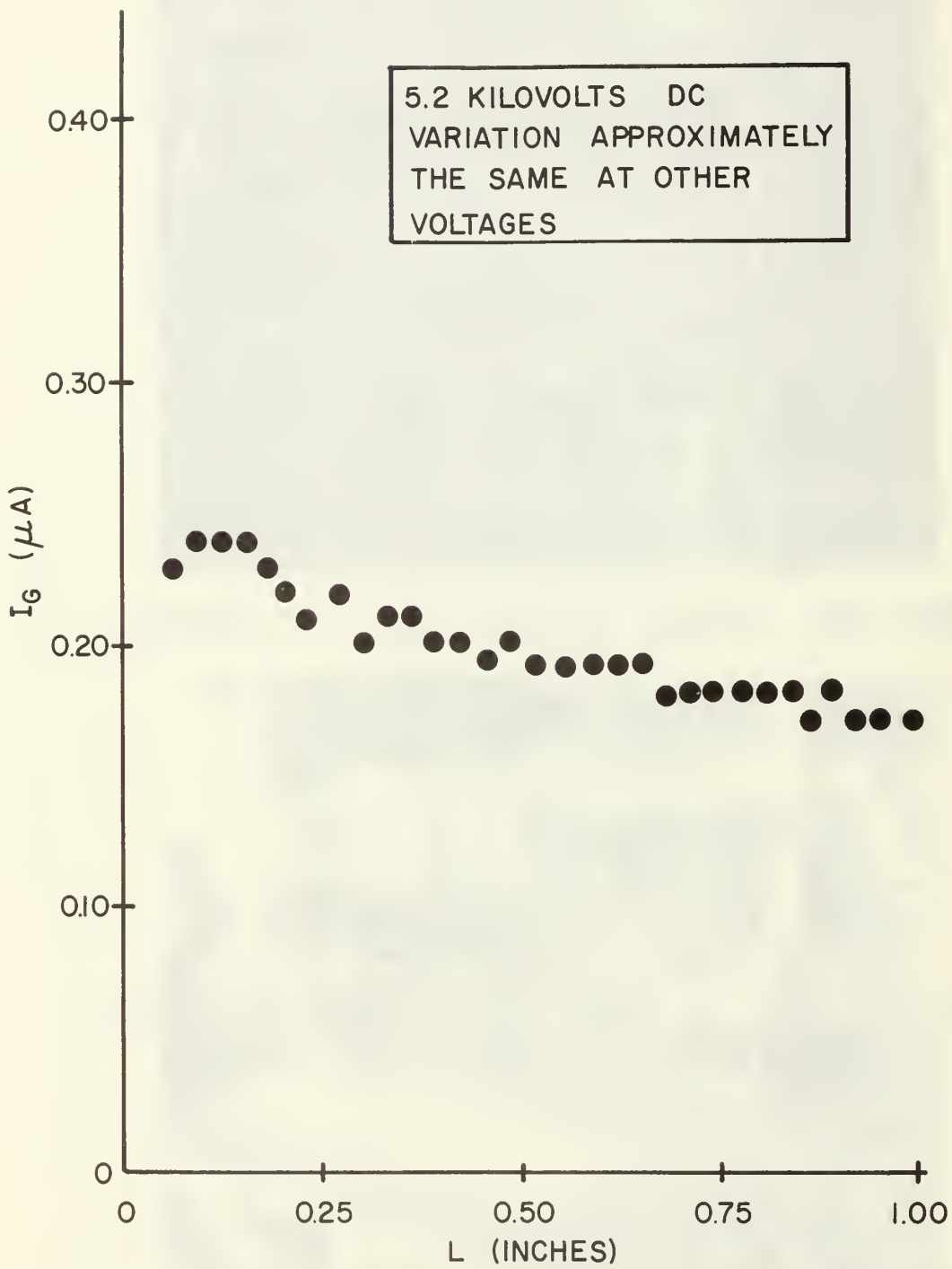

FIGURE XVI GENERATOR CURRENT VS COLLECTOR DISTANCE FROM NOZZLE EXIT

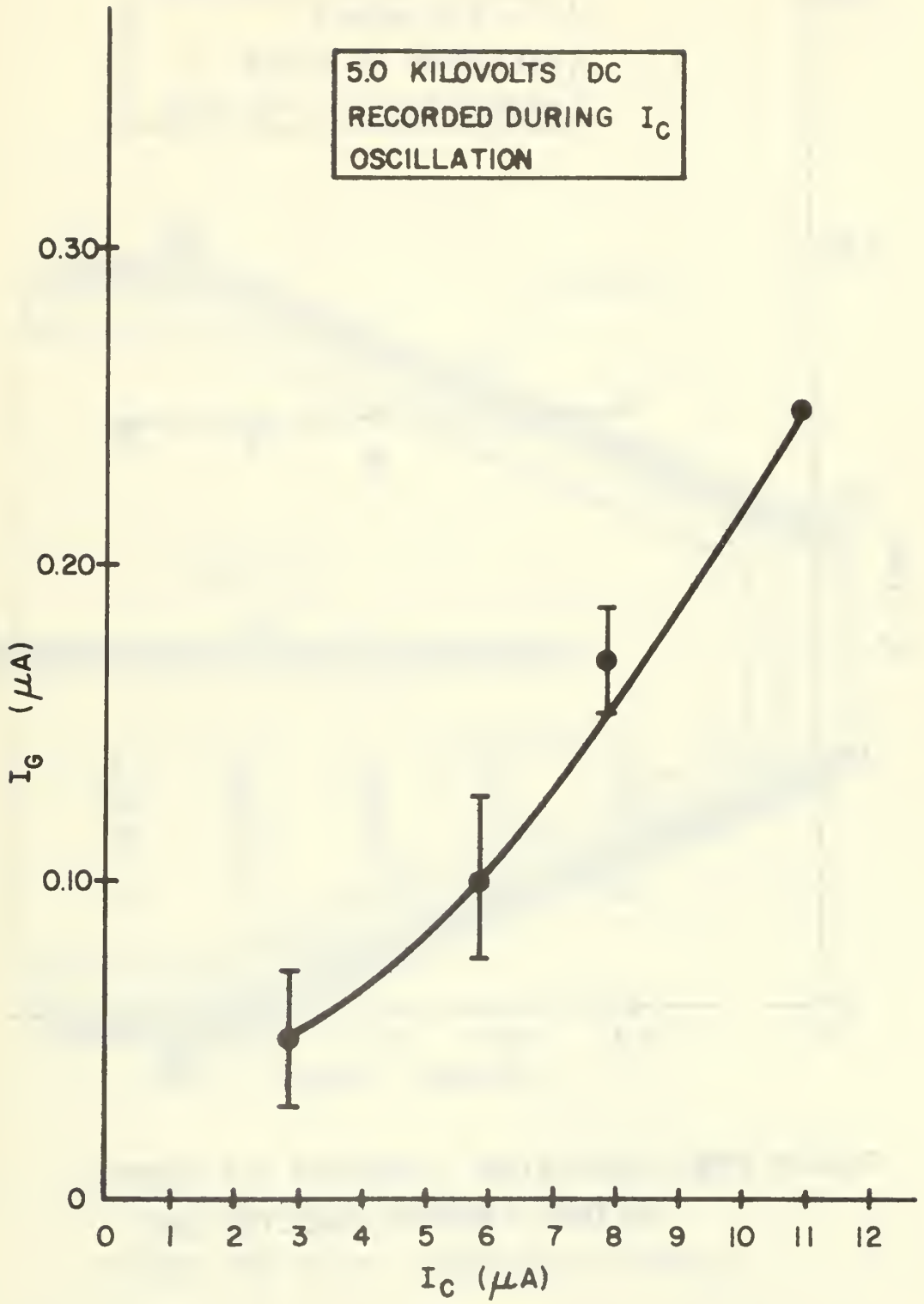

FIGURE XVII GENERATOR CURRENT VS CORONA CURRENT - MICRON INJECTOR UNIT

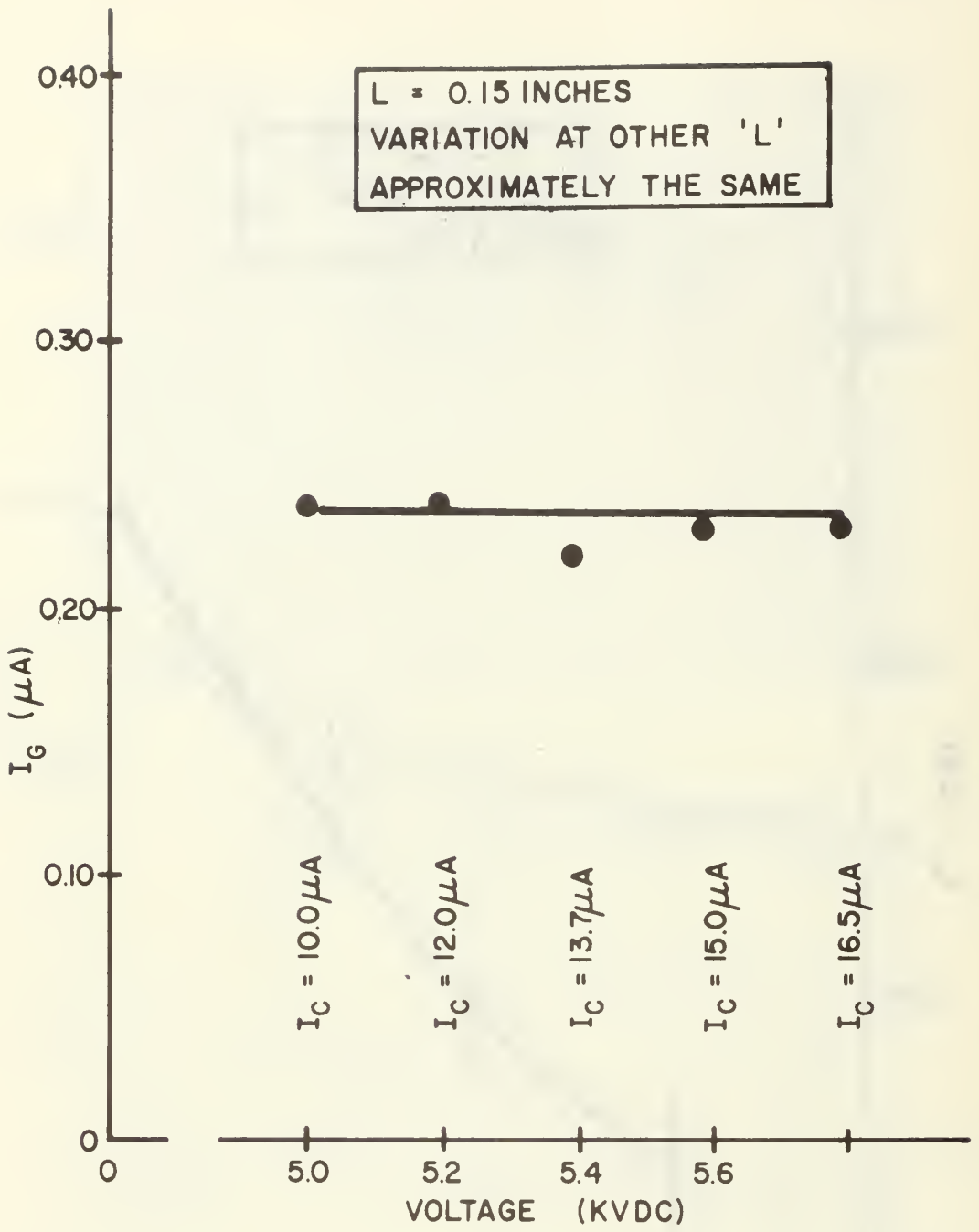

FIGURE XVII GENERATOR CURRENT VS CORONA VOLTAGE - MICRON INJECTOR UNIT

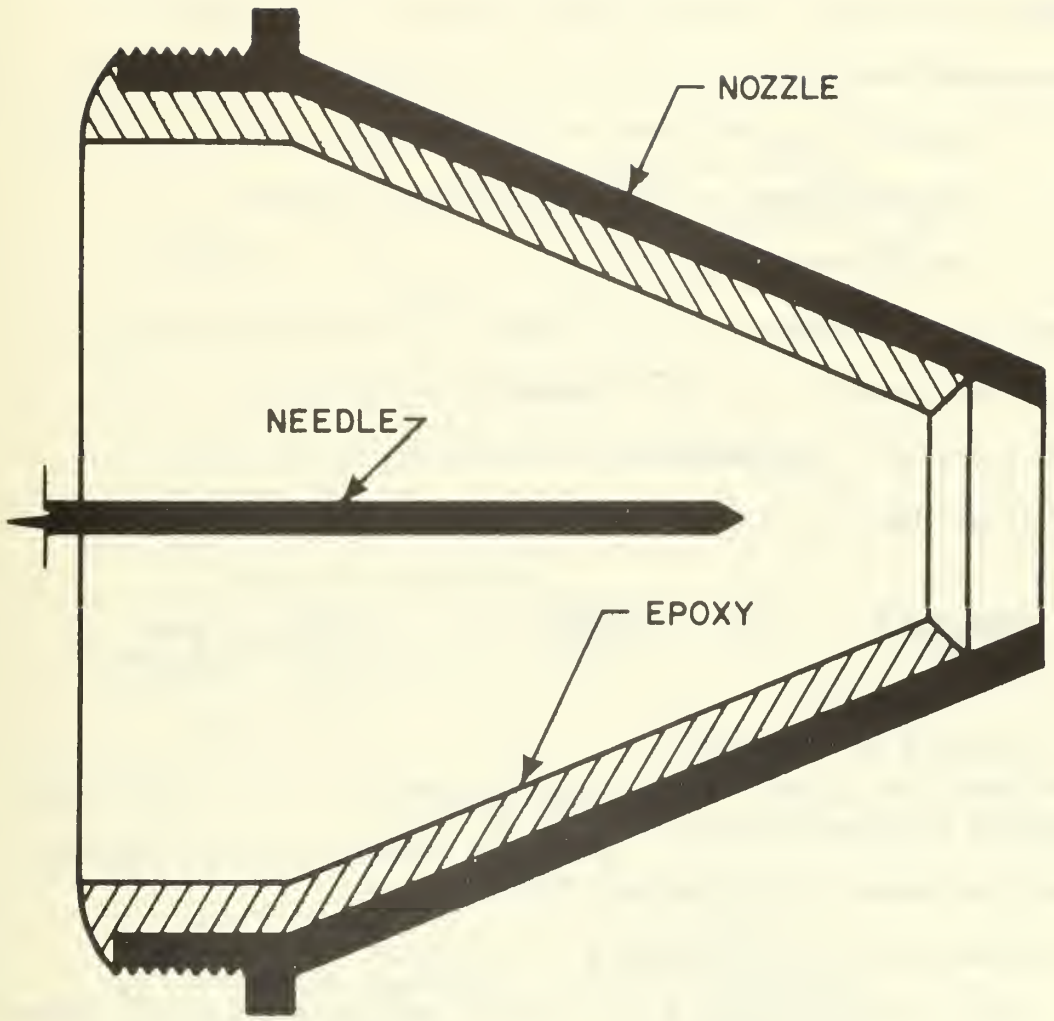

FIGURE XIX EPOXY COATING ON NOZZLE

APPENDIX A

CALCULATION OF NECESSARY STEAM FLOW RATE

Basic assumptions:

1. maximum desired current = 10^{-4} amperes
2. average charge per ion = 10^{2} electron charges
3. micron sized ions

1 amp = 1 coulomb/sec $\therefore$ 10^{-4} amp = 10^{-4} coulomb/sec

1 electron charge = 1.6×10^{-19} coulomb

$\therefore$ 1.6×10^{-17} coulomb/ion

It follows that, for a current of 10^{-4} amp:

$$\frac{\text{ions req'd}}{\text{sec}} = 10^{-4} \frac{\text{coulomb}}{\text{sec}} \times \frac{\text{ion}}{1.6 \times 10^{-17} \text{ coulomb}}$$

$$= 6.25 \times 10^{12} \text{ ions/sec}$$

Volume of 1 micron particle = 5.25×10^{-13} cm^3

Density of water = 2.204 lbm/cm^3 (liquid)

$\therefore$ Flow rate for 100% charging efficiency =

6.25×10^{12} ions/sec X 5.25×10^{-13} cm^3/ion X 2.2×10^{-3} lbm/cm

$= 7.25 \times 10^{-3}$ lbm/sec

With this flow rate as a basis, steam mass flow rates were chosen which would bracket the theoretical value.

APPENDIX B

CALCULATION OF NOZZLE EXIT AREAS

Assumption:

1. Superheated steam may be approximately treated as an ideal gas.

The analysis below represents a preliminary estimate of the exit areas.

Ideal gas equation used[8]:

$$\left(\frac{W}{A}\right)_{max} = \frac{W}{A^*} = \sqrt{\frac{k}{R}\left(\frac{2}{k+1}\right)^{\frac{k+1}{k-1}}}\frac{P_o}{\sqrt{T_o}}$$

where:

W = mass flow rate lbm/sec

A* = nozzle exit area for choked flow

$k = c_p/c_v$ for steam = 1.33

R = 85.6 ft-lbf/ R-lbm

P_o = 30 psi

T_o = 710° R

Substituting into the above equation, the following exit areas were obtained for each selected flow rate:

1. W = 0.01 lbm/sec, $A = 0.02157\ in^2$
2. W = 0.005 lbm/sec, $A = 0.01079\ in^2$
3. W = 0.001 lbm/sec, $A = 0.002157\ in^2$

Nozzles were designed with the following guidelines:

1. Add 10% to exit area for real gas effects
2. Nozzle half angle to be approx. 30°.
3. Max nozzle length to be approx. 1 cm.
4. Max entrance to exit area ratio = 20.

The nozzle dimensions are shown in Figure B-1. No attempt has been made as yet to determine what the actual flow rate for each nozzle is.

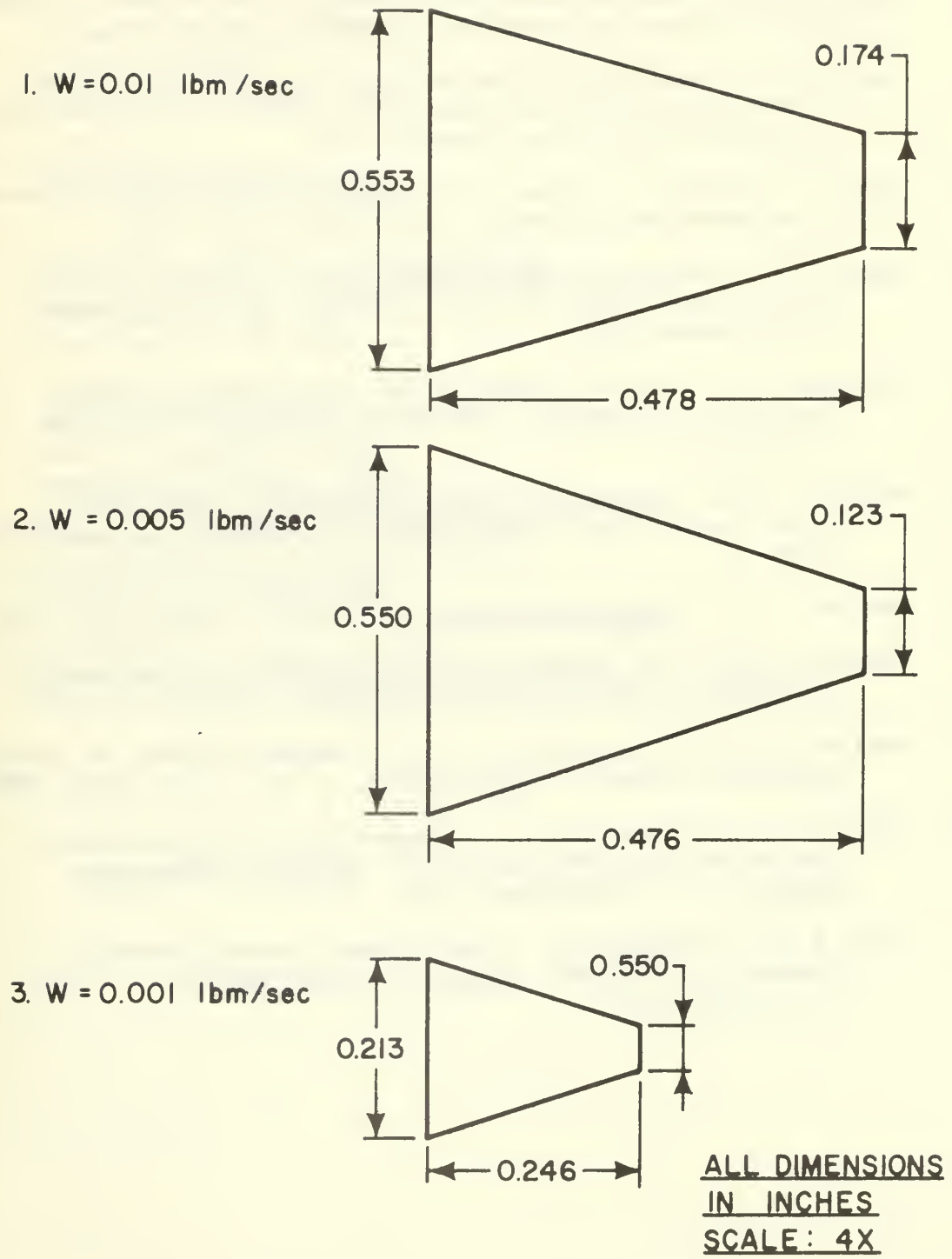

FIGURE B-I NOZZLE DIMENSIONS

BIBLIOGRAPHY

1. Smith, J. M., Electrodynamic Power Generation-Experimental Studies, Space Sciences Laboratory Report R62SD27, March 1962.

2. Marks, A., Experimental Investigation of a High Potential, High Voltage Electrogasdynamic Generator, Marks Polarized Corporation Report Now-0582-c, December 1967.

3. Marks, A., Barreto, E., Chu, C. K., Charged Aerosol Energy Converter, AIAA Summer Meeting Report 63-158, June 17-20, 1963.

4. Kahn, B., A Continuation of the Basic Study of Slender Channel Electrogasdynamics, Aerospace Research Laboratory Report 65-4, January 1965.

5. Gourdine, M. C., Study of MHD and EHD Free Convection Energy Converters, Plasmadyne Corporation Report ASD-TDR 62-320, June 1962.

6. Wallace, D. W., Molecular Ion Electrogasdynamic Flow Channel, M. S. Thesis, Naval Postgraduate School, Monterey, California, 1969.

7. Cobine, J. D., Gaseous Conductors, p. 248-281. McGraw-Hill, 1941.

8. Shapiro, A. H., The Dynamics and Thermodynamics of Compressible Fluid Flow, p. 85, Ronald Press, 1953.

9. Pfeifer, R. J. and Hendricks, C. D., "Parameter Studies of Electrogasdynamic Spraying", AIAA Journal, v. 16, p. 496, March 1968.

10. Hirth, J. P. and Pound, G. M., "Condensation and Evaporation, Nucleation and Growth Kinetics", Progress in Materials Science, v. 11, MacMillan, 1963.

11. Hill, P. G., "Condensation of Water Vapor During Supersonic Expansion in Nozzles", Journal of Fluid Mechanics, v. 25-3, p. 593-620, 1966.

INITIAL DISTRIBUTION LIST

		No. Copies
1.	Defense Documentation Center Cameron Station Alexandria, Virginia 22314	20
2.	Library Naval Postgraduate School Monterey, California 93940	2
3.	Commander, Naval Air Systems Command Attn: Mr. Milton A. Knight (Code AIR-34001) Department of the Navy Washington, D. C. 20360	1
4.	Professor O. Biblarz Department of Aeronautics Naval Postgraduate School Monterey, California 93940	4
5.	Chairman, Department of Aeronautics Naval Postgraduate School Monterey, California 93940	1
6.	LTJG William T. Ober III, USN 76 Salem Street Andover, Massachusetts 01810	1

DOCUMENT CONTROL DATA - R&D

(Security classification of title, body of abstract and indexing annotation must be entered when the overall report is classified)

1 ORIGINATING ACTIVITY (Corporate author)	2a REPORT SECURITY CLASSIFICATION
Naval Postgraduate School Monterey, California 93940	Unclassified
	2b GROUP

3 REPORT TITLE

Ion Injectors for Single- and Two-Phase Electrogasdynamic Generators

4. DESCRIPTIVE NOTES (Type of report and inclusive dates)

Master's Thesis; June 1969

5. AUTHOR(S) (Last name, first name, initial)

William Taylor Ober II

6 REPORT DATE	7a TOTAL NO. OF PAGES	7b. NO. OF REFS
June 1969	47	11

8a CONTRACT OR GRANT NO.	9a. ORIGINATOR'S REPORT NUMBER(S)
b. PROJECT NO.	
c.	9b. OTHER REPORT NO(S) (Any other numbers that may be assigned this report)
d	

10. AVAILABILITY/LIMITATION NOTICES

Distribution of this document is unlimited

11. SUPPLEMENTARY NOTES	12. SPONSORING MILITARY ACTIVITY
	Naval Postgraduate School Monterey, California 93940

13. ABSTRACT

Systems suitable for the injection of ions into electrogasdynamic (EGD) generator devices were built and tested. The mechanism of injection was based on a corona discharge, whereby ions moving through an electric field can be intercepted by a gaseous flow. The intercepted ions are of one polarity, insuring selective ion injection. Two types of injector units were investigated. One was a molecular ion device which produced ions directly from the carrier gas, and the other created larger sized ions, resulting in an aerosol flow. The latter consisted of passing saturated steam through a corona discharge and injecting it into an air stream. In order to aid the injection process, the wake of a cylinder in the air stream was utilized in both cases. Most of the work done here was devoted to the design and testing of the aerosol flow device. The degree of success was moderate.

DD FORM 1 JAN 64 1473

14 KEY WORDS	LINK A		LINK B		LINK C	
	ROLE	WT	ROLE	WT	ROLE	WT
Electrogasdynamic						
Ion						
Micron Sized Particles						
Generator						

United States
Naval Postgraduate School

THESIS

MOLECULAR-ION ELECTROGASDYNAMIC

FLOW CHANNEL

by

David William Wallace

June 1969

pages D1 - D56

Molecular-ion Electrogasdynamic

Flow Channel

by

David William Wallace
Lieutenant (junior grade), United States Navy
B. S., United States Naval Academy, 1968

Submitted in partial fulfillment of the
requirements for the degree of

MASTER OF SCIENCE

IN

AERONAUTICAL ENGINEERING

from the

NAVAL POSTGRADUATE SCHOOL
June 1969

ABSTRACT

This investigation evaluates the operating characteristics of an EGD (electrogasdynamic) generator system which utilizes air both as the carrier fluid and as the source of injected ions. The design and construction of a flow channel and a corona ion injector are discussed, the performance of the ion injector is examined, and the results of attempts to obtain work by EGD energy conversion are presented. The experimental results presented and discussed are in reasonable agreement with expectations. The high mobility of molecular ions inhibits the conversion process and only 0.5% of the ions were removed from the corona by the air flow. Suggestions for improvements on the present system and the design of an advanced system are made.

TABLE OF CONTENTS

LIST OF ILLUSTRATIONS

LIST OF SYMBOLS

Symbol	
A'	Percent of test channel cross-section within boundary layer
b	Barometric pressure (in. Hg.)
D_2	Orifice diameter (inches)
h_w	Pressure differential across the orifice (in. H_2O)
I_c	Corona current
I_g	Collector current
K	Dimensionless discharge coefficient
KV	Kilovolt (10^3 volts)
M	Mach number
P_b	Absolute pressure at test section (psi)
P_1	Absolute pressure at orifice (psi)
ΔP	Pressure differential of pitot-static tube (cm H_2O)
q	Rate of heat loss
RMS	Root-mean-square
T	Temperature (°R)
T_f	Flow field temperature
T_w	Wire temperature
U_∞	Freestream velocity (ft/sec)
u	Average velocity in the boundary layer (ft/sec)
$\bar{u}$	Mass-mean velocity (ft/sec)

V_c	Corona voltage
Y_1	Dimensionless expansion factor
α	Dimensionless area multiplier
ρ_b	Fluid density at test channel (lb/ft^3)
ρ_1	Fluid density at orifice (lb/ft^3)
μA	Micro-ampere (10^{-6} amp)

ACKNOWLEDGEMENT

The author expresses his sincere appreciation to Professor Oscar Biblarz of the Naval Postgraduate School, Monterey, California, for his assistance and guidance, and to Mr. Pat Hickey, Naval Postgraduate School technician, for his many technical services. Special thanks are given to fellow student W. T. Ober, LT(j.g.), USN, for principally providing the corona ion injector.

I. INTRODUCTION

High voltage, low current power sources have not been exploited commercially due to their high cost and the generally bulky size of the necessary equipment. The most familiar apparatus of this type is the Van de Graaff generator which 'pumps' charges from ground to a collector device by means of a moving belt, thereby generating a high electric potential between the collector and ground. In 1959, W. E. Bennett[1] pointed out that since a greater charge could be carried in a volume than on a surface (such as the belt of a Van de Graaff generator) and since the charge transfer rate could be much higher with a moving fluid flow, the fluidic Van de Graaff generator promised higher currents and greater efficiency. Such a device is variously termed an electrogasdynamic (EGD), electrohydrodynamic (EHD), or electrofluiddynamic (EFD) generator, depending on the transport medium used, and is the subject of this investigation.

As indicated by the title of this report, we have chosen to pursue the investigation of the electrogasdynamic type device, henceforth referred to as the EGD system. Although it has been shown by various researchers[3] that higher efficiencies and greater currents are obtained if micron-sized charged particles are injected into the system, we have confined ourselves in this project to molecular ions, using air both as the transport fluid and the source of charged particles. It should

be noted that this investigation is the preliminary stage of a more comprehensive, long-term project being carried on by Professor Oscar Biblarz, Department of Aeronautics, Naval Postgraduate School.

An experimental EGD generator system was fabricated and installed in Building 230 at the Naval Postgraduate School, Monterey, California, utilizing a corona discharge to provide charged particles. A test program was carried out to determine the basic performance of the flow channel and ion injector, and to evaluate the molecular-ion EGD generator system as a whole.

II. PRINCIPLES OF OPERATION

The electrogasdynamic generator is analogous to the Van de Graaff generator in principle: a moving medium transports charged particles against an electric field to a collector. Thus the kinetic energy of the transport medium is converted into electrical energy. In the case of the Van de Graaff generator, a moving belt is used to transport the charged particles. For the Van de Graaff generator, the amount of charge transported is limited by two physical criteria --- the surface area of the belt and the velocity of the belt. By using a moving fluid for the transport medium, the amount of charge transportable is greatly increased because: 1) the amount of charge carried is now more a function of volume rather than surface area; and 2) the fluid can travel at a higher speed than a mechanical belt.[2]

An EGD generator consists of three basic components: 1) a charged-particle injector; 2) a dielectric conversion section; 3) a collector. Figure 1 is a schematic of an EGD generator system.

Charged particle injection at near-atmospheric pressures is most easily accomplished using a corona discharge[4]. A high voltage is placed across a needle and ring, producing an intense electrical field in the region between the needle and the ring. Ionization of gas molecules in this region is caused by the electric field, with a sheath of oppositely charged particles being formed around the needle. This charge sheath intensifies the field adjacent to the needle, and diminishes

the field external to the sheath extending to the ring. Ions of like charge to the needle then drift toward the ring, as shown in Figure 2. The ionization process is exponential in nature, and produces electron avalanches which are a mechanism by which current flows across the corona gap. Each avalanch decreases the gap potential. Thus at low voltages, complete ionization across the gap is stopped by the associated potential decrease before breakdown can occur. At a sufficiently high voltage, however, the gap potential, even with the loss due to the electron avalanches, is sufficient to cause complete ionization and a direct current flow across the gap. Breakdown is undesireable because ions are no longer drifting alone towards the ring.[5]

In the case of a positive needle corona, gas molecules are stripped of an electron and drift towards the ring as positive charged particles. With a negative needle corona, the drifting particles may be free electrons or negative ions formed by electron attachment. Since both free electrons and negative ions have a higher mobility than positive ions, a negative needle corona produces higher current than a positive needle corona. As long as the breakdown potential of the gas is not exceeded, any current flowing through the corona unit will be due to ions reaching the ring and being neutralized. Ideally, if an external force could be applied which would remove all the charged particles drifting toward the ring before they reached it, thus preventing current flow across the corona, the net work done by the corona circuit power source would be zero.

The external force used to remove the charged particles from the corona field may be derived from the kinetic energy of a gas flow. For the ions drifting toward the ring to be removed by the air flow, the kinetic energy imparted to them by the flow must be greater than the electrostatic energy of the corona unit. In the case of molecular-sized particles this transfer of kinetic energy is accomplished by molecular collisions between the air flow particles and the charged ions, and thus is dependent on the mobility of the charged particles. (Mobility is defined as the average drift velocity per unit electric field, where the average drift velocity is related to the reduction of the ion mean free path by collisions with the gas molecules). Mobility decreases as density increases, and therefore is also inversely related to pressure. Thus the removal of charged particles from the corona, which increases as mobility decreases, increases with the increasing pressure.

Once the gas molecules, now charged, are removed from the corona, their electrical energy is retrieved by means of a collector. This may be a wire mesh, a hollow cylinder, or a conducting rod. The rod seems to be the most efficient method of collection, although it is not understood exactly how the collection process occurs.[6]

The retrieval of charges at the collector causes a buildup of a potential between the collector and ground, and the resulting current flow through the collector circuit is the work done by the air flow, or the output of the EGD system.

Figure 3 shows the wiring circuit of an EGD system. Ideally, there will be no current flow through the corona circuit ($I_C = 0$) since the ions will be swept downstream to the collector, producing a collector current (I_G).

With the corona-conversion process acting as a generator, a typical load curve might be obtained by placing the generator output across a suitable variable resistance. For a given resistance, a voltage versus current curve could be obtained which would include the maximum voltage-no current case (open circuit) and the no voltage-maximum current case (short circuit) as its limits. Since the conversion process at the corona was of primary interest, e.g., the percentage of corona ions being forced to the collector, the short circuit setup which indicated largest current through the collector was first used. After a significant collector current had been detected, the generator performance would have been further evaluated by determining the entire load curve, had more time been available.

III. EXPERIMENTAL APPARATUS

The EGD system fabricated was designed for approximate flow speeds of Mach 0.3 and for minimum flow turbulence at the test section where the corona unit was placed. Figure 4 shows the system schematic, while Figure 5 shows the flow channel in detail. A photograph and engineering drawing of the flow channel are provided in Figures 6 and 7, respectively. Air was supplied by a Carrier three stage centrifugal compressor (Figure 8) with a 4000 $ft^3/min.$ maximum inlet capacity and a maximum pressure ratio of two. The exit air temperature varied from 65°F to 240°F. The flow could be regulated, as shown in Figure 4, by two valves and exhausted to the atmosphere. The flow orifice shown in Figure 4 was used only to determine the accuracy of the pitot-static tube located in the flow channel, which in conjunction with the manometer bank was used to determine the flow rate setting (See Appendix A). The cooling bank was used to keep the temperature of the air flow close to ambient and to hasten the temperature stabilization. An iron-constantan thermocouple was used to determine the flow temperature.

The test channel was made of three-eighths inch Plexiglass which was chosen because of its high dielectric properties (volume resistivity=10^{12} ohms-cm). In addition, Plexiglass permitted the investigator to observe the interior of the test channel. A test channel plenum to test section area ratio of 10 to 1, and a series of consecutively finer honeycomb and wire mesh were used to reduce the freestream flow

turbulence to a level comparable to contemporary flow channels--0.14% RMS (i.e., the time-averaged magnitude of velocity fluctuations was 0.14% of the freestream velocity) according to a Ballantine RMS voltmeter. Using a Security Associates single-channel hot-wire probe, the channel boundary layers were determined so that the corona unit might be placed outside of the boundary layers. The boundary layers were found to be not fully developed, and at most only 0.15 inch thick which presented no interference with the test region.

Because the efficiency of a corona discharge depends in part on pressure, being more efficient at lower pressures, the corona unit was mounted on the downstream side of a Plexiglass cylinder placed horizontally in the flow channel. Thus, due to the pressure drop downstream of the cylinder, the pressure at the needle where the corona action is strongest was relatively low compared to the pressure at the ring, where the conversion process occurs. It was observed that the corona performance was also affected by turbulence in that turbulence tended to inhibit breakdown. Although this aspect of the corona unit was not investigated, turbulence levels in the wake of the cylinder were determined, and are given in Figure 9. The ring and needle leads were buried in the Plexiglass to minimize the possibility of point discharges and subsequent current leaks. Figure 10 is an isometric of the corona unit, while Figure 11 provides an engineering drawing of the corona device. The cylinder was three-eighths inch in diameter. The Reynolds number based on freestream velocity and cylinder diameter

for M=0.3 was 6.63×10^4, which is subcritical, indicating separation close to 90° from the horizontal centerline. The needle and ring were made of pure platinum wire with wire sizes of 0.010 and 0.020 inches respectively. Three different corona configurations were used. Their pertinent dimensions are summarized as follows:

Ring	Needle Length	Distance From Cylinder to Ring (smallest)	Ring Diameter
1	0.187 inch	0.187 inch	0.394 inch
2	0.062 inch	0.187 inch	0.315 inch
3	0.187 inch	0.187 inch	0.750 inch

The collector unit consisted of an iron rod (1/8" Dia.), sharpened to a needle point, which was mounted on an insulated traversal unit allowing vertical and horizontal movement for any axial position.

High voltage power was supplied to the corona unit by a Sorensen High Voltage D.C. Power Supply. This power supply produces up to 30KV and 20MA of current with a ripple of 2%, and has trip controls for both voltage and current. It also has the feature of reversible polarity.

The high voltage across the corona was measured with a Sensitive Research electrostatic voltmeter. This instrument has an internal impedance of 5×10^{15} ohms and reads RMS voltages up to 40KV on four scales.

Corona currents were measured with a Simpson 0-100 μA ammeter.

Collector currents were read using a Calico Digital Multimeter which had an amperage range of 0.01-1000 μA through the use of various scales.

Figure 12 is a photograph of the experimental setup.

IV. EXPERIMENTAL PROCEDURE

This investigation was divided into two parts: 1) design and construction of apparatus and determination of its airflow properties, and 2) testing of the EGD system.

The first part was preliminary to the second and consisted of determining and reducing, if necessary, the freestream turbulence; determining the test channel wall boundary layers; and exploring the corona-cylinder wake (See Appendix B). Turbulence levels were determined using the RMS voltmeter in conjunction with the hot-wire anemometer, assuming the boundary layer to start where the velocity dropped to 0.99 of the freestream velocity. After the freestream turbulence was lowered to an acceptable level by means of honeycomb and wire mesh screen, and the boundary layers were determined, the corona cylinder was placed in the test channel. Turbulence levels and wake boundaries were determined in order to insure that the corona ring was placed within the wake region where high turbulence levels would inhibit breakdown. This completed preliminary work and actual testing of the corona unit was begun.

The corona unit was first tested for continuity of all electrical connections. An effort was then made to minimize point sources which might enable current leakage. This problem was primarily attacked by devising the brass connector spheres shown in Figure 13. Then data for corona curves was taken without air flow, followed by data for

corona curves with air flow. Curves were obtained by holding the flow velocity constant and varying corona voltage, and by keeping corona voltage constant and varying flow velocity. Finally, the collector unit was positioned downstream of the corona unit. If a collector current was detected, the unit was moved about to determine the effect of position on collector current. Prior to each test run, the corona unit was cleansed with freon. This procedure was carried out for each of the three corona units.

V. RESULTS AND CONCLUSIONS

Figures 14 thru 17 show the data obtained by the procedure outlined previously. The general pattern is the same for each corona configuration (see page 19, this report), and thus only curves for a single configuration are given. Data reproductability was generally good. The main cause of data error was improper circuit connection; specifically, if the contact screws were not seated properly, internal corona discharges would occur, causing noticeable errors. Small data variances from run to run were caused by the relative insensitivity of the ammeter in the corona circuit. The smallest scale division of this ammeter was 2 μA and the meter itself had an accuracy no better than ± 2 μA. Other data discrepancies may have been due to humidity variations, misalignment of the corona needle, or power supply irregularities.

Figure 14 is a typical comparison of corona current versus voltage with no airflow for positive and negative needle coronas, using corona unit 1. As shown, a negative needle corona produces much higher corona currents for a given voltage than a positive needle corona, and the breakdown of a negative needle corona greatly exceeds that of the positive needle. However, in subsequent data runs the positive needle corona was used since this polarity produces ions drifting toward the ring of a lower mobility than those produced by a negative needle corona. Thus greater collector currents would be expected with a positive needle corona.

The next chart, Figure 15, shows the results of adding airflow to the positive needle corona. At low test section Mach numbers ($M < 0.3$), the corona current at a given voltage is considerably less and the breakdown potential is slightly higher than that of the no-flow corona. At higher Mach numbers ($M > 0.3$), the corona currents at a given voltage are only slightly less than that of a no-flow corona but the breakdown potentials have dropped considerably. It is believed that this behavior of the corona current --- first decreasing, then increasing as the velocity is increased at a given voltage --- is due to interaction between the velocity and pressure effects on corona efficiency. At low velocities and pressures velocity has a greater effect than pressure, thus causing decreasing current with increasing velocity. After a certain increase in velocity and accompanying decrease in pressure, however, the pressure effect becomes dominant over the velocity effect, causing an increasein corona current with further velocity increase.

The current-voltage-velocity relationship was investigated with a different approach by holding the corona voltage constant and examining how the corona current reacted to changes in air flow rate. The results are shown in Figure 16. It can be seen that addition of flow rate causes an initial drop in corona current at any voltage. The corona current then increases as velocity increases, but tends to remain below the no-flow level. Both the initial drop and gradual increase are more pronounced at high voltages. Data points cross-plotted from Figure 16 to Figure 15 lie on the existing data curves.

Efforts to detect collector current using corona unit 1 at any air flow rate were generally unproductive, and led to the designing of corona unit 2. This unit had the feature of a shorter needle but because of a smaller-radius ring the distance between the needle tip and the ring was the same as that of corona unit 1. Thus the electric field between the needle and the ring would tend to help drive the drifting ions downstream. A main problem encountered was the action of the collector needle as a corona needle when placed close enough to the ring to detect generated current. Any collector current which may have been present was being overshadowed by the backward flowing current of the unwanted corona. This problem was eliminated by placing a set of three International Rectifier Corporation diodes in the collector circuit which prevented any reverse current. Since no collector current was yet detectable, another corona unit, unit 3, was built. This unit had a larger diameter ring which reduced the electric field on the charged ions, enhancing their chances of receiving enough kinetic energy to be blown downstream to the collector. Figure 17 shows the results of this final effort. Since no current was detected with corona units 1 and 2 in the same range of voltages using the diodes to prevent a reverse corona, the currents obtained were reasonably assured to be collector currents rather than reverse current leakage through the diodes. The bars representing data points are due to the fact that these currents were read from a digital ammeter on the last digit of the readout. Thus it was deemed inappropriate to average the values which fluctuated over

the range shown. Collector current increased with increasing voltage, being limited by the breakdown potential of the corona. The optimal collector position was on the corona ring centerline, one inch downstream of the ring plane. Any horizontal or vertical movement from this position caused a decrease in collector current. Changes in air flow rate seemed to make little difference in the amount of collector current, although as can be seen by Figure 17, the amount of current detectable was so minute that changes may have been unreadable due to limitations of the ammeter. The trend of the curve is reasonable in that increased voltage causes increased corona current. As corona current rises, more ions are available for conversion.

VI. RECOMMENDATIONS

As stated earlier, for an EGD system to produce power, the force imparted by the gas flow on the ions of the corona must exceed the attractive force of the corona field. Since variation of the corona voltage is relatively restricted by breakdown, the most apparent improvement would be to increase the rate of energy transfer between the flow particles and the injected ions. On this basis, the following recommendations are made:

a. Investigate further the pressure wake of the cylinder to re-evaluate its effect on the EGD process. The benefits to corona efficiency caused by the decreased pressure of the cylinder wake may be less than the detrimental effects on the conversion process, which is more efficient at higher pressures.

b. Conduct further modified experiments by injecting micron-sized particles (such as dust) into the air flow upstream of the corona unit. Such particle ions have a much lower mobility than air ions and thus should lead to higher conversion efficiencies.

c. Develop a new injection system which would inject micron-sized charged particles into the air flow. (Such a system might use steam as the injection medium. LT(jg) W. T. Ober, USN, has conducted an investigation of a system of this type.[7]) These lower mobility ions would again increase the conversion efficiency.

d. Since ion mobility is reduced by increased pressure, the conversion process would be enhanced if the operating pressure (atmospheric for this investigation) could be increased.

e. Continue efforts to improve data reproductibility by eliminating sources of current leakage and other adverse system variables.

APPENDIX A

Flow Measurements

The experimental facility air flow delivery tube had a square-edged orifice, built to ASME standards,[8] for determination of flow rates. However, the equation for mass flow as determined by this device is awkward and requires an iterative procedure to obtain a value. Since frequent flow rate changes were necessary for this investigation and extremely accurate flow rate determination was not a requirement, it was deemed sufficient to measure flow rate using a pitot-static tube located in the test section. However, the following calculations were made to ascertain how closely the pitot-static and orifice measurements correlated.

The development of the orifice flow rate equation is, according to reference 8:

$$W = 359.1(D_2)^2 Y_1 \propto K\sqrt{\rho_1 h_w} \quad \text{(lb/hr)} \qquad \text{(A-1)}$$

D_2 = orifice diameter, inches

ρ_1 = fluid density at orifice, lb/ft^3

h_w = pressure differential across orifice, inches H_2O

Y_1 = dimensionless expansion factor

K = dimensionless discharge coefficient

$\propto$ = dimensionless area multiplier

$$K = 0.6876 \qquad \text{(Ref. 8, p. 221)} \tag{A-2}$$

ρ_1 may be determined as follows:

$$\rho_1 = MP_1/(10.73)T_1\mu_1 \tag{A-3}$$

T_1 = temperature above orifice, °R

P_1 = absolute pressure above orifice, lb/ft^2

M = 28.96 for air, $\frac{lbm}{lb\text{-mole}}$

$\mu_1 \simeq 1.0$ (Ref. 8, Fig. 138)

Y_1 is obtained from the following formula:

$$Y_1 = 1-(.41 + .35\beta^4)h_w/KP_1 \tag{A-4}$$

β = orifice to pipe diameter ratio

K = 1.4 for air

Y_1, δ, and α are all very close to unity. For D_2 = 2.15 inches, the orifice flow rate equation reduces to:

$$W = 1131\sqrt{\rho_1 h_w} \quad (lb/hr) \tag{A-5}$$

or by the continuity equation:

$$\bar{u} = W/\rho_b A \tag{A-6}$$

A = test channel cross-sectional area

$\bar{u}$ = mass-mean velocity

ρ_b = fluid density in test channel

The equation for flow determination by the pitot tube is derived from Bernoulli's equation:

$$p_a + \rho_a U_a^2/2g = p_b + \rho_b U_b^2/2g \qquad \text{(A-7)}$$

but $U_a = 0$, $\rho_a = \rho_b$, giving after rearrangement:

$$U_\infty = \sqrt{2g\Delta P/\rho_b} \quad \text{(ft/sec)} \qquad \text{(A-8)}$$

$g = 32.2$ ft/sec^2

ΔP = pitot tube pressure differential, cm H_2O.

However, the orifice equation gives mass-mean flow rate while the pitot tube indicates freestream velocity. Therefore, the pitot tube value is corrected according to Reference 9, page 536. For a 1/7-power velocity distribution, in the boundary layer,

(u/U_∞) average = .875.

Therefore, the mass-mean velocity can be computed by the following formula:

$$\bar{u} = [A' \times u] + [(1-A') \times U_\infty] \qquad \text{(A-9)}$$

u = average velocity in the boundary layer

U_∞ = freestream velocity

A' = percent of cross-sectional area within the boundary layer.

Assuming a boundary layer thickness of 0.1 inch, A-9 reduces to:

$$\bar{u} = .28u + .72U_\infty \qquad \text{(A-10)}$$

or

$$\bar{u} = .965U_\infty \qquad \text{(A-11)}$$

The following data is reduced for comparison:

Orifice	Pitot Tube
$t_1 = 69°F$	$t_2 = 68°F$
$h_w = 26.1$ cm H_2O	$\Delta P = 46.3$ cm H_2O
$P_1 = 86.6$ cm H_2O	$P_2 = 70.0$ cm H_2O
b = 30.06 in Hg	b = 30.06 in Hg
$\rho_1 = .0819$ [by (A-3)]	$\rho_b = .0806$ [by (A-3)]
	$U_\infty = 276$ ft/sec [by (A-8)]
$\bar{u} = 280$ ft/sec [by (A-6)]	$\bar{u} = 266$ ft/sec [by (A-11)]

Thus flow rate determination using the pitot-static tube yields values approximately 5% in error on the low side. Assuming constant density for air, the following formula, which includes a factor to correct for this error, was used to compute flow velocities:

$$\bar{u} = 40.95\sqrt{\Delta P} \quad \text{(ft/sec)}$$

As before, ΔP is the pitot-static tube pressure differential in centimeters of water.

APPENDIX B

Flow Determination Instrumentation

Before choosing the means of determining the flow properties of the test channel, four different devices were considered: the hot-wire anemometer, thermistor, conductivity probe, and pitot-static tube. The thermistor and conductivity probes are devices which measure temperature and temperature fluctuations. The thermal sensitivity of the thermistor is about twice that of the conductivity probe (-4%/°C versus -2%/°C) but has a slower frequency response. However, both the thermistor and the conductivity probe are insensitive to velocity fluctuations.[10] Inasmuch as the flow properties which were under investigation were velocity and velocity fluctuations (turbulence), the thermistor and conductivity probe were immediately eliminated as useful.

Thus it was decided to use the hot-wire anemometer which gives both the relative velocity (generally the output indicator is adjusted to maximum scale for a specific local velocity) and, in conjunction with a RMS voltmeter, velocity fluctuations. This device utilizes King's Law which gives the rate of heat loss from an electrically heated fine wire exposed to a flow:

$$q = (A + B\sqrt{U})\ (T_w - T_f)$$ where

q = rate of heat loss

T_w = wire temperature

T_f = flow field temperature

U = velocity normal to the wire

A and B are constants dependent on geometrical factors and fluid property values. A hot-wire system may be operated in one of two modes: constant current or constant temperature. The constant temperature mode has a frequency response several orders higher than the constant current mode and thus has better response characteristics. In this mode a feedback amplifier is employed which senses the wire resistance and adjusts the wire heating current to maintain a constant wire temperature. Changes in flow velocity over the wire cause heating loss rate changes which are sensed by the amplifier as resistance changes. The hot-wire anemometer system used was a Security Associates Constant Temperature Hot-Wire Anemometer which utilizes a built-in analogue computer circuit to linearize the output.

In addition, a pitot-static tube was used to measure the flow mean velocity.

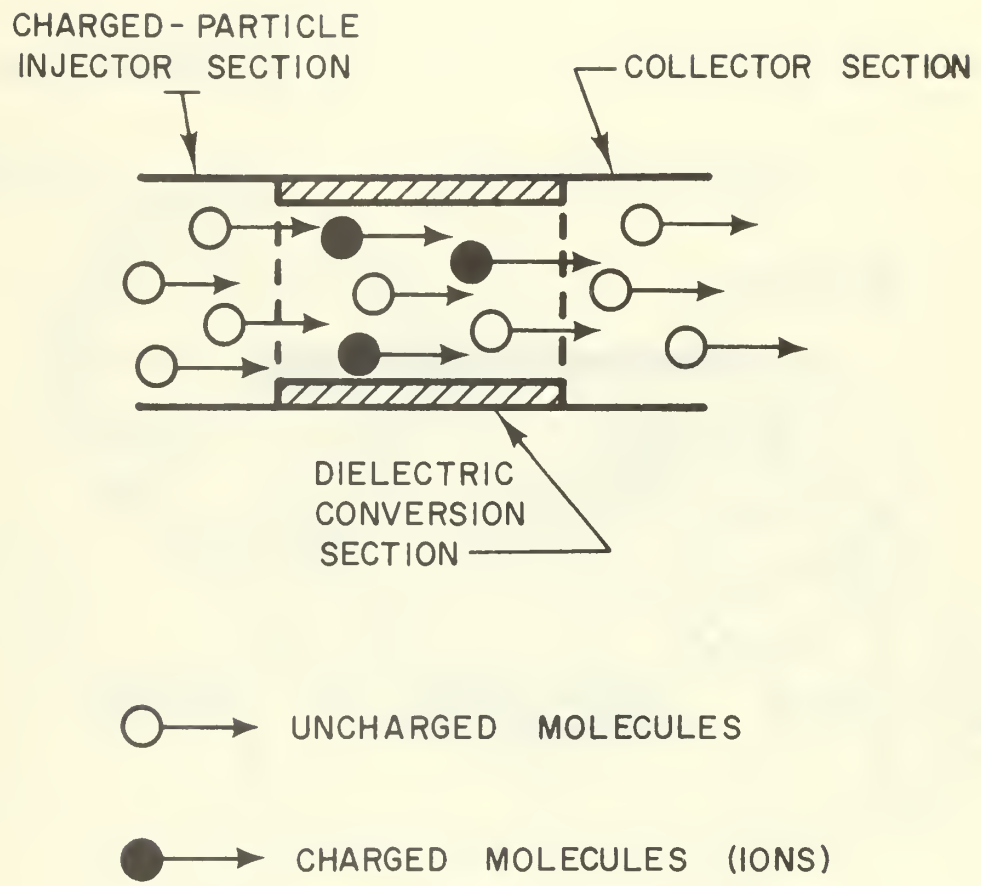

FIGURE I. EGD GENERATOR SCHEMATIC

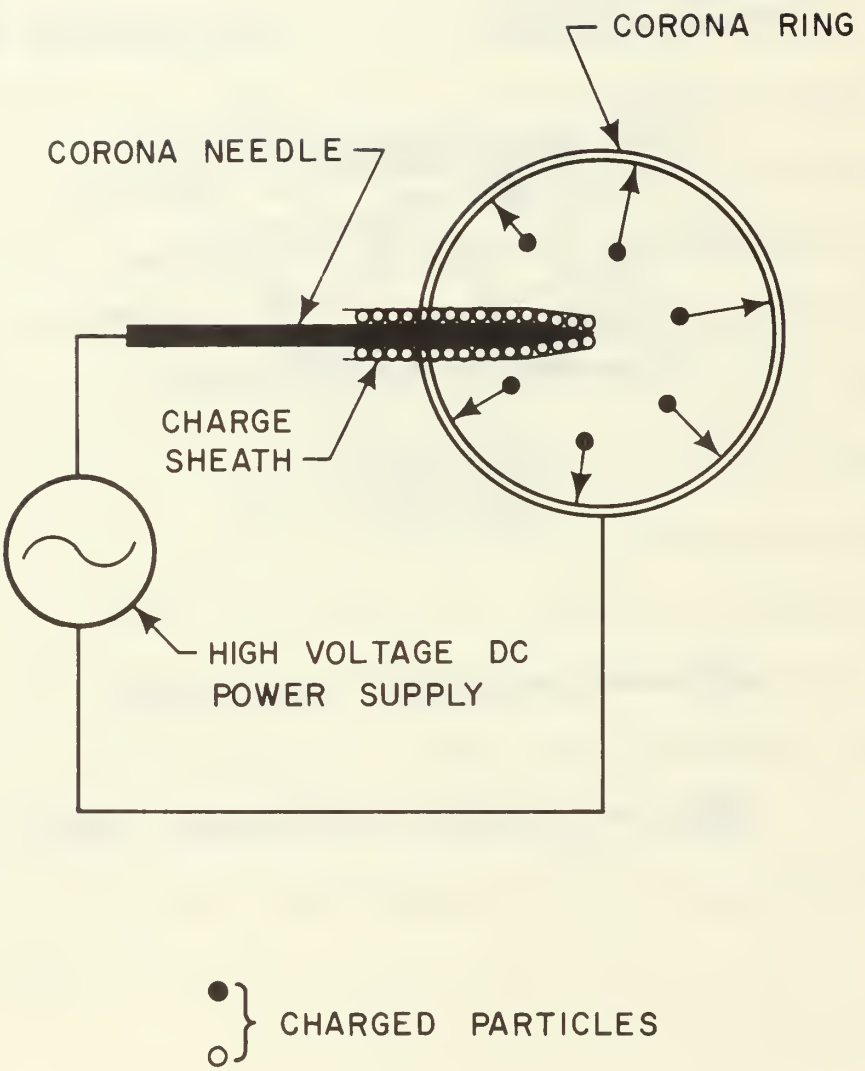

FIGURE 2. CORONA DISCHARGE PRINCIPLE

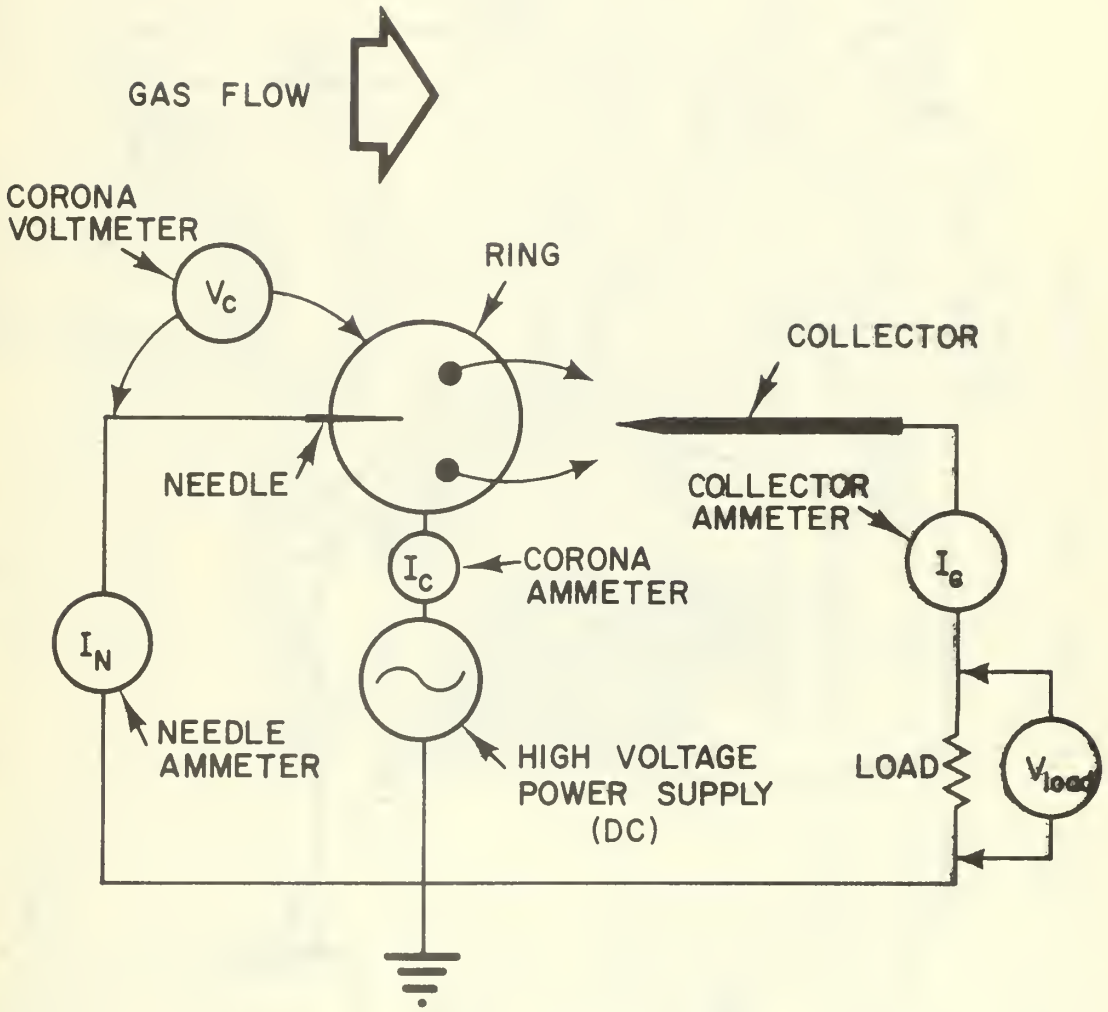

FIGURE 3. EGD SYSTEM WIRING CIRCUIT

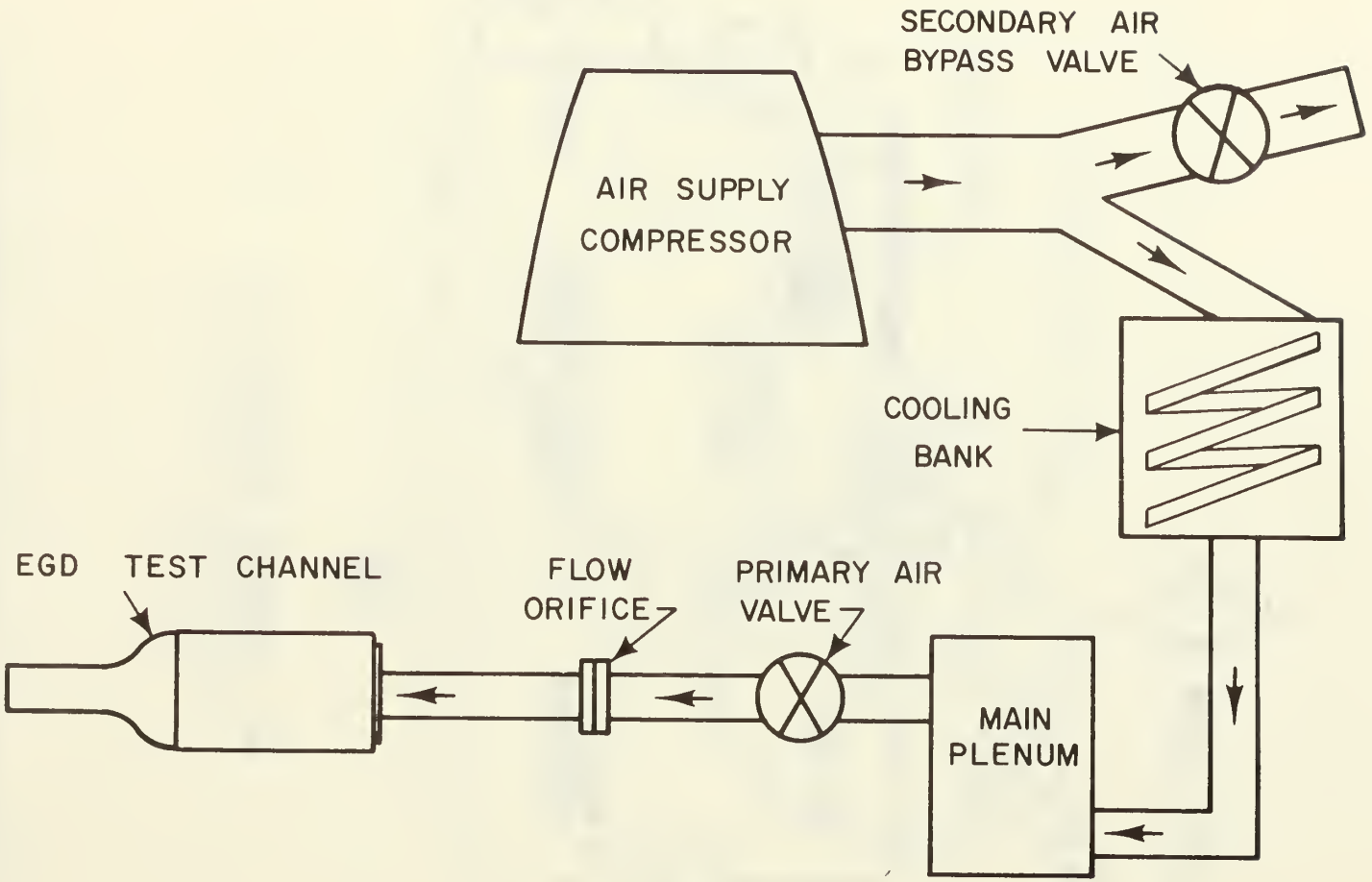

FIGURE 4. EGD SYSTEM SCHEMATIC

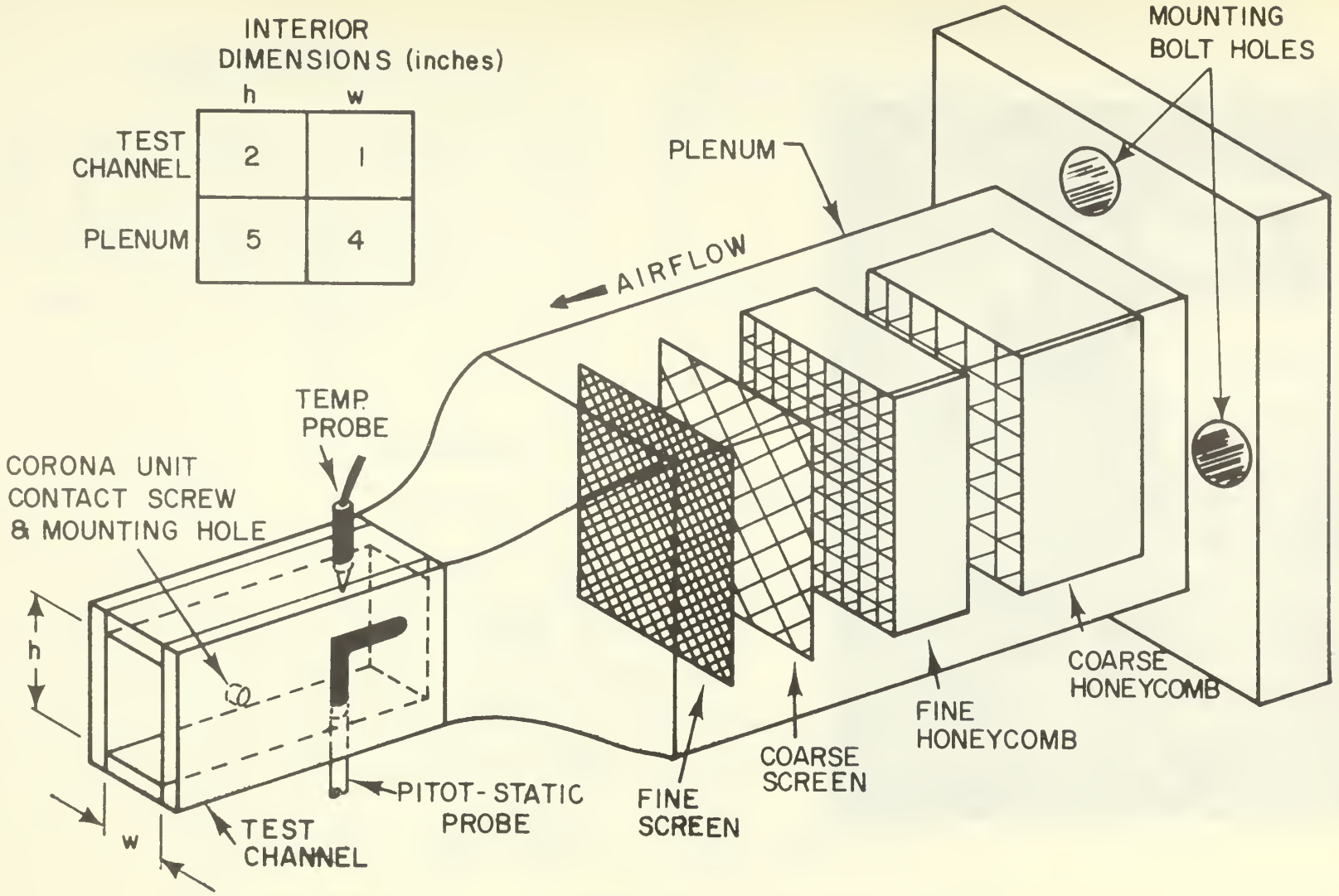

FIGURE 5. EGD SYSTEM FLOW CHANNEL

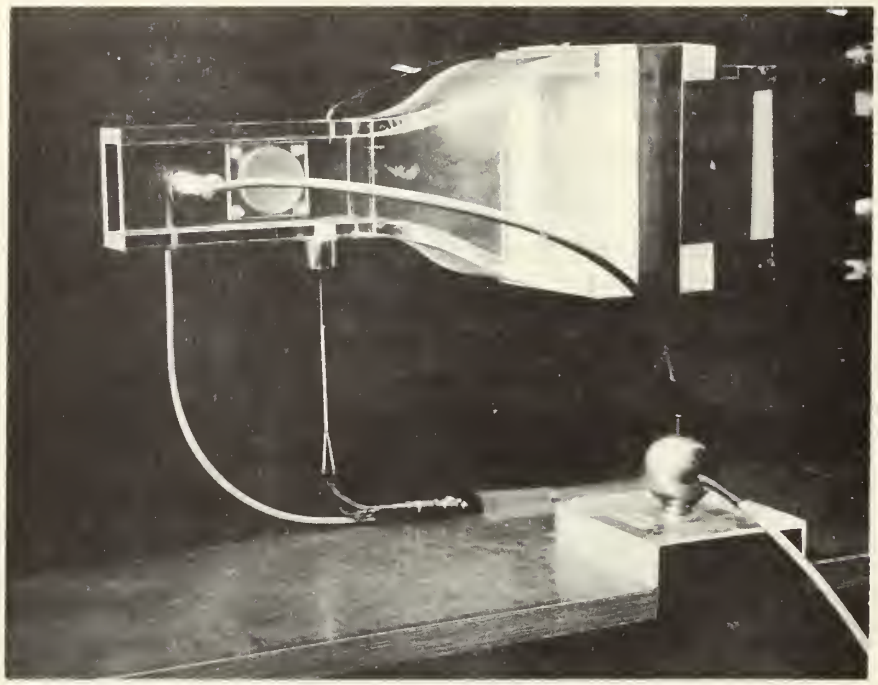

FIGURE 6 EGD SYSTEM FLOW CHANNEL

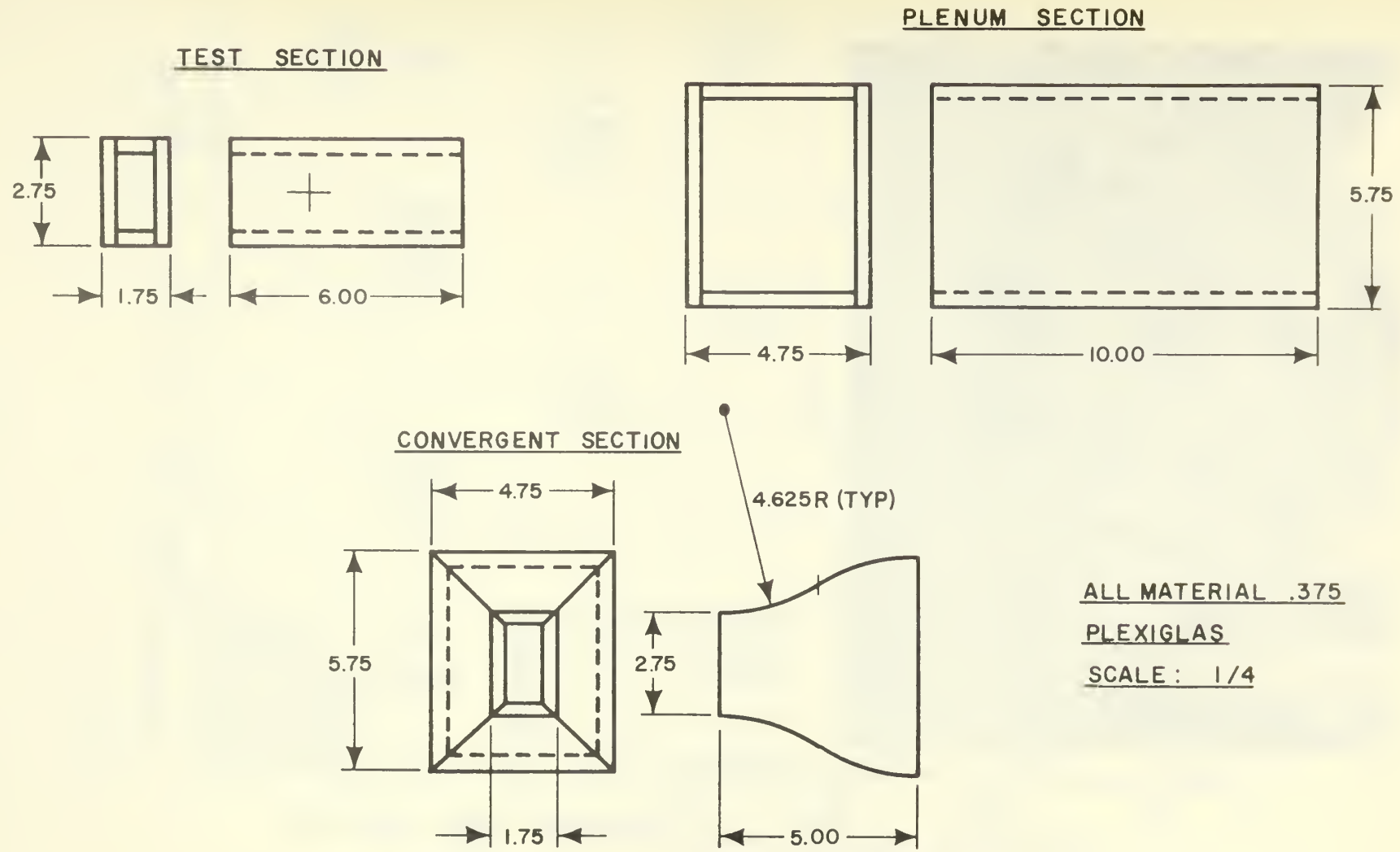

FIGURE 7. EGD SYSTEM FLOW CHANNEL

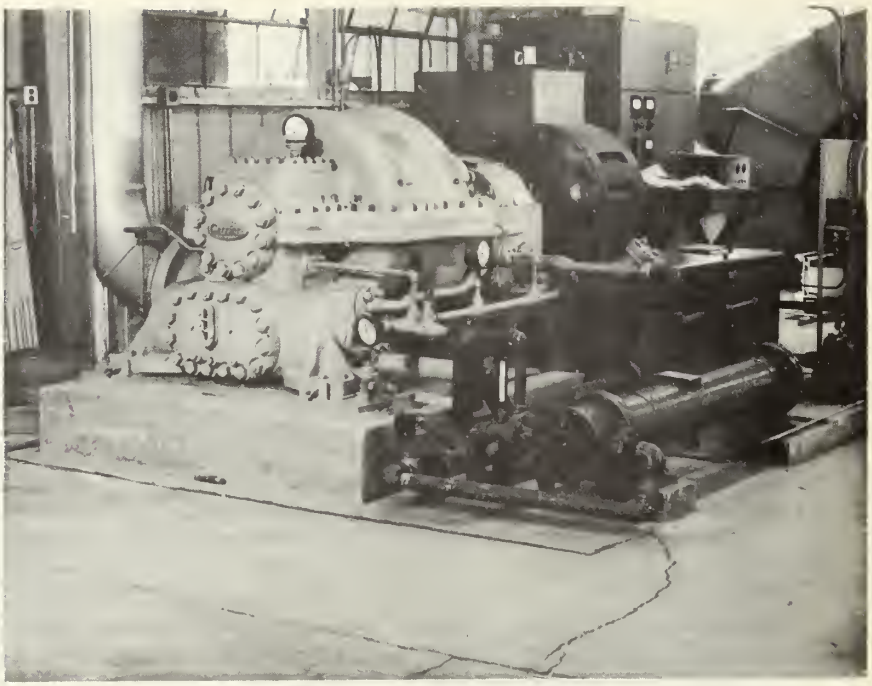

FIGURE 8. COMPRESSOR

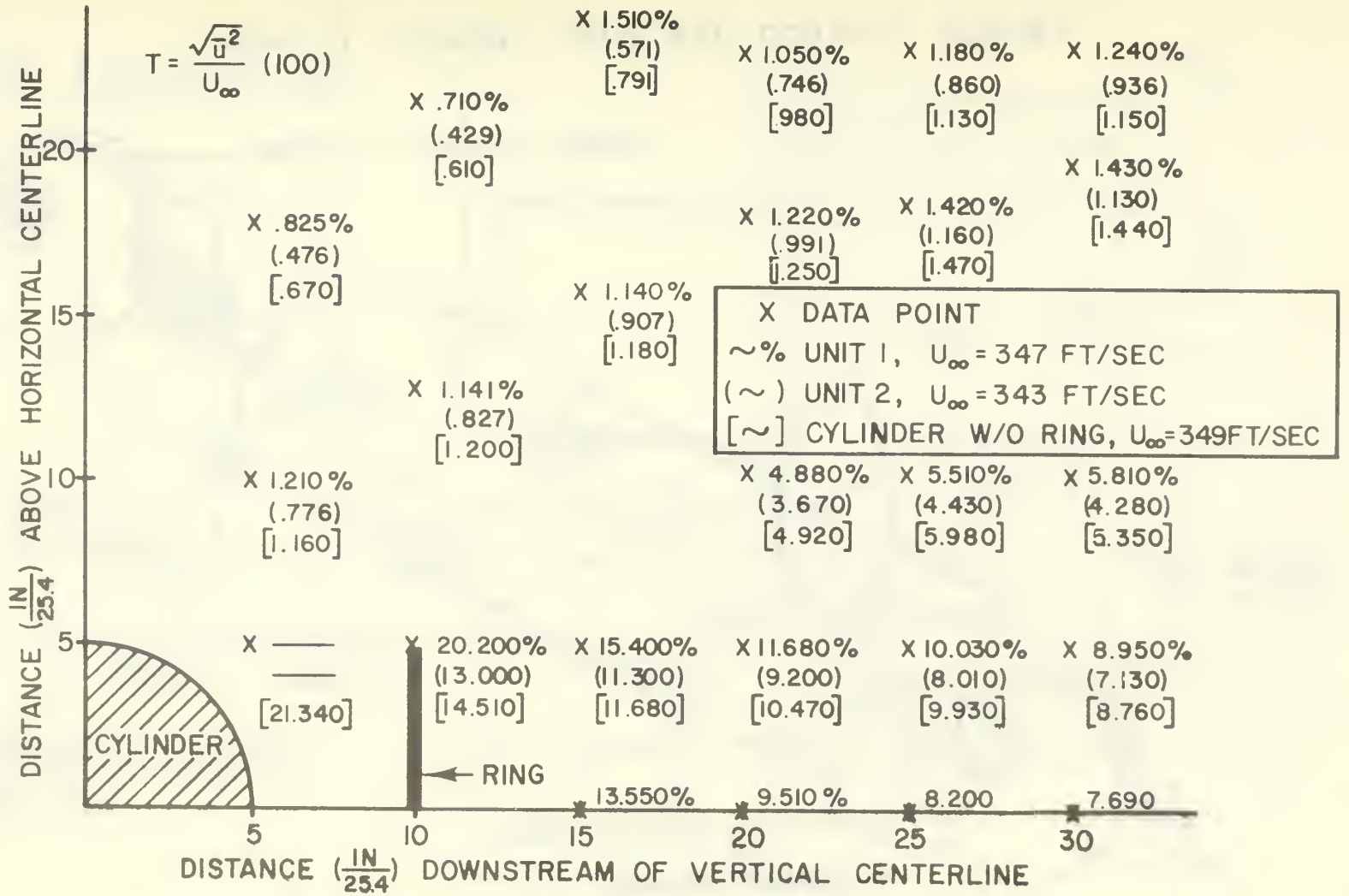

FIGURE 9. TURBULENCE LEVELS AT VARIOUS WAKE POSITIONS

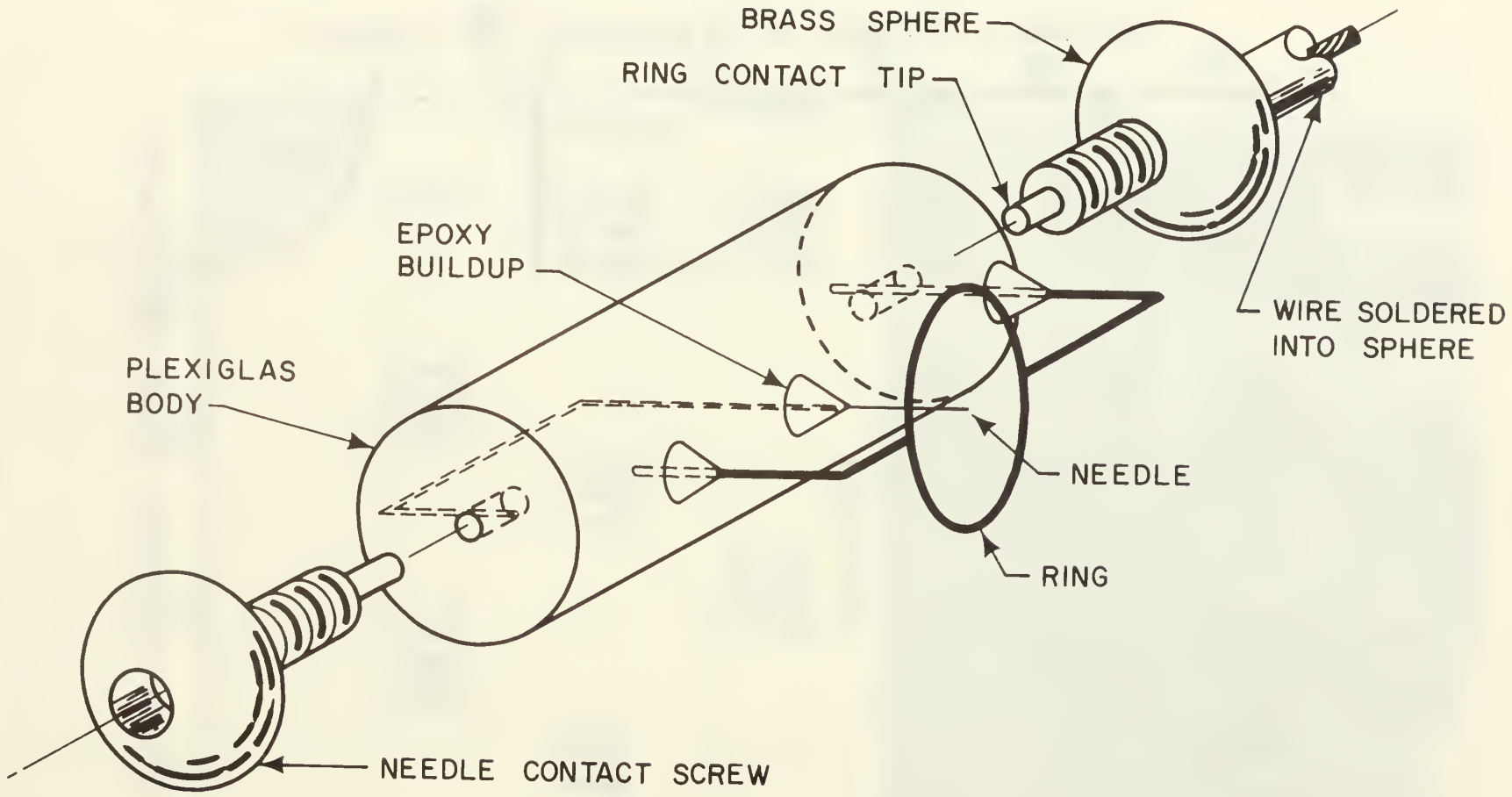

FIGURE 10. CORONA UNIT AND CONTACT SCREWS

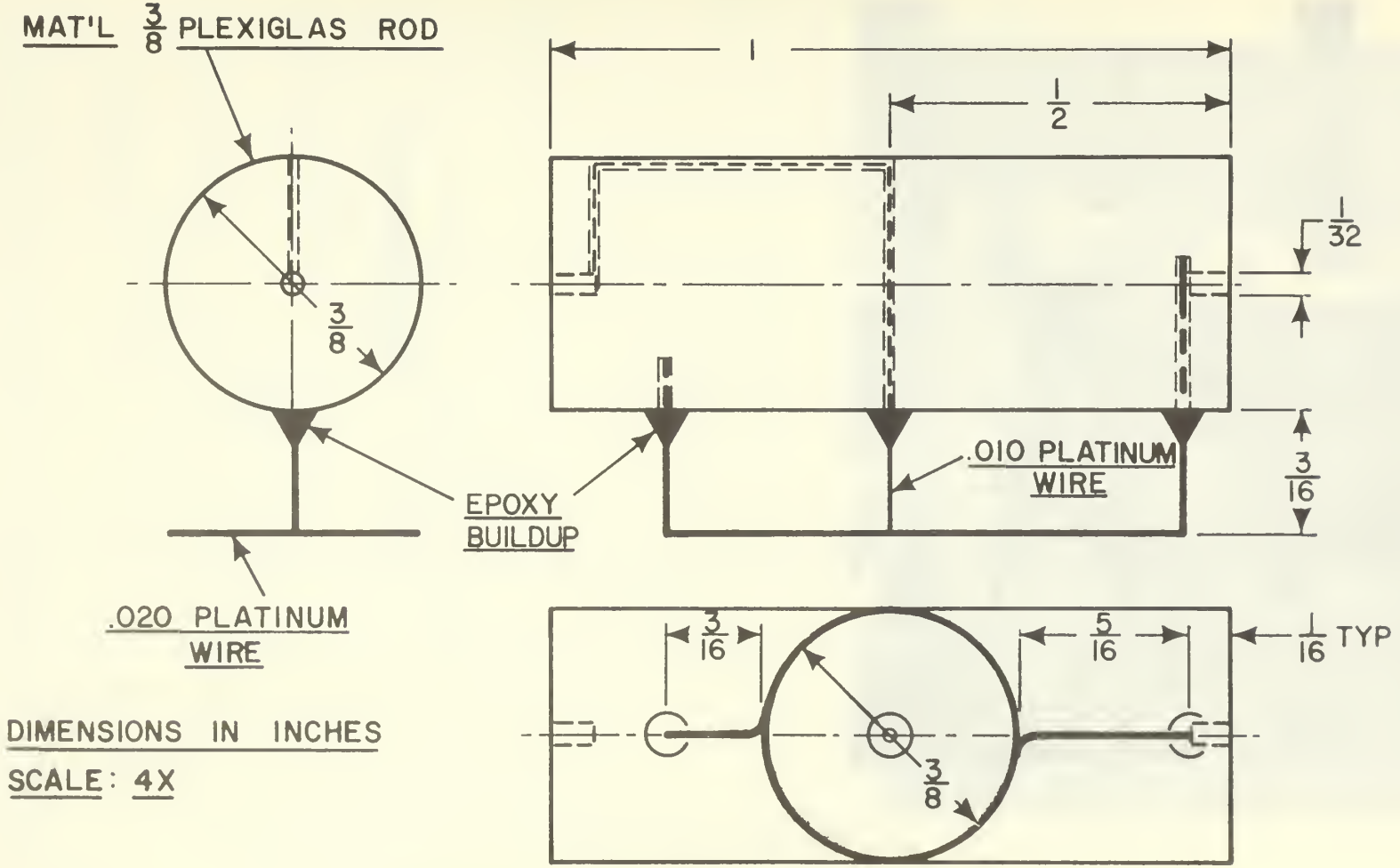

FIGURE 11. CORONA UNIT

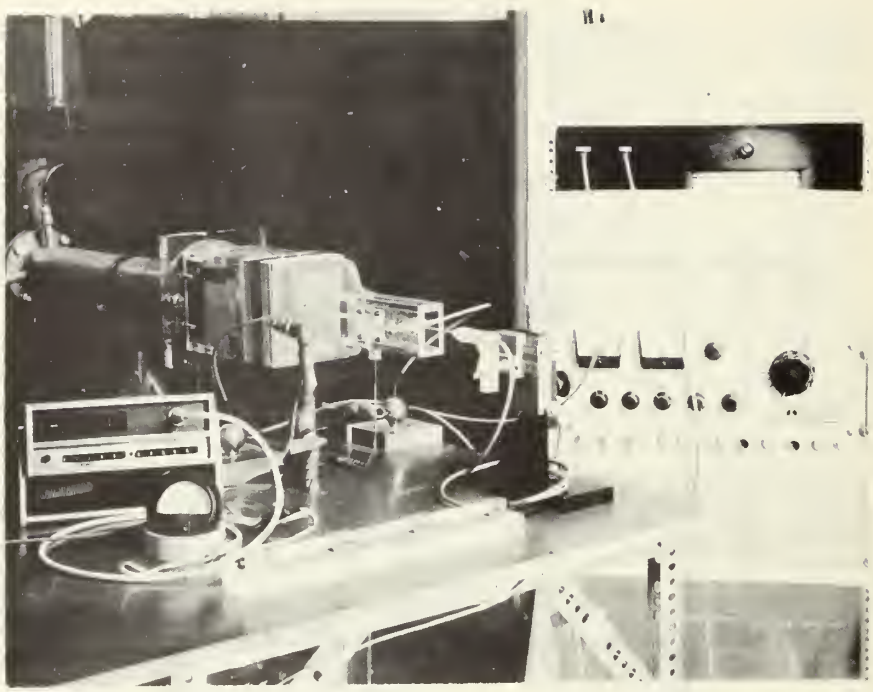

FIGURE 12. INSTRUMENTATION

FIGURE 1). CONNECTOR SPHERE

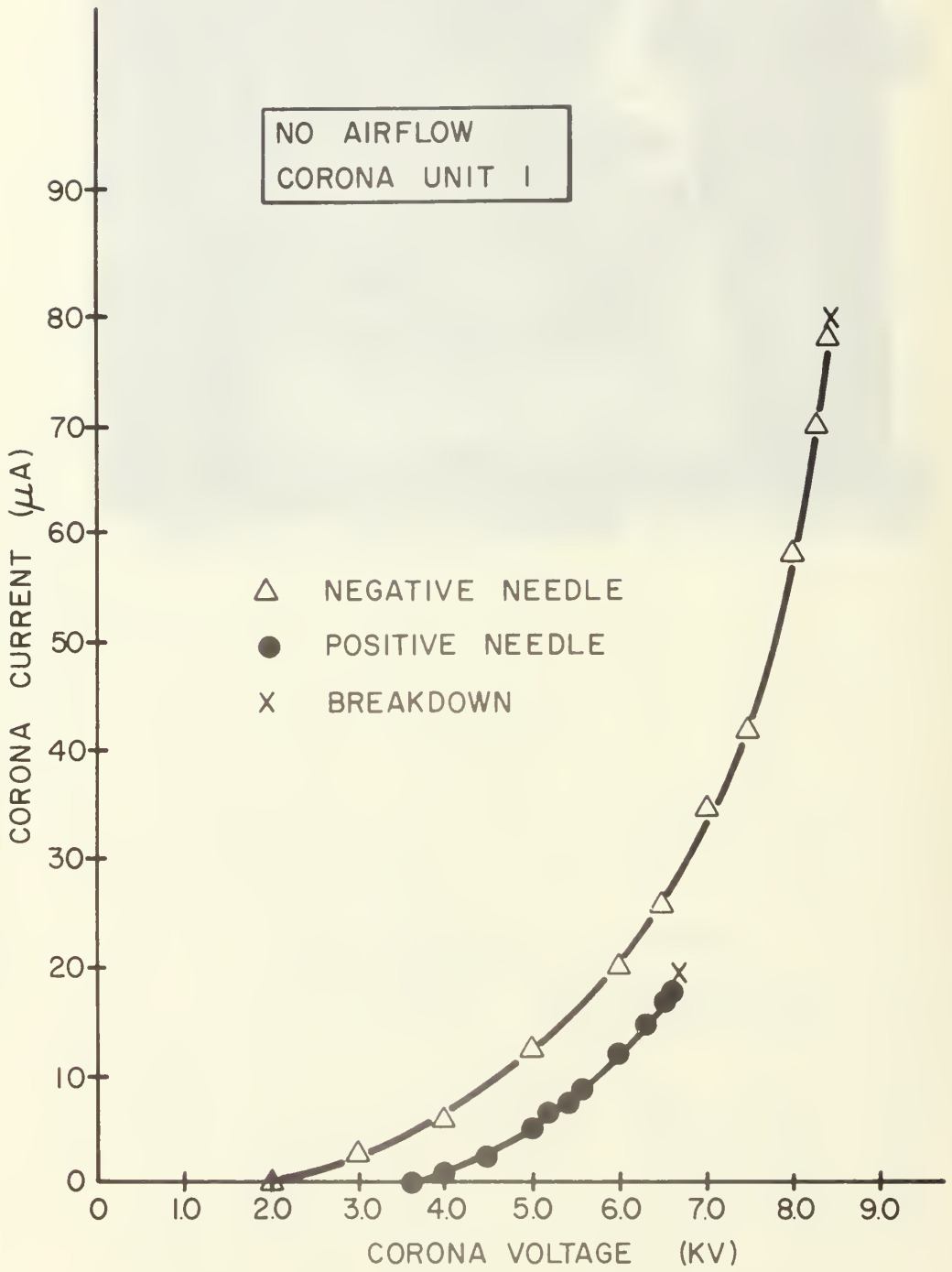

FIGURE 14. CORONA CURRENT VS VOLTAGE

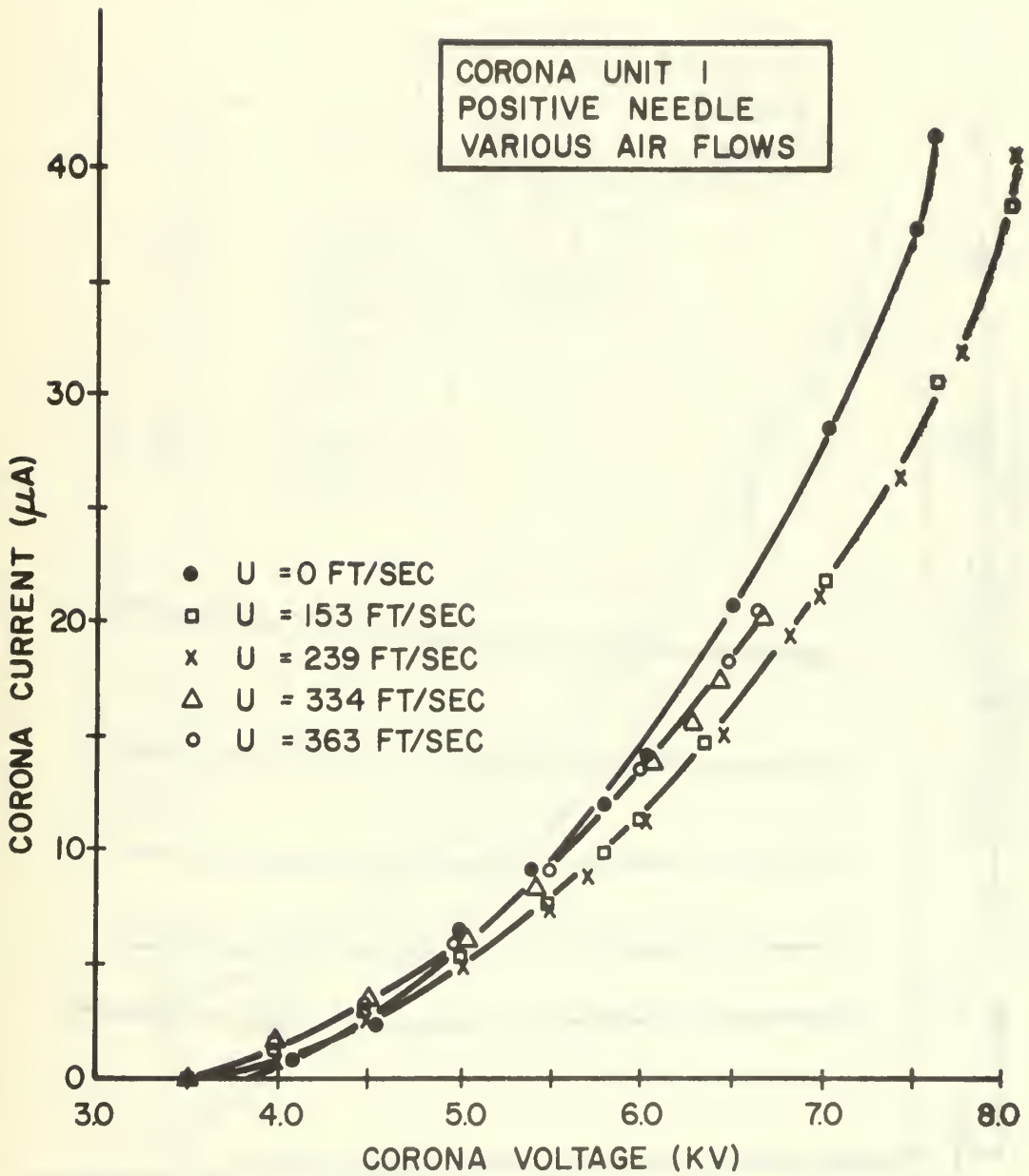

FIGURE 15. CORONA CURRENT VS VOLTAGE

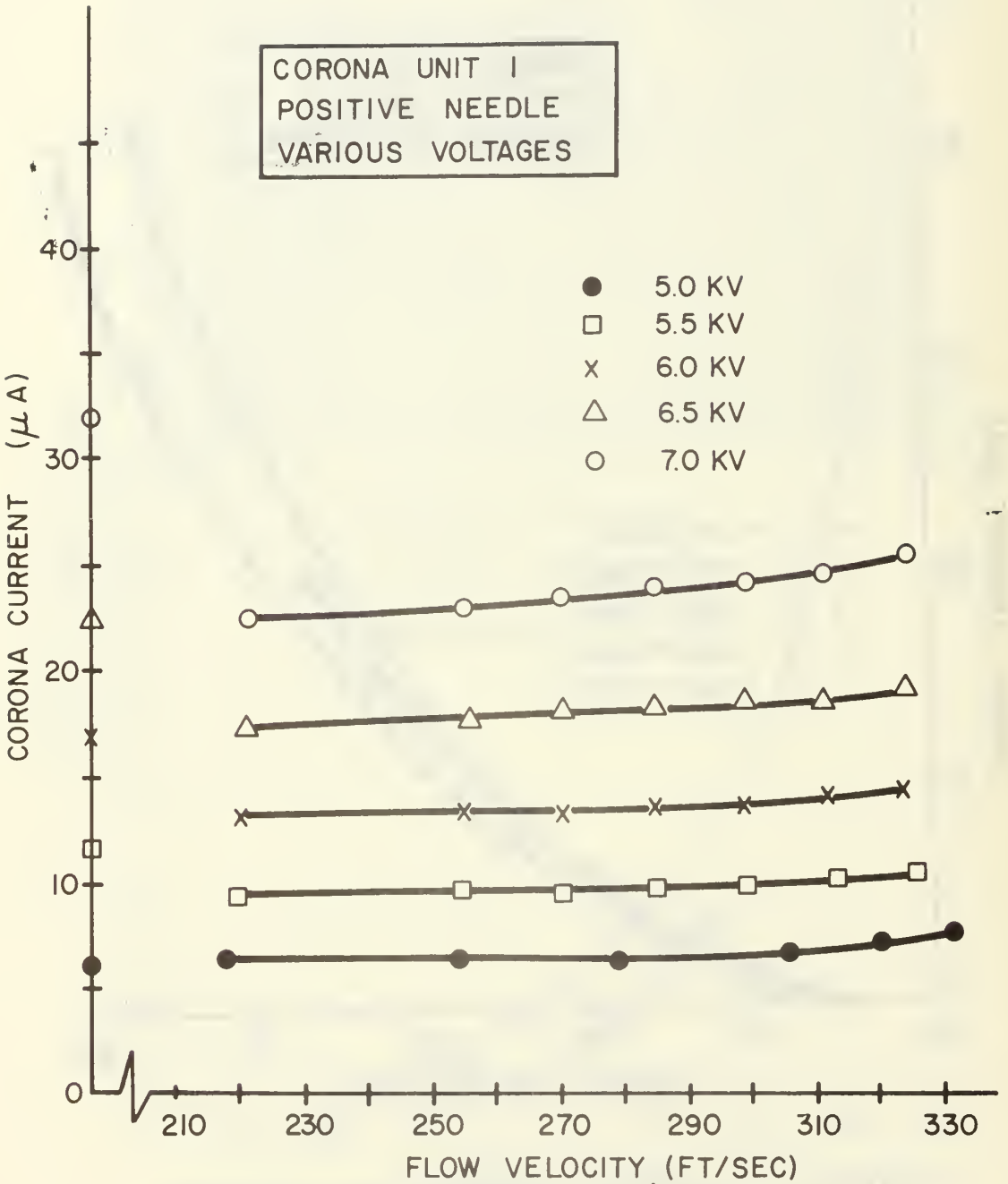

FIGURE 16. CORONA CURRENT VS FLOW RATE

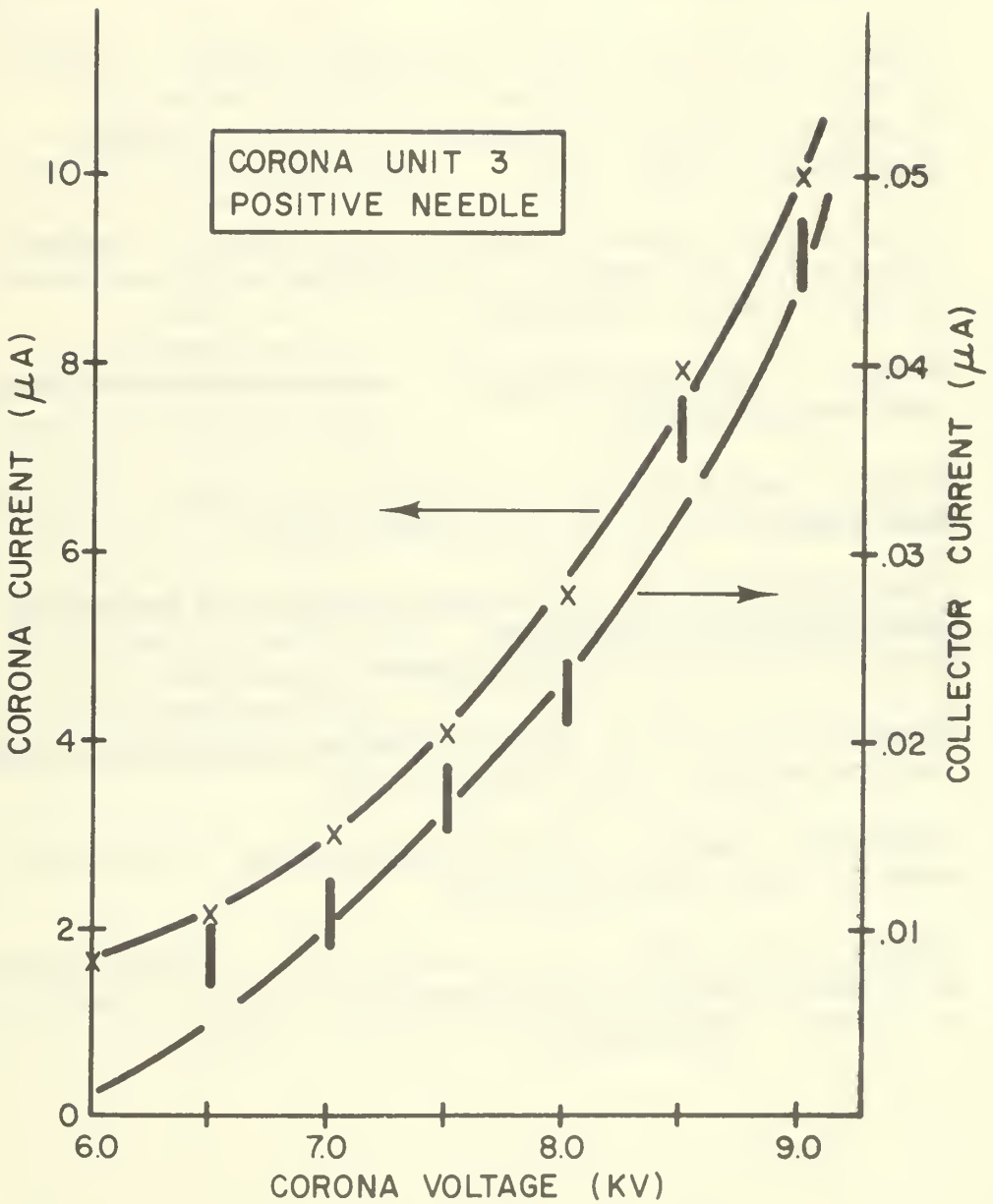

FIGURE 17. CORONA AND COLLECTOR CURRENT VS VOLTAGE

BIBLIOGRAPHY

1. Bennett, W. E. "The Generation of Direct Current at High Potentials." Research Applied in Industry, Vol. 12, No. 12, December 1959, England.

2. Smith, J. M. Electrohydrodynamic Power Generation--- Experimental Studies. General Electric Space Sciences Laboratory Report, March 1962.

3. Decaire, Capt. John A. and Wifall, Capt. James R. "Charge Generation by Corona Discharge in Electrofluiddynamic Conversion Processes." Advances in Energy Conversion Engineering. ASME, 1967.

4. Charged Particle Power Generation and Propulsion. Maremont Corporation, Final Report on Contract NOw 64-0594-f, Bureau of Naval Weapons, Washington, D. C., July, 1966.

5. Cobine, J. Gaseous Conductors. ~~McGraw-Hill Book Company, Inc., New York, 1969~~ Dover, 1958.

6. Marks, A. and Barreto, E. "Charged Aerosol Energy Converter." AIAA Journal, Vol. 2, No. 45, January 1964.

7. Ober, LT(jg) William. Ion Injector for Single and Two-phase Electrogasdynamic Generators. Master Thesis, Naval Post-graduate School, Monterey, California. June, 1969.

8. Stearnes, R. F., et al. Flow Measurement with Orifice Meters. Van Nostrand Co., Inc., New York, 1960.

9. Schlichting, Hermann. Boundary Layer Theory. McGraw-Hill Book Co., Inc., New York, 1960.

10. Gibson, C. H., Chen, C. C., and Lin, S. C. "Measurements of Turbulent Velocity and Temperature Fluctuations in the Wake of a Sphere." AIAA Journal, Vol. 6, No. 4, 1968.

INITIAL DISTRIBUTION LIST

		No. Copies
1.	Defense Documentation Center Cameron Station Alexandria, Virginia 22314	20
2.	Library Naval Postgraduate School Monterey, California 93940	2
3.	Commander Naval Air Systems Command Department of the Navy Attention: Mr. Milton Knight, Code AIR-340C Washington, D. C. 20360	1
4.	Professor O. Biblarz Department of Aeronautics Naval Postgraduate School Monterey, California 93940	4
5.	LT(jg) D. W. Wallace, USN 2207 Jameson St., S.E. Washington, D. C. 20031	1
6.	Chairman, Department of Aeronautics Naval Postgraduate School Monterey, California 93940	1

Security Classification

DOCUMENT CONTROL DATA - R & D

(Security classification of title, body of abstract and indexing annotation must be entered when the overall report is classified)

1. ORIGINATING ACTIVITY (Corporate author)	2a. REPORT SECURITY CLASSIFICATION
Naval Postgraduate School Monterey, California 93940	Unclassified
	2b. GROUP

3. REPORT TITLE

Molecular-ion Electrogasdynamic Flow Channel

4. DESCRIPTIVE NOTES (Type of report and inclusive dates)

Master's Thesis; June 1969

5. AUTHOR(S) (First name, middle initial, last name)

David William Wallace

6. REPORT DATE	7a. TOTAL NO. OF PAGES	7b. NO. OF REFS
June 1969	52	10

8a. CONTRACT OR GRANT NO.	9a. ORIGINATOR'S REPORT NUMBER(S)
b. PROJECT NO.	
c.	9b. OTHER REPORT NO(S) (Any other numbers that may be assigned this report)
d.	

10. DISTRIBUTION STATEMENT

Distribution of this document is unlimited

11. SUPPLEMENTARY NOTES	12. SPONSORING MILITARY ACTIVITY
	Naval Postgraduate School Monterey, California 93940

13. ABSTRACT

This investigation evaluates the operating characteristics of an EGD (electrogasdynamic) generator system which utilizes air both as the carrier fluid and as the source of injected ions. The design and construction of a flow channel and a corona ion injector are discussed, the performance of the ion injector is examined, and the results of attempts to obtain work by EGD energy conversion are presented. The experimental results presented and discussed are in reasonable agreement with expectations. The high mobility of molecular ions inhibits the conversion process and only 0.5% of the ions were removed from the corona by the air flow. Suggestions for improvements on the present system and the design of an advanced system are made.

DD FORM 1 NOV 65 1473 (PAGE 1)

S/N 0101-807-6811

Security Classification

A-31408

14 KEY WORDS	LINK A		LINK B		LINK C	
	ROLE	WT	ROLE	WT	ROLE	WT
electrogasdynamic corona discharge ion injector energy conversion						

DISTRIBUTION LIST

		No. Copies
1.	Defense Documentation Center Cameron Station Alexandria, Virginia 22314	20
2.	Library Naval Postgraduate School Monterey, California 93940	2
3.	Commander Naval Air Systems Command Department of the Navy Attn: Dr. H. R. Rosenwasser, Code AIR-310C	3
4.	Chairman Department of Aeronautics Naval Postgraduate School Monterey, California 93940	1
5.	Professor T. H. Gawain Department of Aeronautics Naval Postgraduate School Monterey, California 93940	1
6.	Professor K. E. Woehler Physics Department Naval Postgraduate School Monterey, California 93940	1
7.	Professor Oscar Biblarz Department of Aeronautics Naval Postgraduate School Monterey, California 93940	10
8.	Professor J. R. Melcher Dept. of Elec. Engr., Room 31-141 Mass. Inst. of Technology Cambridge, Massachusetts 02139	1
9.	Professor Albert Solbes Dept. of Aero., Room 37-375 Mass. Inst. of Technology Cambridge, Massachusetts 02139	1
10.	Mr. Alvin M. Marks Marks Polarized Corp. 153-16 10th Avenue Whitestone, New York 11357	1

11. Dr. M. C. Gourdine — 1
Gourdine Systems, Inc.
112 Naylon Avenue
Livingston, New Jersey 07039

12. Dr. Hans von Ohain — 1
Aerospace Research Laboratory
U. S. Air Force
Wright-Patterson AFB, Ohio 45433

13. Dr. A. E. Fuhs — 1
Chief Scientist-Code APX
Aero Propulsion Laboratory
Wright-Patterson AFB, Ohio 45433

14. Dr. Ernesto Barreto — 1
Atmospheric Research Center
State University of New York
130 Saratoga Road
Scotia, New York 12302

15. Professor H. R. Velkoff — 1
Dept. of Mech. Engr.
Ohio State University
Columbus, Ohio 43210

16. Dr. Otmar M. Stuetzer — 1
Sandia Corporation
P. O. Box 5800
Albuquerque, New Mexico 87115

17. Dr. Ralph Roberts — 1
Office of Naval Research
Power Program, Code 473
Washington, D. C. 20360

18. Mr. John A. Stakowski — 1
Office of Naval Research
Power Program, Code 473
Washington, D. C. 20360

19. Dr. H. J. Mueller — 1
Naval Air Systems Command
Code AIR 310
Washington, D. C. 20360

20. Dr. S. J. Magram — 1
Army Research Office
Arlington, Virginia 22200

21. Air Force Office of Scientific Research — 1
Washington, D. C. 20333
ATTN: Power Systems Group

22. Mr. Robert C. Hamilton — 1
Institute of Defense Analysis
400 Army - Navy Drive
Arlington, Virginia 22202

23. Dr. George C. Szego — 1
Institute of Defense Analysis
400 Army - Navy Drive
Arlington, Virginia 22202

24. Mr. S. Cohen — 1
NASA Lewis Research Center
21000 Brookpark Road
Cleveland, Ohio 44135

25. Mr. M. Lawson — 1
Aerospace Research Laboratory
U. S. Air Force
Wright-Patterson AFB, Ohio 45433

26. Dean of Research Administration — 2
Naval Postgraduate School
Monterey, California 93940

27. LTJG William T. Ober III, USN — 1
76 Salem Street
Andover, Massachusetts 01810

DOCUMENT CONTROL DATA - R & D

(Security classification of title, body of abstract and indexing annotation must be entered when the overall report is classified)

1. ORIGINATING ACTIVITY (Corporate author)
Naval Postgraduate School
Monterey, California 93940

2a. REPORT SECURITY CLASSIFICATION
Unclassified

2b. GROUP

3. REPORT TITLE
EHD Research
Final Report for the Year 1968-69

4. DESCRIPTIVE NOTES (Type of report and inclusive dates)

5. AUTHOR(S) (First name, middle initial, last name)
Oscar Biblarz

6. REPORT DATE
December 1969

7a. TOTAL NO. OF PAGES

7b. NO. OF REFS
28

8a. CONTRACT OR GRANT NO.
AIRTASK No A34340/551/69R01002010

b. PROJECT NO.

c.

d.

9a. ORIGINATOR'S REPORT NUMBER(S)
NPS-57ZI9121A

9b. OTHER REPORT NO(S) (Any other numbers that may be assigned this report)

10. DISTRIBUTION STATEMENT
This document has been approved for public release and sale; its distribution is unlimited.

11. SUPPLEMENTARY NOTES

12. SPONSORING MILITARY ACTIVITY
Naval Air Systems Command
Washington, D. C.

13. ABSTRACT

The present research in electrohydrodynamics is concerned with how charged particles can be generated in the laboratory with a potentially useful range of sizes, of charge, and of number density. It is suggested that refined measurement techniques are needed to check on just what is being injected into the flow. The effects of turbulence on the EHD process and, particularly, on breakdown are being studied. The report discusses in some detail the possible role of turbulence on the mean effective mobility of charged particles.

On the experimental side, a laboratory facility has been built and then improved by the addition of a larger test section and other equipment. Work is proceeding to further develop and refine the instrumentation. Two types of injectors have been operated, namely, molecular and two phase and the latter shows potential for efficient operation.

It has been concluded tentatively that turbulence in the carrier fluid increases its breakdown potential, and that turbulent air may be a suitable medium for the EHD energy conversion process.

Research plans for the coming year are outlined in the report.

14 KEY WORDS	LINK A		LINK B		LINK C	
	ROLE	WT	ROLE	WT	ROLE	WT
Electrohydrodynamics						
Turbulence						
Breakdown potential						
Charged Particle injector						
Mobility						
Direct Energy Conversion						